PRODUCTION AND CHARACTERIZATION OF BORON CARBIDE POWDER BY MECHANOCHEMICAL METHOD

A THESIS SUBMITTED TO
THE GRADUATE SCHOOL OF NATURAL AND APPLIED SCIENCES
OF
MIDDLE EAST TECHNICAL UNIVERSITY

BY

BERKAY BÜYÜKLÜOĞLU

IN PARTIAL FULFILLMENT OF THE REQUIREMENTS
FOR
THE DEGREE OF MASTER SCIENCE
IN
METALLURGICAL AND MATERIALS ENGINEERING

JANUARY 2023

Approval of the thesis:

PRODUCTION AND CHARACTERIZATION OF BORON CARBIDE POWDER BY MECHANOCHEMICAL METHOD

submitted by **BERKAY BÜYÜKLÜOĞLU** in partial fulfillment of the requirements for the degree of **in Master of Science, Metallurgical and Materials Engineering, Middle East Technical University** by,

Prof. Dr. Halil Kalıpçılar
Dean, Graduate School of **Natural and Applied Sciences** _____

Prof. Dr. Ali Kalkanlı
Head of the Department, **Metallurgical and Mat. Eng. METU** _____

Assist. Prof. Dr. Irmak Sargın
Supervisor**, Metallurgical and Materials Eng, METU** _____

Examining Committee Members:

Prof. Dr. Caner Durucan
Metallurgical and Materials Eng, METU _____

Assist. Prof. Dr. Irmak Sargın
Metallurgical and Materials Eng, METU _____

Prof. Dr. Arcan Dericioğlu
Metallurgical and Materials Eng, METU _____

Assoc. Prof. Dr. Simge Çınar Aygün
Metallurgical and Materials Eng, METU _____

Prof. Dr. Ziya Esen
Department of Material Science and Eng, Çankaya University _____

Date: 27.01.2023

I hereby declare that all information in this document has been obtained and presented in accordance with academic rules and ethical conduct. I also declare that, as required by these rules and conduct, I have fully cited and referenced all material and results that are not original to this work.

Name Last name : Berkay Büyüklüoğlu

Signature :

ABSTRACT

PRODUCTION AND CHARACTERIZATION OF BORON CARBIDE POWDER BY MECHANOCHEMICAL METHOD

Büyüklüoğlu, Berkay
Master of Science, Metallurgical and Materials Engineering
Supervisor: Assist. Prof. Dr. Irmak Sargın

January 2023, 127 pages

In this study, the production of boron carbide (B_4C) powders at room temperature by mechanochemical alloying is investigated. The conventional production methods of this industrially important material requires high energy consumption, whereas the low energy production methods could only produce small amounts. By optimizing the mechanochemical alloying, the know-how for the larger scale production is developed. The mechanochemical method consists of mechanical grinding and acid leaching to remove by-products and impurities from the system. A mechanical chamber is designed with high friction strength, resistance to pressure and temperature and that is also suitable for scaled-up production while avoids large amounts of contamination. The process parameters, namely ball to powder ratio (BPR), ball mill speed (RPM), and grinding time are optimized. For the second stage, acid leaching, the parameters acid molarity, magnetic stirrer table speed, and temperature, and leaching time are optimized. The powders that produced with different processing parameters are characterized for present phases, particle size and morphology by X-ray diffraction (XRD), laser diffraction, and scanning electron microscopy (SEM), respectively. Also, kinetics of B_4C formation is studied. Within

the scope of these studies, boron carbide particles with a particle size of approximately 2 μm and a purity of 98% are produced by mechanochemical method at room temperature with low energy consumption.

Keywords: Boron Carbide, Mechanochemical Operation, Ball Mill, Mechanical Alloying, Acid Leaching, Room Temperature Production

ÖZ

MEKANOKİMYASAL YÖNTEMLE BOR KARBÜR TOZU ÜRETİMİ VE KARAKTERİZASYONU

Büyüklüoğlu, Berkay
Yüksek Lisans, Metalurji ve Malzeme Mühendisliği
Tez Yöneticisi: Assist. Prof. Dr. Irmak Sargın

Ocak 2023, 127 sayfa

Bu çalışmada, bor karbür (B_4C) tozlarının mekanokimyasal yöntem ile oda sıcaklığında üretimi çalışılmıştır. Endüstriyel açıdan önemli olan bu malzemenin geleneksel üretim yöntemleri, yüksek enerji tüketimi gerektirirken, düşük enerjili üretim yöntemleri ile sadece küçük miktarlarda üretim yapabilmektedir. Mekanokimyasal üretim optimize edilerek daha büyük ölçekli üretim için know-how geliştirilmiştir. Mekanokimyasal yöntem, yan ürünleri ve safsızlıkları sistemden uzaklaştırmak için mekanik öğütme ve asit liç operasyonlarından oluşur. Yüksek sürtünme mukavemetine, basınca ve sıcaklığa karşı dirence sahip bir hazne tasarımı gerçekleştirilmiştir. Bu hazne aynı zamanda kontaminasyonu önemli ölçüde önlerken, daha büyük ölçekli üretime de uygun olabilecektir. Proses parametreleri, yani bilye-toz oranı (BPR), bilyalı değirmen hızı (RPM) ve öğütme süresi optimize edilmiştir. İkinci aşama olan asit liç operasyonu için asit molaritesi, manyetik karıştırıcı tabla hızı ve sıcaklığı ile liç süresi parametreleri optimize edilmiştir. Farklı parametreler ile üretilen tozlar sırasıyla X-ışını kırınımı (XRD), lazer kırınımı ve taramalı elektron mikroskobu (SEM) ile mevcut fazlar, parçacık boyutu ve morfoloji açısından karakterize edilmiştir. Ayrıca, B_4C oluşumunun kinetiği de incelenmiştir. Bu çalışmalar kapsamında yaklaşık 2 μm parçacık boyutuna ve %98 saflığa sahip

bor karbür parçacıkları mekanokimyasal yöntemle oda sıcaklığında düşük enerji tüketimi ile üretilmiştir.

Anahtar Kelimeler: Bor Karbür, Mekanokimyasal Yöntem, Bilyalı Değirmen, Mekanik Alaşımlama, Asit Liç, Oda Sıcaklığında Üretim

I dedicate this thesis to my parents, Fethiye, Adnan and dear brother Mert. For their endless love, encouragement, and support.

ACKNOWLEDGMENTS

I would like to express my endless gratitude to my supervisor Assist. Prof. Dr. Irmak Sargın for guidance at every stage, encouragements, advices and for teaching me the academic approach.

I also wish to thank the members of examining committee, Prof. Dr. Caner Durucan, Prof. Dr. Arcan Dericioğlu, Prof. Dr. Ziya Esen, and Assoc. Prof. Dr. Simge Çınar Aygün for their valuable criticism, suggestions, and comments to make this thesis better during the defense period.

I would like to express my endless thanks to my family, my mother, my father and my brother, who have supported me with their endless love at every stage of my life, encouraged me and enabled me to achieve significant success in life.

I would like to express my special thanks to my friends, too many to name, for their help, support, and encouragement during the process of writing this thesis.

TABLE OF CONTENTS

ABSTRACT v

ÖZ vii

ACKNOWLEDGMENTS x

LIST OF TABLES xiv

LIST OF FIGURES xv

LIST OF ABBREVIATIONS xvii

CHAPTERS

1 LITERATURE REVIEW 1

1.1 Introduction to Boron Carbide 1

1.2 Production of B_4C 6

1.2.1 Carbothermic Reduction 7

1.2.2 Self-Propagating High-Temperature Synthesis (SHS) 10

1.2.3 Vapour Phase Reaction 10

1.2.4 Synthesis From Polymer Precursors 12

1.2.5 Liquid Phase Reaction 12

1.2.6 Vapour-Liquid-Solid (VLS) Growth 13

1.2.7 Mechanical Alloying and Comparison of Production Routes 14

1.3 Mechanochemical Synthesis 19

1.4 Mechanism of Alloying 24

1.5 Mechanochemical Synthesis Parameters 27

1.5.1 Mill Type 28

1.5.2 Milling Container and Material 34

1.5.3 Milling Speed 35
1.5.4 Milling Time 36
1.5.5 Grinding Medium Material and Size 37
1.5.6 Ball-to-powder weight ratio 38
1.5.7 The extent of filling the vial 39
1.5.8 Milling atmosphere 40
1.6 Acid Leaching 40
1.7 Kinetic Modelling of the System 44
2 EXPERIMENTAL PROCEDURE 47
2.1 Steps of Mechanochemical Synthesis 47
2.2 Mechanical Jar Design 50
2.3 Mechanochemical Synthesis Parameters 52
2.4 Acid Leaching and Obtaining Final Powder 55
2.4.1 Acid Leaching 55
2.4.2 Powder Extraction 56
2.4.3 Washing 57
2.5 Characterization 58
2.5.1 Particle Size Analysis and Optimization 58
2.5.2 Phase Analysis 59
2.5.3 Morphological Characterization 59
2.6 Kinetics modelling 60
3 RESULTS AND DISCUSSION 61
3.1 Mechanical Design 61
3.1.1 Mechanical Jar Design 61

3.1.2 Relief Valve Design and Optimization 65
3.1.3 Material Selection 68
3.1.4 Inert Gas Selection 70
3.2 Raw Material Characterization 71
3.2.1 Particle Size Analysis and Optimization 71
3.3 Mechanochemical Operation Parameters 74
3.3.1 BPR (Ball to Powder Ratio) Optimization 74
3.3.2 RPM Optimization 75
3.3.3 Milling Time Optimization 77
3.4 Acid Leaching 82
3.4.1 Acid Molarity 83
3.4.2 Leaching Temperature 85
3.4.3 Magnetic Stirrer RPM 86
3.4.4 Leaching Time and Final Results 87
3.5 Steps Following Acid Leaching and Obtaining Final Powder 93
3.5.1 Centrifuge Operation Optimization 93
3.5.2 Drying 93
3.6 Kinetic Modelling of the System and General Results 95
4 CONCLUSION 101
5 REFERENCES 105

LIST OF TABLES

TABLES

Table 1.1. Process type, parameters, and final quality of some production methods. 17

Table 1.2. Comparison of advantages and disadvantages table of B_4C production methods. 17

Table 1.3. Rise in Temperature during MA [107]. 23

Table 1.4. Conventional capacities of various kinds of mills. 34

Table 2.1. Experimental conditions used in this study. 54

Table 3.1. Raw material particle size before and after an additional milling operation. 72

Table 3.2. Summary of BPR optimization studies. 74

Table 3.3. RPM Optimization results. 75

Table 3.4. Fixed mechanochemical milling parameters. 77

Table 3.5. Acid molarity optimization results. 83

Table 3.6. Leaching temperature optimization results. 85

Table 3.7. Stirrer RPM optimization. 86

Table 3.8. Purity of 8h milled sample and purity of acid leached sample. 90

Table 3.9. Weight percentage transformed of B_4C and MgO with respect to milling duration for 450 RPM, 15:1 BPR. 96

Table 3.10. Curve fitting of the B_4C and MgO transformation. 99

LIST OF FIGURES

FIGURES

Figure 1.1. Boron carbide's lattice structure [3] 2

Figure 1.2. B_4C lattice exhibiting correlation between the hexagonal (blue) unit cells and rhombohedral (red). [3] 3

Figure 1.3. Phase diagram of B-C system. 4

Figure 1.4. Thermogravimetric analysis plot: Boric acid's carbothermic reduction. 8

Figure 1.5. The impact of feed temperature and composition on the estimated product composition during one mol B_2O_3 (l)'s carbothermic reduction [47] 9

Figure 1.6. The differences in temperature of the grinding vial during MA at the time of the burning reaction [97]. 21

Figure 1.7. Powder mixture collision between powder and ball during mechanical alloying (MA) [108]. 25

Figure 1.8. Distribution of narrow particle size distribution due to the tendency of small particles to weld together and large particles to fracture under steady-state conditions [110]. 26

Figure 1.9. Grinding time with relation to particle refinement and grain sizes. 27

Figure 1.10. SPEX 8000 mixer mill. (b) Tungsten carbide vial set consisting of the lid, vial, balls, and gasket. Courtesy of SPEX CertiPrep, Metuchen, NJ. 29

Figure 1.11. (a) Fritsch Pulverisette P-5 4 station ball mill. (b) Diagram illustrating the ball moves within a ball mill. (c) Planetary ball mill angular velocity explanations. Courtesy of Gilson Company, Inc., Worthington, OH. 31

Figure 1.12. (a) Model 1-S attritor. (b) Configuration of spinning arms on a shaft within an attrition ball mill. Courtesy of Union Process, Akron, OH [108]. 32

Figure 1.13. Grinding of TiB_2 powder to achieve comparable particle sizes in (a) planetary ball mill and (b) attritor [108]. 33

Figure 2.1. Summary of the production steps and the optimized parameters in this study. 49

Figure 3.1. A simple schematic of milling operation[60]. 63
Figure 3.2. Jar technical drawing without bottom jar Radius (upper), jar technical drawing with 20 mm jar bottom radius (bottom). 64
Figure 3.3. Relief valve. 66
Figure 3.4. Relief valve opening pressures. 67
Figure 3.5. Particle size analysis results from Mastersizer 72
Figure 3.6. Particle size analysis results before and after B_2O_3 milling operation. 73
Figure 3.7. 550 RPM and more than 12 hours of mechanochemical milled powder. 76
Figure 3.8. Particle size change with the milling time. 78
Figure 3.9. 3 hour, 5 hours and 8 hour XRD results. 79
Figure 3.10. SEM images of the samples taken at different time intervals in the mechanochemical operation, 3 hours milling (upper), 5 hours milling (middle), and 8 hours milling (below). 81
Figure 3.11. GSAS-II software Rietveld analysis, (a) 8 hour milled sample, and (b) acid leached sample. 89
Figure 3.12. Before and after SEM images for acid leaching operation, 8 hours milling (upper), 8 hours milling and after acid leaching (middle), and acid leached 20.000x magnification (below). 91
Figure 3.13. EDS result obtained by SEM device after acid leaching operation. .. 92
Figure 3.14. (a) Percentage transformed as a function of milling time. 96
Figure 3.15. Change of percentage transformed for MgO and B_4C as function of time (symbols) and the Avrami equation curve fitting (lines). 98

LIST OF ABBREVIATIONS

ABBREVIATIONS / SYMBOLS

AISI D2	: Cold Work Tool Steel
BPR	: Ball-to-Powder Ratio
CNC	: Computerized Numerical Control Machine
CR	: The charge ratio
DI	: Distilled
DLC	: Diamond-like Carbon
E	: Elastic Modulus
EDS	: Energy-Dispersive Spectroscopy
GSAS-II	: General Structure Analysis System-II
HEL	: Hugoniot Elastic Limit
HRC	: Hardness Rockwell C
JMAK	: Johnson–Mehl–Avrami–Kolmogorov
MA	: Mechanical Alloying
MM	: Mechanical Milling
pH	: Potential of Hydrogen
PTFE	: Polytetrafluoroethylene
RPM	: Revolutions per minute
SAE304	: Stainless Steel Grade 304
SAE316	: Stainless Steel Grade 316
SAE316L	: Stainless Steel Grade 316L
SEM	: Scanning Electron Microscopy
SHS	: Self-Propagating High-Temperature Synthesis
SPEX mill	: High-Energy Ball Mill
TDS	: Total Dissolved Solids
TEM	: Transmission Electron Microscopy

VLS : Vapor–Liquid–Solid Method

X-RAY : A Form of Electromagnetic Radiation

XRD : X-Ray Diffraction Analysis

" : inch

% : Percent

M_V : Molar Volume

$\boldsymbol{\mu_S}$: Strain Modulus

ΔG : Gibbs Free Energy

°C : Degree Celsius

μm : Micrometer

at% : percentage by time

Bar : Unit of Pressure

cm : centimeter

g : gram

g/cm3 : Grams per cubic centimeter

GPa : Gigapascals

k : Rate constant

kg : Kilogram

$kJmol^{-1}$: Kilojoule per mole

M : Molar

m/s : meter per second

m^2 : square meter

Ml : Milliliter

mm : millimeter

n : Order of reaction

nm : nanometer

$t_{0.5}$: Half time period

wt% : percentage by weight

k : Rate Constant

t : Time Period

y	: Fracture of transformation
ρ	: Density
Al	: Aluminium
Al_2O_3	: Aluminum Oxide
B	: Boron
B_2O_3	: Boron oxide
B_4C	: Boron carbide
MgO	: Magnesium oxide

CHAPTER 1

LITERATURE REVIEW

1.1 Introduction to Boron Carbide

B_4C is the general chemical formula used for boron carbide. However, it is only an empirical formula. The boron carbide is made up of dodecahedral clusters of 12 boron (B) atoms linked to linear rods of 3 carbon (C) atoms. However, stoichiometry is not constant; instead, it ranges from B_6C_5 to B_4C. One major characteristic of boron carbide is its extreme hardness, which is 9.3 on the Mohs scale. Due to its hardness, it is utilized as an abrasive [1]. Moreover, it holds a particular space.

The B_4C compound was first discovered in 1858. After that, B_3C was synthesized and identified by Joly in 1883 [2]. In 1934, the B_4C 'stoichiometric formula' was assigned [3]. Boron carbide's other properties, such as high hugoniot elastic limit (HEL) and low density combined with its extreme hardness, make it highly suitable for protective body armor. B_4C’s unique properties result from a distinctive lattice structure with strong covalent bonds and high interatomic electron density [4].

The hardness of B_4C ranges from 29 to 41 GPa, making it the third hardest material [5]. The first and second hardest materials are diamond and cubic boron nitride, respectively. Andrievski et al. claim that the hardness of B_4C can rise to 49 GPa [6]. The capacity of elemental boron to create caged structures of different sizes results in icosahedra within the boron carbide structure [7], [8]. Some of the properties of B_4C are high elastic modulus (450 GPa), low density (2.52 g/cm^3), good wear resistance, good strength, good chemical inertness at room temperature, and exceptional hardness (29.1 GPa) [3], [9], [10].

Because of its thermal stability and extremely high melting point (2450 °C), B_4C possesses refractory characteristics. The boron carbide lattice structure given in Figure 1.1. [5], [11].

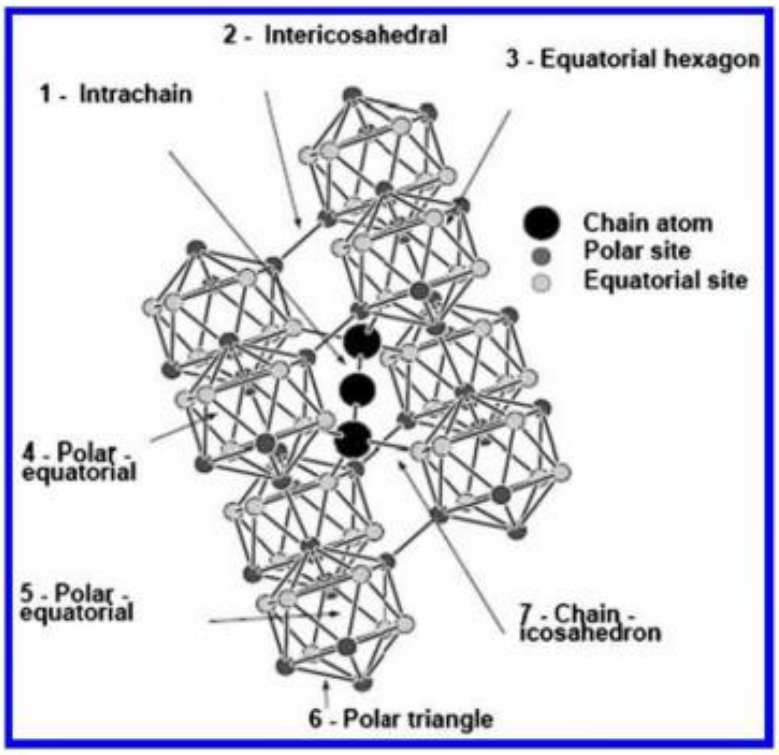

Figure 1.1. Boron carbide's lattice structure [3]

Some researchers have extensively described the boron carbide's atomic structure. As shown in Figure 1.2, the B_4C 's primary structural units are the 3-atom linear chains that attach icosahedra with the (111) rhombohedral axis and 12-atom icosahedra present at the rhombohedral lattice of trigonal symmetry's vertices (R3m space group). This structure can also be characterized by the notion of a non-primitive unit cell-based hexagonal lattice, where the [0001] axis correlates to the [111] rhombohedral direction [3], [12]–[14]. In Figure 1.2, the arrows represent inequivalent lattice sites. The B_4C 's icosahedra are the two pentagonal pyramids

joined together. Equatorial and polar are the two distinctive locations possibly present in an icosahedron. The equatorial locations are the places where 3-atom chains are joined together. Moreover, it makes up a hexagonal chair in the icosahedron as shown in Figure 1.1. On the other hand, the atoms that bond icosahedra together are corresponded to polar locations. In the crystal structure, the polar atoms inside the cage are also the three atoms from each of the two planes that confront each other [15].

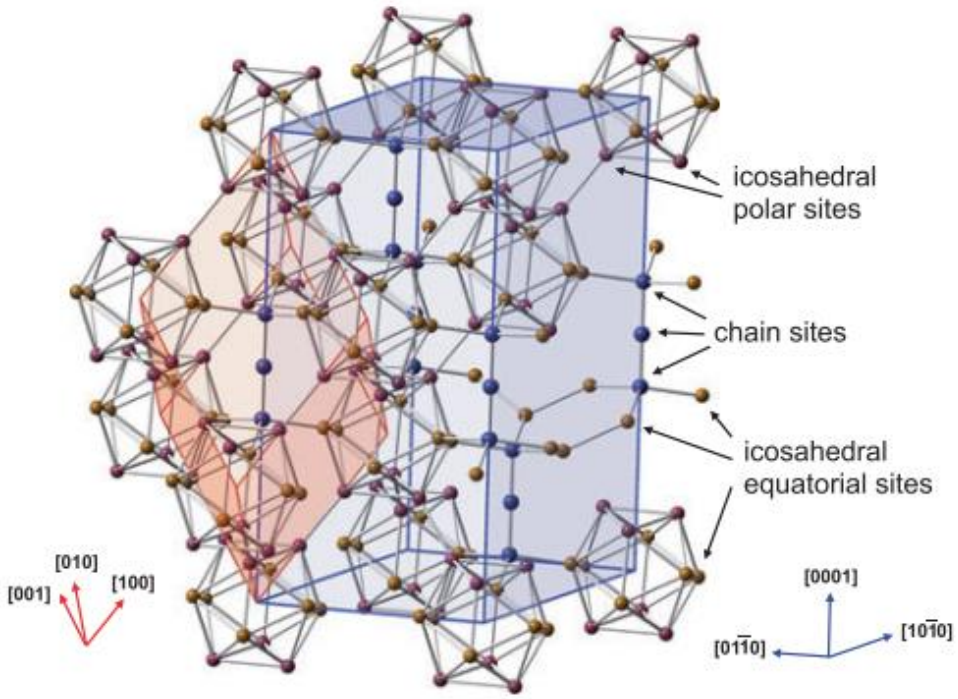

Figure 1.2. B_4C lattice exhibiting correlation between the hexagonal (blue) unit cells and rhombohedral (red). [3]

Rhombohedra is the crystal structure of B_4C. It consists of 3-atom linear chains that join the icosahedra with (111) rhombohedral axis and 12-atom icosahedra positioned at the unit cell's corners, see Figure 1.1 [5]. The unit cell's composition is represented as $B_{12}C_3$ or B_6-C-C-C-B_6. The B and C's exchange is possible in the

interstitial atoms' row, with $B_{13}C_2$ or B_6-C-B-C-B_6 being ideally stable composition. Figure 1.3 illustrates that the B_4C can be present in various compositions per the B-C system. This range is between B_4C to $B_{10.5}C$ [16].

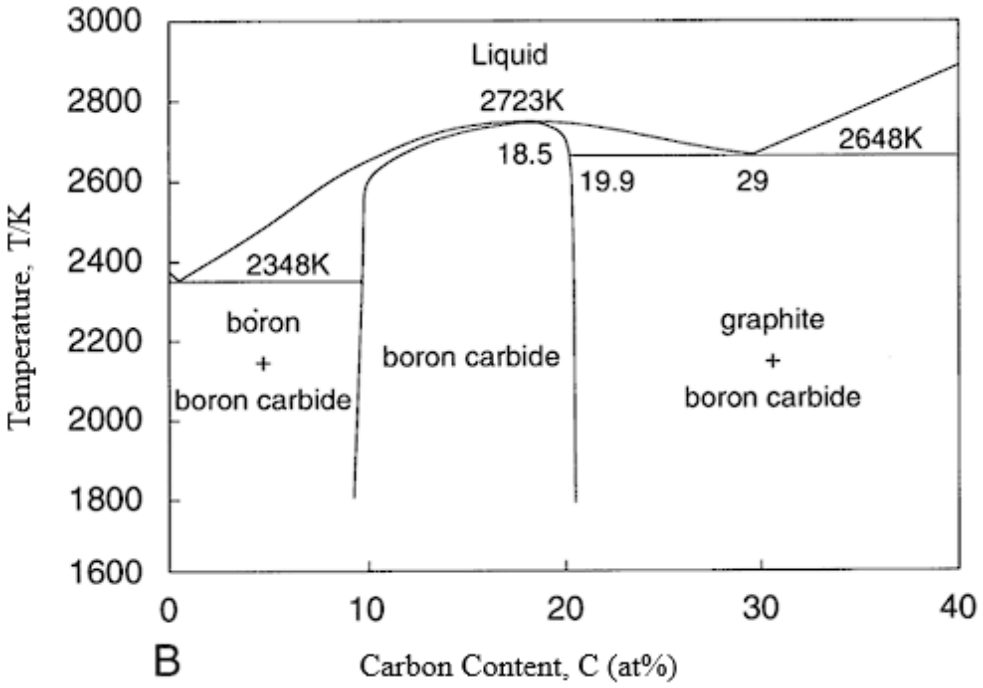

Figure 1.3. Phase diagram of B-C system.

Three-atom linear chains are present on the biggest diagonal of the rhombohedral unit cell (C-B-C). Each chain link is covalently connected to an atom of three distinct icosahedra [17]. Generally, icosahedra are composed of one carbon atom and eleven boron atoms. Carbon atom positions inside various icosahedra are not arranged relative to one another. Boron's lack of valence electrons leads to a predisposition to create three-center covalent bonds [18], resulting in the icosahedral structure. There are two crystallographically distinct locations in the icosahedron. Six atoms occupy polar triangles at opposing extremities of the icosahedron, whereas the remaining six atoms hold equatorial positions. The atoms at polar locations along

the cell borders are directly connected to adjacent icosahedra by strong two-center connections. The atoms at equatorial positions directly link to neighboring icosahedra via three-center bonds or form chain structures [18], [19]. A small percentage have a B_{12} structure or a $B_{10}C_2$ structure with two C atoms in antipodal polar sites, while the majority of icosahedra have a B11C structure with the C atom at a polar location [20].

B_4C has many polymorphs, with the energetically preferred B_4C structure having B11C icosahedra containing the C atom at a polar position and a C-B-C chain [16], [21], [22].

Because of these characteristics can be used in engineering for many purposes, such as high-pressure nozzles [23], neutron capture materials, abrasives, and personal body armor [24], [16], [25], [26].

Due to B_4C 's wear resistance and super hardness, it is suitable for different kinds of challenging utilizations. Specifically, wear-resistant coatings for ferrous materials have considerable potential. Due to its vastly superior chemical and thermal stability compared to a diamond and diamond-like carbon (DLC), B_4C should be significantly more appropriate [27].

Furthermore, boron carbide possesses numerous other unique qualities that make it suitable for different applications across various sectors. B_4C is appealing for thermoelectric energy generation [28] due to its good thermoelectric features, such as a comparatively high Seebeck coefficient or low thermal conductivity and a high melting point of 2450 C. B_4C is attractive for novel electronic applications as a high-temperature semiconductor due to its electrical characteristics [16]. Boron carbide with the isotope 10B is employed as a neutron absorber in nuclear applications, especially in nuclear power plants [3], [29]. B_4C is also an effective sintering aid for the increasing density of S-SiC ceramics [30], in addition to its detailed application areas in the aforementioned fields. Rapid growth has occurred in using boron carbide-reinforced aluminum matrix composites in key automotive, aerospace, nuclear engineering, and military applications [31].

B_4C ceramics and related compounds are being investigated as viable possibilities for tribological applications that require minimal friction and wear. B_4C ceramics have lower density and higher hardness than ZrO_2 ceramics, Al_2O_3 ceramics, Si_3N_4 ceramics, and SiC ceramics. Consequently, B_4C ceramics are more appropriate for rotatory tribological and moveable applications where weight reduction is critical. Boron Carbide ceramics are resistant to particle erosion and abrasion due to high hardness. B_4C can be employed as a wear-resistant material in both thin and bulk coating forms. Additionally, B_4C particles can be utilized in alloys as a reinforcing phase to increase their tribological characteristics [32]–[39].

Furthermore, due to its great hardness and low weight, boron carbide has been researched in light reinforcement applications, with improved characteristics than silicon and alumina carbide. Considering these materials' hardness, it is regarded as a perfect material for ballistic applications. However, some studies indicate that boron carbide is inefficient against numerous rounds in practice and shows low ballistic resistance in some scenarios, such as against bullets with a tungsten carbide core [40], [41]. This, combined with processing challenges such as the inability to sinter the material without the presence of dopants or high pressure, lack of plasticity, a high melting temperature, and a low diffusion coefficient, tends to make this material suitable for use in shields resistant to melee weapons and low weapon caliber [9].

1.2 Production of B_4C

A reaction including metal bodies happened in the 19th century, and a by-product known as Boron Carbide was identified. In 1933, early researchers produced B_4C with a purity of less than 75%. A researcher named Ridgway et al. [42] utilized the carbothermic process and produced 90% pure crystalline boron carbide. This section presents different methods for synthesizing boron carbide. [12] The B_4C synthesis methods are carbothermic reduction, self-propagation synthesis (SHS), synthesis

from elements, vapor phase reactions, synthesis from polymer precursors, liquid phase reactions, vapor-liquid-solid method (VLS growth), and mechanical alloying.

1.2.1 Carbothermic Reduction

Carbothermic reduction is the commercial method for producing B_4C. In this method, carbons of boron trioxide and boric acid are reduced. The following formula presented the carbothermic reduction reaction:

$$4H_3BO_3 + 7C = B_4C + 6CO + 6H_2O \quad (1)$$

Before this reaction, the following three crucial steps are carried out [43]:

$$4H_3BO_3 = 2B_22O_3 + 6H_2O \quad (2)$$

$$B_2O_3 + 3CO = 2B + 3CO_2 \quad (3)$$

$$4B + C = B_4C \quad (4)$$

When heated, boric acid transforms into B_2O_3. This transformation is possible because boric acid releases water. As shown in Figure 1.4 [45], above 1400 ℃, the elimination of B_2O_3 with carbon monoxide becomes thermodynamically viable. Typically, the furnace temperature is maintained at 2000 °C to increase the overall reaction rate. The process is extremely endothermic and requires 16.800 kJ per mole of B_4C [44].

Despite the presence of various kinds of furnaces in this process, they all do the same function. Similar to other procedures, there are different furnaces and high-temperature production methods. They all work the same and contain most of the disadvantages of the carbothermic method. The most important disadvantage is the degree of purity.

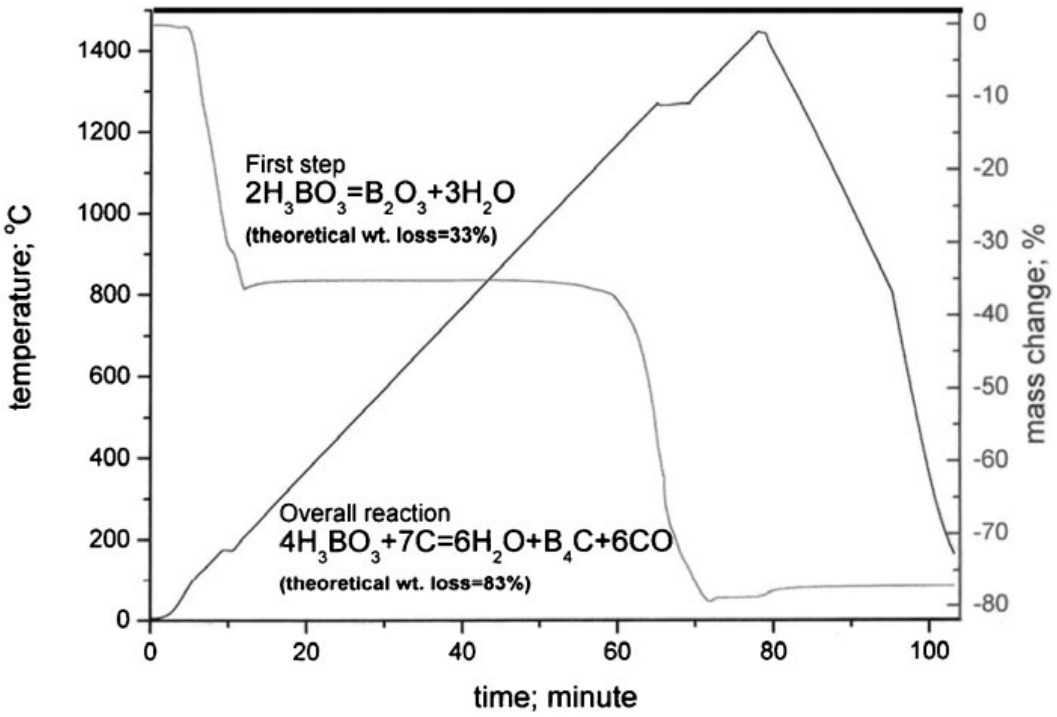

Figure 1.4. Thermogravimetric analysis plot: Boric acid's carbothermic reduction.

The boron carbide's production using carbothermal has primarily been a batch procedure. Tumanov [45] has reported developing a steady method for producing boron carbide by inductively heating a carbon black and boron oxide-based charge. Rafaniello [46] presented another improved reduction method in his patent. It describes the production of submicrometer-sized B_4C particles. Fine particles are the consequence of the kind of carbon employed, rapid heating rates (70–10.000 °C/min) and the manner of preparing the charge combination. Also, the impact of feed temperature and composition on the estimated product composition during the 1 mol B_2O_3 (l)'s carbothermic reduction is examined, as shown in Figure 1.5.

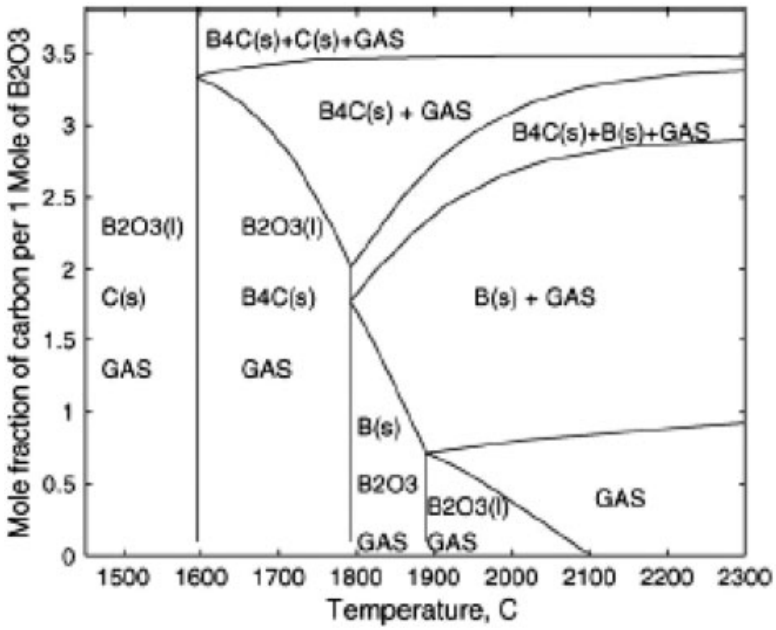

Figure 1.5. The impact of feed temperature and composition on the estimated product composition during one mol B_2O_3 (l)'s carbothermic reduction [47]

Boron carbide can also be formed from the elemental boron using the carbothermic process. Due to the high cost of elemental boron, the boron carbide's synthesis from its elements is deemed unviable, therefore, only used for specialized purposes [48], [49]. Owing to boron retention in the furnace and boron loss, a carbothermic reduction is unsuitable for the boosted boron carbide's synthesis; thus, this is the only economical way, but it results in low purity. Despite the fact that B_4C 's formation is thermodynamically feasible at room temperature using pure elements, the heat of the reaction 239 kJ/mol is insufficient for self-sustenance [50]. Formation of the B_4C layer tends to slow additional reaction because of reacting species' slow diffusion across this layer. Therefore, longer durations and higher temperatures are needed to complete the reactions. Carbon and boron are carefully mixed for elemental synthesis to generate a homogenous powder combination. After that, this powder is pelletized and reacts at around 1500°C in an inert environment or vacuum. The partially sintered boron carbide pellet is crushed and milled to get fine B_4C

powders. Typically, highly pure elemental boron powder generated by the merged salt electrolytic process is utilized to make B_4C of high purity [51], [52].

As can be seen from the preceding information, the manufacture of boron carbide using this approach requires a tremendous amount of energy. Despite its status as conventional practice, alternative ways have begun to gain prominence globally, with a greater emphasis on energy use in recent years.

1.2.2 Self-Propagating High-Temperature Synthesis (SHS)

Gray [53] patented the SHS process and described the manufacture of B_4C powders from alkaline $Na_2B_4O_7$ or B_2O_3's magnesiothermic reduction in the carbon presence at temperatures between 1650 and 1700 °C. It has been discovered that using metallic sulfates as a catalyst lowers the temperature of the reaction to 700°C [54]. The heat generated by a magnesiothermic reaction is adequate for a self-high temperature synthesis pathway. Zhang et al. [55] and Khanra et al. [54], [56] explored the use of (SHS) to produce fine B_4C powder from the C, H_3BO_3, and Mg powders. This mixture's activation temperature was determined to be 670 °C.

Though boron carbide has been produced by magnesiothermic reduction and used for applications defined by its high calorific value. However, because of this calorific value, the productions made by this method are uncontrolled. So with this method, it becomes impossible to get controlled and equal quality products every time.

1.2.3 Vapour Phase Reaction

Extensive research has been conducted on the B_4C's synthesis by performing a reaction between gaseous compounds of carbon and boron. This approach is advantageous; therefore, effectively utilized for the synthesis of submicron-sized whiskers and powders and thin B_4C coatings. Many boron halides are acceptable as

boron sources; for example, BI_3, BBr_3, and BCI_3 [60]. Nevertheless, due to the moderate cost and ease of availability, BCI_3 is the preferred option. In addition to boron halides, some boron sources are oxide (B_2O_3) and borane (B_6H_6). Moreover, some hydrocarbon gases are also utilized as sources of carbon. These hydrocarbon gases are carbon tetra chloride (CCl_4), C_2H_6, CH_4, C_2H_2, and C_2H_4. The B_4C is synthesized in the reaction jar. The reaction jar is maintained at the proper temperature, pressure, and atmosphere. Hydrogen is typically found in the atmosphere, where it reacts with halogens to generate hydrogen chloride according to the following reactions [60]:

$$4\mathrm{BCl_3} + \mathrm{C}Cl_4 + 8H_2 = B_4C + 16HCl \quad (5)$$

$$4\mathrm{BCl_3} + \mathrm{C} + 6H_2 = B_4C + 12HCl \quad (6)$$

$$4\mathrm{BCl_3} + \mathrm{C}H_4 + 4H_2 = B_4C + 12HCl \quad (7)$$

Bourdeau describes a similar setup for vapor phase reaction in his patent [61]. He described the method for manufacturing B_4C by reacting a boron halide in a vapor phase with hydrocarbon between 1500 and 2500 °C. Clifton et al. [62] described a method for manufacturing B_4C whiskers in the range of 0.05 to 0.25 mm. These B_4C whiskers are formed by reacting hydrocarbon gas with B_2O_3 vapors at temperatures between 700 °C to1600 °C. Cree et al. [63] have invented a method for manufacturing B_4C whiskers that utilizes catalytic components to boost the productivity of the gas phase reaction mechanism. Another method for producing B_4C powder with a surface area greater than 100 m^2g has been patented by MacKinnon et al. [64], who discovered that when CH_4–H_2 mixture is combined with BCl_3 in a radio frequency argon plasma, submicron powders of boron carbides with varying B/C ratios might be produced, where the resultant stoichiometry depends on the reactant components.

1.2.4 Synthesis From Polymer Precursors

As a low-temperature alternative to high-temperature reaction methods, there is significant effort towards utilizing polymer precursors to produce ceramic materials. Some boron-containing organic substances, such as triphenyl borane, carborane (C_2BnHnz_2), borazines, and polyvinyl pentaborane, are used to produce B_4C upon pyrolysis. Ordinarily, temperatures between 1000 and 1500 °C in an inert atmosphere are needed to perform this procedure. The method for producing unrestrictedly flowing B_4C powder using sugar and boric acid was described by a US patent "Method of producing boron carbide from water-alcohol solution of carbon source" [65]. The ethylene glycol-dissolved mixture was first air-dried at 180 °C and then reheated at 700 °C in hydrogen. This product is crushed and heated for 7 hours at 1700 °C to produce B_4C powder. Mondal and Banthia [66] reported a low-temperature synthesis approach in which an "amine-treated B_2O_3 fiber" is heated at 2000–2350 °C in an inert atmosphere. Cihangir et al. [67] have developed a process for synthesizing a precursor material which results and B_4C and B_4C/SiC composites when heated at a temperature between 1400 °C and 1600 °C. The method of creating precursor material is formed by the dehydration of sugar with sulfuric acid.

1.2.5 Liquid Phase Reaction

Attempts have been made to produce ultrafine B_4C powder utilizing liquid precursors by liquid phase reactivity. This technique is also known as the reduction technique or the solvothermal process. This one can be utilized at far lower temperatures to produce B_4C with the appropriate characteristics compared to many modern production routes. Shi et al. [68] have researched the synthesis of ultrafine boron carbide particles by the co-reduction of carbon tetrachloride and boron tribromide employing sodium as the reducing agent according to the reaction,

$$4\mathrm{BBr_3} + \mathrm{C}Cl_4 + 16\mathrm{Na} = B_4C + 4NaCl + 12NaBr \qquad (8)$$

An autoclave was used for performing this reaction at the temperature of 450°C. The resultant B_4C crystals were either rod-like with a diameter of 200 nm and a length of 2.5 mm or they are homogenous spherical particles with a diameter of 80 nm [68]. Gu et al. [69] discovered the production of nanocrystalline B_4C in an autoclave at 600 °C by solvothermal reduction of CCl_4 with Li during the amorphous boron powder with the presence of the following reaction,

$$4\mathrm{B} + \mathrm{CCl} + 4\mathrm{Li} = \mathrm{B}C + 4LiCl \qquad (9)$$

By reacting polyvinyl alcohol with boric acid, a polymeric precursor is produced, which, upon pyrolysis at temperatures between 400°C and 800 °C, yields crystalline boron carbide. Sinha et al. [70] have developed a method for producing a persistent gel from a solution of citric acid and boric acid in water. This gel is subsequently processed to produce a precursor. The precursor has yielded B_4C when heated to 1450 °C under a vacuum.

1.2.6 Vapour-Liquid-Solid (VLS) Growth

The carbothermal VLS growth method can be used to generate a B_4C whisker. This method includes the transit of gas-phase carbon and boron to a liquid catalyst metal (Co, Fe, or Ni) in which whisker components dissolve. B_4C whiskers emerge off the metal droplets when the catalyst gets fully saturated with carbon and boron. Carlsson et al. [71] produced platelets and boron carbide whiskers using this method. Carbon and boron were obtained from carbon black and B_2O_3, respectively. The addition of Co and NaCl facilitated the development of whiskers. The interaction of NaCI with B_2O_3 generates BCl, which, together with carbon, dissolves in liquid cobalt before precipitating as B_4C whiskers. Krishnarao et al. [72], [73] have investigated B_4C whisker formation by utilizing NiC_2 and K_2CO_3. $NiCl_2$ and K_2CO_3 are used as catalysts and low-melting liquids to promote B_4C platelet and whisker formation. B_4C nanowire formation by adding iron in a boron trioxide,

boron, and carbon mixture has been examined by Ma et al. [73]. The mixture is used as a precursor. This procedure caused a decrease in nanowire diameter from 50–200 nm to 10–30 nm.

1.2.7 Mechanical Alloying and Comparison of Production Routes

Mechanical Alloying (MA) is an effective and convenient technique for powder fabrication. The processing parameters affect the final composition of the product [74].

The process of MA begins with combining a specified amount of powders and loading the mixture into the chamber along with the grinding medium. After that, the mixture is milled for a definite duration until the constitution of each powder particle matches [60]. Occasionally, the powder is ground either to attain certain qualities or to generate metastable phases. The resultant powder is then compacted into a bulk form and subjected to heat treatment to create the desired characteristics and microstructure. The MA raw materials are generally accessible in the form of commercially pure powders. Particle sizes as small as 200 μm can be typically reached by MA [75].

Various explanations of mechanical alloying mechanisms have been offered [14], [19]. One of the theories focuses on thermal effects and states that heat generated by the friction and impact of granules with the grinding medium and with one another is responsible for the chemical processes' activation [15]. The second theory is based on dislocations and suggests that the activation happens at the cost of the energy for the dislocations leaving particle surfaces due to the plastic deformation upon milling [16], [76]. Numerous processes, including emission of charged particles such as electrons, luminescence, 'evaporation' of crystalline components, and the emergence of electric charges on the surface, contribute to developing the 'deformation' concept. The third theory states that activation of the chemical processes is linked to the development of a transient active center and the 'trip-out' of durable energy upon solid distraction [76]–[80].

Recently, mechanochemistry has become a prominent production method for a number of products. Numerous types of refractory compounds, master alloys, pure metals, and pre-alloyed powders are produced by MA have been offered. The production of B_4C in mechanochemistry is also feasible through mechanical alloying [81].

In synthesizing B_4C by MA, extended planetary milling at room temperature is utilized to activate the powder particles. After that, the alloyed mixture is subsequently annealed to produce B_4C. The magnesiothermic reduction of submicron boron carbide particles has also been accomplished through mechanical alloying [58]. There are limited examples of boron carbide production via the mechanochemical synthesis in the scientific literature.

Wang et al. [59] have investigated the production of boron carbide fiber–MgO composite materials by burning B_2O_3, Mg, and C in the fiber form in an argon-filled jar. The pressure of the surrounding argon gas affects the proportion of the conversion since it dictates the level of Mg's evaporation and, by extension, the degree of conversion and burning temperature. Calcium can also be employed in place of Mg as a reductant. Recently, Berchman et al. [82] reported the fabrication of B_4C powder by calciothermic reduction of B_2O_3 or borax ($Na_2B_4O_7$) in carbon's presence at 1000 °C under an argon atmosphere.

According to the research of F. Deng et al. [58], submicron boron carbide particles are formed after 72 hours of milling with raw materials B_2O_3, Mg, and C. The parameters of this process are the ball mill's RPM which was 200 RPM, whereas the containers' RPM along their axis was 400 RPM. The balls are made of steel, and their diameter is 19 mm. The BPR is approximately 5:1. The load consisted of graphite, boron oxide, and magnesium with particles smaller than 3 mm. Each container comprised 66 grams of the powder mixture, and the bulk ratio of B_2O_3:C:Mg was 10:1:11 [58].

Another research conducted by Sharifi et al. revealed that the production of MgO-B_4C composite is done after 80 hours of grinding the B_2O_2-Mg-C system. At

room temperature, the powder mixture was milled in a planetary ball mill with 20 mm hardened carbon steel balls and 250 RPM, 10:1 BPR ratio. Mechanochemically produced boron carbide particles could be observed after the leaching operation [83].

Mohammad Javad Nasr Isfahani et al. also conducted another study in which boron carbide particles can be produced at room temperature by utilizing a high-energy planetary ball grind. The rotational speed of the vial and ball-to-powder rotation was 700 RPM and 15:1, respectively. The 10-hour-milled sample was excreted in 1M HCl at 80 ℃ for one hour, and based on the findings, boron carbide particles are readily visible [84].

Based on the three studies mentioned above, it is possible to say that the production of B_4C by mechanochemical milling with different process parameters is possible. The same powder that can be produced at lower speeds in 70 hours using conventional attritor mills can be produced in 10 hours using a planetary ball mill. The BPR used in 3 different studies is 5:1, 10:1, and 15:1. In this case, although different BPR ratios are used, it is seen that the production operations are completed without a major difference. In fact, increasing or decreasing some parameters indirectly affects other parameters. In the case of correct proportioning, it is always possible to obtain a quality product.

The product quality by different methods is summarized and compared in Table 1.1. This table gives the boron carbide synthesis parameters and summary results with several different production methods using some reactants. Different results are obtained in different methods, but since the free carbon ratio is undesirable, it can be deduced that the most successful result is obtained with SHS and mechanical alloying. Mechanical alloying stands out among others because it can produce the smallest powder size with lower energy input.

An overall comparison of the production methods can be found in Table 1.2. It can be seen in this that high temperatures are required in many manufacturing methods of B_4C. Although the methods that require high temperatures have become traditional, using methods in which low temperature is sufficient is becoming critical

with every passing day. Furthermore, some manufacturing methods have highly complex steps, such as vapor phase reactions, liquid phase reactions, and VLS growth. On the other hand, even though it is possible to develop a product with excellent purity and small particle size using mechanochemical alloying. There are only two main production stages in mechanical alloying. Therefore, mechanical alloying has the advantages of low energy requirements, high product purity, and small particle size over other techniques for the fabrication of sophisticated materials to be used in qualified industries [53], [57], [85].

Table 1.1. Process type, parameters, and final quality of some production methods.

No	Reactants	Process type	Process parameters	Quality of B_4C	Ref.
1	$B_2O_3 + Mg + C$	Tubular furnace	950-1200°C, H_2	Fine powder	[93]
2	$B_2O_3 + Mg + C$	SHS	…	Fine powder 98% pure	[96]
3	$B_2O_3 + Mg + C$	Batch	700°C, Ar, 1 h catalyst: K_2SO_4	Boron: 74.6% carbon: 25.2%	[95]
4	$B_2O_3 + Mg + C$	Mechanical alloying	Rotation speed ratio: 200 rev min^{-1} Ball to load ratio: 5:1 72 h	Submicrometre particles	[88]
5	$B_2O_3 + Mg + C_{fibre}$	Combustion synthesis	Ar	B_4C fibre + MgO composites	[99]
6	$H_3BO_3 + Mg + C$	SHS	670°C, Ar,	8-24 μm size, 8% free carbon	[97]
7	$Na_2B_4O_7 + Mg + C$	Continuous	1650-1700°C, H_2	Powder boron: 77.5% carbon: 21.3%	[94]

Table 1.2. Comparison of advantages and disadvantages table of B_4C production methods.

Production Method	Advantages	Disadvantages	Reference
Carbothermic Reduction	Information is easily accessible, the most common method	Energy consumption (up to 2400°C)	[69], [83]
Self-Propagation Synthesis (SHS)	Fast and low investment cost	Difficult to control process parameters	[54]-[59]
Vapour Phase Reaction	Good for whisker particles	High rates of uncontrolled reactions, long time required	[60]-[64]
Synthesis from Polymer Precursor	Organic compound usage	Relatively high-temperature synthesis (up to 1500°C)	[67]
Liquid Phase Reaction	Fine particle size (nearly 15 nm)	Contain so many steps, complicated production	[68], [69], [70]
Vapour Liquid Solid (VLS) Growth	Fine particles can be produced up to 10 nm	Not suitable for bulk production	[71], [72], [73]
Mechanical Alloying	Room temperature synthesis, low energy consumption, consistent product quality	Because of high amount of by-products acid leaching required	[74], [85]

To compare in general, a very important part of the amount of boron carbide, which is the most well-known, easy-to-apply and traditional production method, is currently produced by carbothermic production methods. As stated in Table 1.2, this

method can be performed at temperatures of 2000 °C and above. Today, less energy-consuming and more environmentally sustainable methods gain importance, especially when problems such as climate change and global warming are considered. Mechanochemical synthesis is powered only by a simple electric motor in the system. The same amount of boron carbide can be produced with almost 15 times less energy consumption by mechanochemical synthesis. To give a more detailed example, energy costs come to the forefront when comparing mechanochemical alloying and the traditional production method, the carbothermic method. Cost comparisons were made for the two methods. For the carbothermic method, a furnace with an energy consumption of 10 kWh for 8 hours of production at 2200 ℃ will consume approximately 80 kWh. In this case, the energy consumption value for boron carbide produced is 11.09 $. However, in order to produce similar amounts of B_4C in mechanochemical alloying, approximately 450 RPM and 8 hours of milling time were taken into consideration. The energy consumption value of the device in this condition is 600 W. The total energy consumed is 2.8 kWh. The energy consumption for this amount is 0.66 $. While performing the calculations, January 2023 Turkey energy unit price was used. With the help of calculations, mechanochemical alloying consumes 16 times lower energy consumption than the traditional production method of carbothermic reduction.

The disadvantage of this method is the formation of a high amount of by-products. However, for bulk productions in carbothermic methods that are compared with each other, the particle size reduction is carried out with jaw crushers or industrial crushers, causing additional energy consumption and contamination of the final product with impurities originating from the crusher material. However, when the main goal is to obtain a product with a small particle size with the mechanochemical operation, it is possible to produce 1 micron and below without any additional operations. In contrast, carbothermic methods can only yield similar particle sizes by adding a third stage of mechanical milling.

Considering all these factors, starting from raw material preparations, this study aimed to gain know-how about critical points such as milling parameters, acid leaching parameters, and powders' drying conditions.

1.3 Mechanochemical Synthesis

In 1989, it was reported for the first time that MA could be employed to generate a range of solid-solid and even liquid-solid reactions [86], [87]. It was shown that ball milling CuO with a bit more reactive metal, such as Ca, at room temperature could convert CuO into pure Cu metal. The development of β'-brass is possible by grinding ZnO and CuO together [87]. However, the use of such chemical reactions was witnessed in 1894. In that era, mechanical energy was converted into chemical energy to cause more chemical reactions [88]. This conversion has been reported in the literature as mechanochemical synthesis or mechanochemical synthesis. The majority of the mechanochemical synthesis reactions investigated were displaced reactions of the type:

$$\mathrm{MO} + \mathrm{R} = \mathrm{M} + RO \qquad (11)$$

MO represents metal oxide and is converted to pure metal (M) by utilizing a more reactive metal which is a reductant, R [89] [90].

Due to the mechanical reaction characteristics of having free negative energy change at a large scale, these are possible at ambient temperature. The existence of these processes at room temperature is thereby restricted solely by kinetic considerations [91].

The formation of product stage(s) at the surfaces of the reactants is a property shared by all solid-state processes. Subsequent expansion of the bulk solution entails diffusing atoms from the reactant phases into the product phase, forming a barrier layer that prevents additional reaction. As a result, greater temperatures are required for these interactions to happen at an appropriate rate [92].

Mechanical alloying has the potential to accelerate the rate of reduction reactions significantly [93] because repeated fracturing and welding of powder particles increase the contact area between reactant granules owing to particle size reduction and enable new surfaces to interact with each other repeatedly. This allows the reaction to proceed without the need for dispersion through the product layer. Furthermore, the fusion distance is reduced due to the fibrous structure. All of these decrease the temperature required for chemical activation [94].

Two fundamentally distinct reaction mechanisms are feasible based on the grinding conditions [94], [95]:

1. A self-propagating combustion process can be launched if the reaction enthalpy is reasonably high.
2. The interaction may expand to the least volume during each contact, resulting in a slow transformation.

The first mechanism necessitates a critical time for grinding to initiate the reaction. The temperature of the vial increases gradually. Also, reaction temperature the increase in the temperature can be used to mark the chemical reaction initiation [96]. According to Aning et al. [97], the temperature starts to increase rapidly after some time which indicates the start of ignition. The temperature difference with time throughout the grinding process is depicted schematically in Figure 1.6. One of the points worth noting is that during the grinding process, only the refinement of particles takes place until the burning reaction initiates. [97].

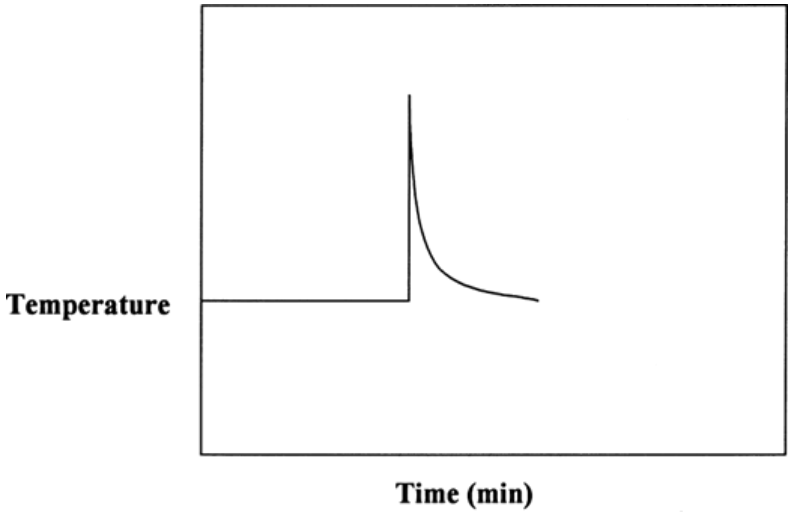

Figure 1.6. The differences in temperature of the grinding vial during MA at the time of the burning reaction [97].

Powders' mechanical deformation causes the development of crystal defects. Additionally, the balance between fracturing operations and cold welding among parts of powder is anticipated to cause an effect on the powder's structural changes. An important factor is the powder's temperature during grinding. The final product's nature can also be identified by the temperature of the powder during grinding. This temperature is based on the balls' kinetic energy. The processes which result in recrystallization and recovery mechanism are caused by the high atomic mobility (higher diffusivity) associated with the increase in the temperature. In this situation, a compound such as intermetallic would form. Nevertheless, in the case of low temperature, the defect recovery would be less, and a nanocrystalline or amorphous would form [98].

Moreover, the system can become overloaded because of energy caused by the MA mechanism. The system's temperature increases despite a stable rate of energy accumulation. There can be two distinctive reasons that might cause the temperature to rise. The first reason is the milling medium's kinetic energy. The second reason for high temperatures is exothermic processes that usually occur during grinding. Nevertheless, in practice, these two reasons combined become the

prime factors of the increased temperature of grinding containers or powder. In addition, the temperature of powders or grinding containers can be increased intentionally [98].

In a few cases, thermocouples have been utilized to measure the macroscopic temperature of the powder or the vial. Koch et al. [99] studied the temperature effects of attritor-type ball mills (Table 1.3). During the experiment, the highest measured temperature of the container with no balls was 40±428C° [99]. On the other hand, the experiment with the SPEX mill with 13 balls was surprising because the temperature rise was approximately 50°C only. Therefore, it can be drawn from this information that the temperature rise is because of bearings and motors. Some researchers have presented temperature rise at a large scale. Table 1.3 shows that the most commonly recorded temperatures range between 100°C and 120°C while the maximum reported temperature is almost 215°C. Although the microscopic, i.e., local, the temperature can rise exponentially and frequently exceed the melting points of some metals used in this process, it is worth noticing that the noted temperature rise is macroscopic [99]. Although SPEX and planetary-type ball mills realize more energy input in a short time, the temperature increase is expected to be at least at the level of attritor-type mills. However, in the measurements taken as a result of the studies, the temperature increase does not occur as expected in both SPEX and planetary varieties. This allows the production to be completed without any deterioration in the structure of the materials or the disadvantages of temperature rise.

The nature of the milling process is dynamic, which causes problems in measuring the microscopic temperature. Nevertheless, Maurice and Courtney [100], Davis et al. [101], Bhattacharya and Arzt [102], Magini et al. [103], and Schwarz and Koch [104] have proposed models that can be used to measure the local temperature.

In addition, the factors that cause temperature increase are the type of mill, not the material used or the ball size. At the same time, crystal and microstructural

changes can cause this temperature increase. Observing crystal structure and microstructural changes (indirect inferences) during the grinding process can help estimate the temperature rise. For instance, a quenched Fe−1.2wt%C steel's tempering reactivity was investigated by Davis et al. [101] during mechanical alloying. Additionally, according to Table 1.3, the maximum estimated temperature rise during the grinding process was almost 300°C [101]. In another study, the estimated rise of microscopic temperature was approximately 570°C minimum which is revealed by noticing the formation of high-temperature orthorhombic Sb_20_3 due to the oxidation of antimony metal and the grinding or Ga-Sb or Sb alloys [105], [106].

Table 1.3. Rise in Temperature during MA [107].

Alloy system	Type of mill	Temperature rise (°C)	Reference
Measured			
-	SPEX 8000	50	[203]
Al−Cr	Conventional ball mill	90	[204]
Al−Mg	SPEX 8000	120	[205]
Al−Mg	Attritor	125	[206]
Co−Fe−Si−B	Vibrational ball mill	100	[207]
Cr−Cu	Vibrational ball mill	100	[208]
Fe−Al	Fritsch Pulverisette 5	80	[103]
Ni-base superalloy	Attritor	< 100−215	[209]
Ni−Ti	High-speed ball mill	172	[172]
Ni−Zr	SPEX 8000	180	[204]
Estimated			
Al−Cu−Mn	Fritsch Pulverisette 5	590	[217]
Fe−1.2wt%C	SPEX 8000	300	[188]
Ni−Al	Planetary ball mill	220	[218]
Ni−Zr	SPEX 8000	180	[210]
Sb or Sb−Ge	Centrifugal ball mill	> 570	[92,214]
7-AlOOH or $Al(OH)_3$	Fritsch Pulverisette 7	> 1000	[215,216]

1.4 Mechanism of Alloying

The chemical reaction between solids capable of interacting is due to thermodynamic considerations. There are two constraints of thermodynamic considerations; the first is to carry the solids together at the acting range of interatomic influences, and the second is to infuse to the atoms sufficient excess energy for the redistribution of electron density, which results in a chemical transformation. The accomplishment of the first constraint is not as complex as the second one. The transmitted average energy density to the matter is much less than the interatomic bond energy. Consequently, some methods of the former at local sites are of sufficient magnitude for the achievement of the second constraint to take precedence [75].

The powder particles are cold-welded, flattened, rewelded, and repeatedly fractured in high-energy grinding. Some of the energy is trapped between two steel balls when they collide. Usually, approximately 1000 particles are trapped when a collision occurs (Figure 1.7), and the weight of these 1000 particles is 0.2 mg. The impact force changes the shape of powder particles plastically, resulting in fracturing and work hardening. The newly formed surfaces allow particles to fuse, causing a larger size of particles. Due to the softness of the particles in the early phases of milling, they tend to fuse and form big particles. Some of the resulting particles are up to three times the size of the initial particles. At this stage, the synthesized particles have a layered structure comprised of numerous permutations of the initial elements. With continuous deformation, particles become shattered and work-hardened through the fragmentation of fragile flakes and a fatigue failure mechanism. Due to the absence of substantial aggregated forces, fragments produced by this method may continue to decrease in size. At this point, fracture propensity occurs predominantly over cold welding. Also, the number of layers in a particle increases and the distance between layers decreases. However, the particle size reduction efficiency is about 0.1% in traditional ball mills. On the contrary, the efficiency can be increased in the high-energy ball milling method, although it

remains less than 1%. The reason is that most of the energy is lost by transforming into heat, although a minor portion is also employed in the plastic and elastic bending of the particles of powders [108].

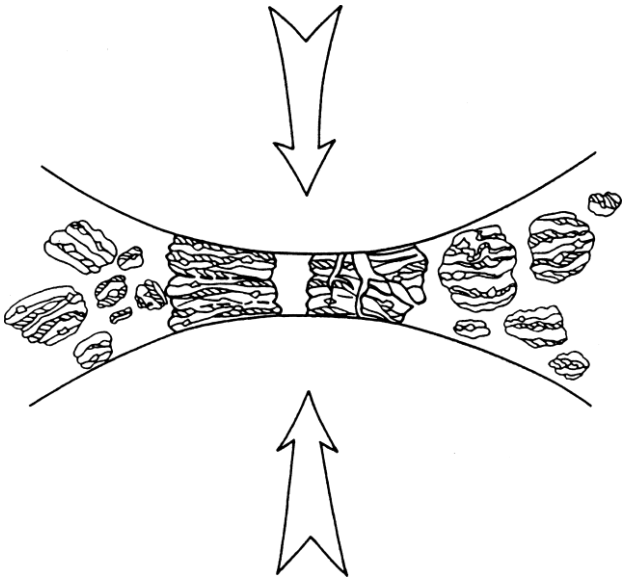

Figure 1.7. Powder mixture collision between powder and ball during mechanical alloying (MA) [108].

The equilibrium state is reached when the fracturing and welding rates are balanced. This stable equilibrium state is usually attained by grinding for a specific time. The fracturing reduces the average synthesized size of the particle, while the welding rate aims to increase the average size of the particle. The smaller size of particles may tolerate compression without shattering and are likely to weld into larger pieces, with a strong pattern to drive both very large and small particles toward an average size [109]. At this point, all the particles consist of the ingredients used initially. The proportion of the ingredients is similar to the amount in which they were blended. The aggregation of strain energy causes saturation hardness of particles. At this phase, the distribution of particle sizes is relatively narrow since particles that are larger than average are being broken down into smaller fragments

at the same rate as fragments that are smaller than average are growing through agglomeration of smaller particles, as shown in Figure 1.8 [110].

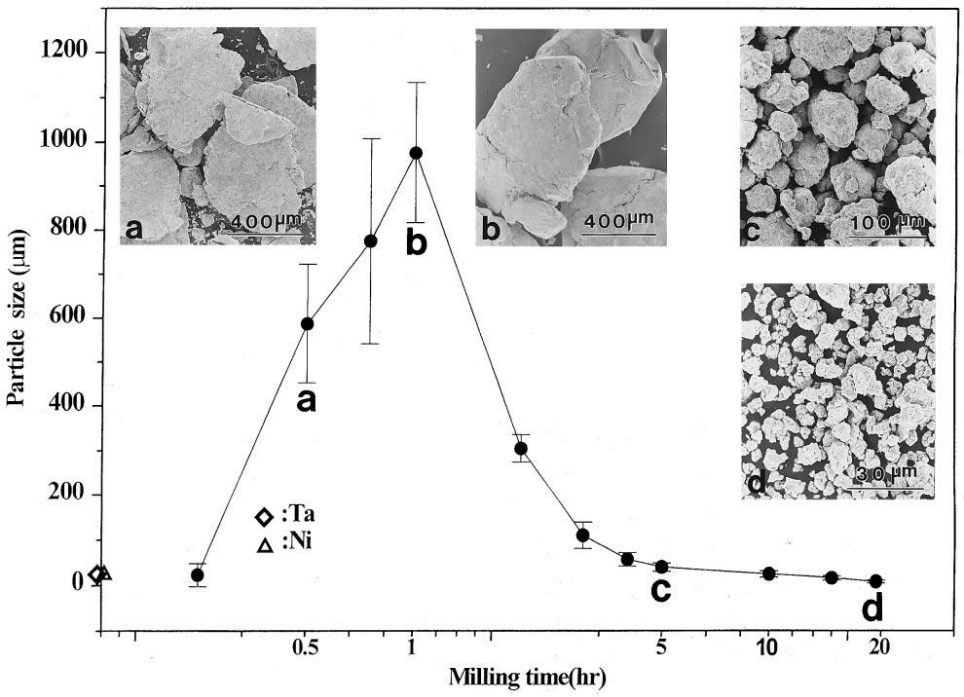

Figure 1.8. Distribution of narrow particle size distribution due to the tendency of small particles to weld together and large particles to fracture under steady-state conditions [110].

Typically, it is understood that particles are deformed during mechanical alloying. Increased density of crystal defects such as vacancies, particle boundaries, dislocations, and stacking faults manifest the deformation. Structural defects increase the diffusivity of the elements into the matrix. Moreover, the decrease in diffusion distances occurred because of clarified microstructural characteristics. In addition, during the grinding process, the temperature rise (even the slightest) increases the rate of diffusion, which results in the constituent element alloying [98].

The particular timeframes necessary to build a certain structure in any mechanism would depend on the properties of the ingredients, the initial size of the particle, the

equipment, and operating parameters. In the majority of instances, however, the degree of refinements of the structure, such as crystallite size, particle size, and lamellar spacing, is nearly logarithmic with time, and hence the initial particle size is rather insignificant. The crystallite size is reduced to nanometer level within a few minutes to one hour. MA has been widely used to generate nanocrystalline materials [111], [112] due, in part, to the efficiency by which nanoparticles can be manufactured. Studies have revealed that the refinement rate increment is related to the BPR, as shown in Figure 1.9 [153], [154], [155], [113], [114].

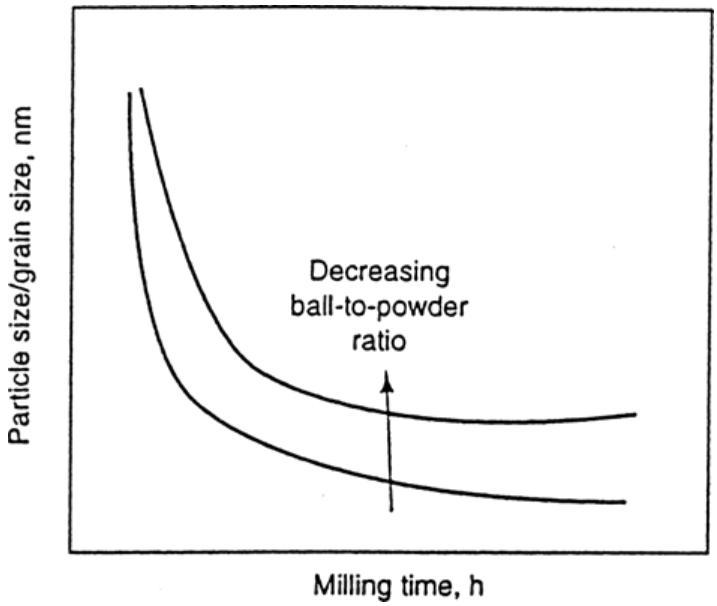

Figure 1.9. Grinding time with relation to particle refinement and grain sizes.

1.5 Mechanochemical Synthesis Parameters

Mechanical Alloying (MA) is a complicated method, and it requires the optimization of a variety of factors in order to attain the desired microstructure and product phase. The factors that affect the final powder's content are mill type, milling container, speed of operation, time of milling, size distribution and type of milling

medium, the weight ratio of BPR, filling volume of the container, and atmosphere of grinding.

The factors mentioned above depend on one another. For instance, the optimal milling duration depends on the size of the milling medium, the mill's type, the ball-to-powder ratio, the milling temperature, and other variables. When the copper oxide is reduced by iron, for instance, a combustion reaction may be triggered; nevertheless, the same reaction advances gradually under minorly modified milling conditions. Therefore, findings from different studies may only be properly compared if the precise settings in which the reactions take place are disclosed. It is necessary to optimize these conditions for the finest products [108].

1.5.1 Mill Type

Mills are often classified into three fundamental groups. These grinders vary in operation speed, capacity, and capability to regulate the process by altering the degree to which they minimize powder contamination and the grinding temperature. A mill can be selected based on the powder quantity, powder type, and final product consistency.

Various kinds of elevated energy milling equipment are employed to generate powders that have been mechanically alloyed. They vary in milling efficiency, capacity, and supplementary heating and cooling arrangements [108]. Below a brief description of the different high-energy milling types is presented.

1.5.1.1 Shaker Mills

Shaker mills are the most commonly used type of mill for industrial production of scientific studies as well as laboratory studies. One example of shaker mills is SPEX mills (see Figure 1.10 (a). Shaker mills grind 10-20 grams of powder

at a time. The most frequently employed type of this mill has only one vial with grinding balls and the sample. Grinding balls are found in the mill's clamp. These balls swing back and forth thousand times per minute. The back-and-forth rattling motion is joined with lateral motions of the vial's ends, giving the impression that the vial is moving in the shape of an infinity sign or a Figure 8. Each time the vial is swung, the balls strike the end of the vial and sample, resulting in mixing and milling the sample. Due to the speed (approximately 1200 RPM) and amplitude (about 5 cm) of the clamp action, the velocities of balls are significant (on the order of 5 m/s), and as a result, the impact force of the ball is notably high. Consequently, these mills are of the high energy type [108].

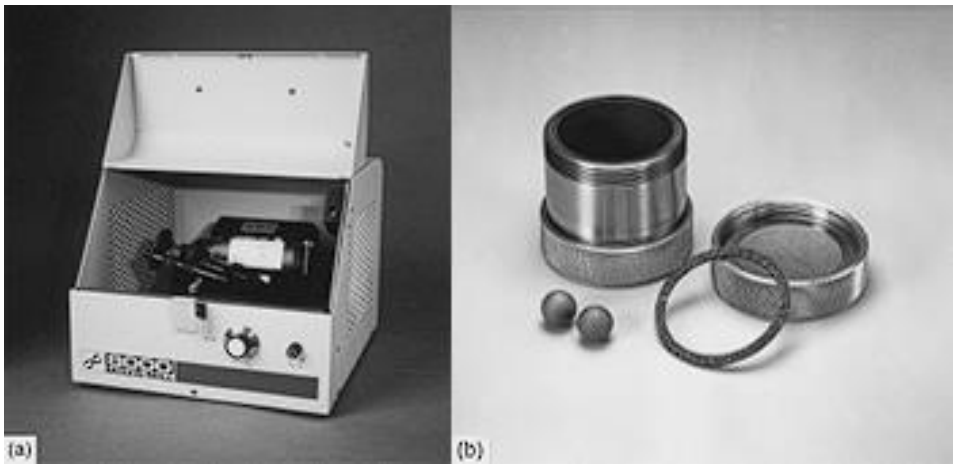

Figure 1.10. SPEX 8000 mixer mill. (b) Tungsten carbide vial set consisting of the lid, vial, balls, and gasket. Courtesy of SPEX CertiPrep, Metuchen, NJ.

1.5.1.2 Planetary Ball Mills

Planetary Ball mills, an example of which is shown in Figure 1.11, are commonly used grinders for conducting mechanical alloying experiments. In this mill, more powder can be ground at a time as compared to the shaker mill. The amount of powder can be a few hundred grams. This mill takes its name from its

vial’s movement, like planets in their orbital. A specific driving mechanism enables these to revolve around their axes as they are stacked on a spinning support disk. Both the centrifugal force generated by the spinning support disk operates on the vial contents and the vials rotating around their axis, composed of the grinding balls and the substance to be ground. As the supporting disk and vials revolve differently, centrifugal forces apply successively in two dimensions. The friction impact is then followed by ‘to be ground material' and the grinding milling balls detaching off and flowing freely through the insider vial' and striking with the opposite inner wall, known as the impact effect.

In older models, the rotational speeds of the vial and the disk could not be regulated individually. However, this is now feasible in the modern versions of planetary ball mills. There could be either 2 or 4 milling sites in a single mill. Eight distinct grinding ball and vial materials are available: Cr-Ni or Cr steel, agate, plastic polyamide, silicon nitride, zirconia, tungsten carbide, and sintered corundum. Although the linear velocity of the balls in the planetary ball mill is greater than that of a SPEX mill, the recurrence of impacts is significantly greater in the SPEX mills [108].

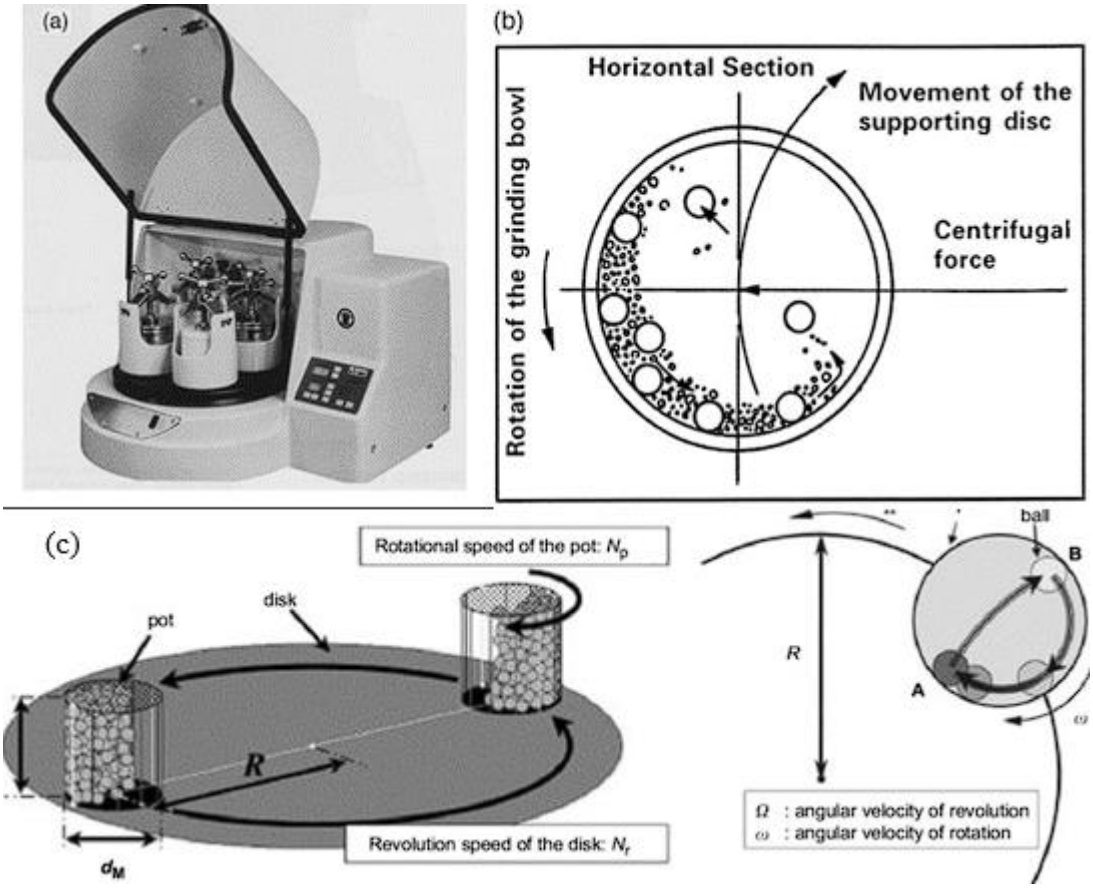

Figure 1.11. (a) Fritsch Pulverisette P-5 4 station ball mill. (b) Diagram illustrating the ball moves within a ball mill. (c) Planetary ball mill angular velocity explanations. Courtesy of Gilson Company, Inc., Worthington, OH.

1.5.1.3 Attritor Mills

The traditional grinder is made up of a spinning horizontal drum. This drum is partially filled with small steel balls. The rotation of the drum makes balls fall on the powder, which will be ground. In this way, it can be said that the grinding speed depends on the rotation of the drum. The gravity force is exceeded by the centrifugal force, which acts on steel balls when the speed of rotation increases; therefore, the balls are placed on the drum walls. After this, the process of grinding stops. The attritor mill is composed of a vertical drum with impellers. This ball mill has the

ability to generate higher energies as compared to other types of grinding mills. The impellers are gradually set to right angles to one another; hence, the ball charges are stimulated. The stimulated balls cause a reduction of powder size due to impact/effect between the container and wall, between balls, and among agitator shaft, balls, and impellers. Nevertheless, sometimes, powder size reduction occurs due to the collisions of the particles and ball sliding. The rotation of the impellers takes place because of the powerful motor resulting in the agitation of the balls present in the drum. The attritors can grind powder in large quantities at a time, such as 0.5 kg to 40 kg as shown in Figure 1.12. (a) [108]. Also, a comparison of the milling type required to reach similar particle sizes in a planetary ball mill and attritor mill can be seen in Figure 1.13 for TiB_2 powders [60].

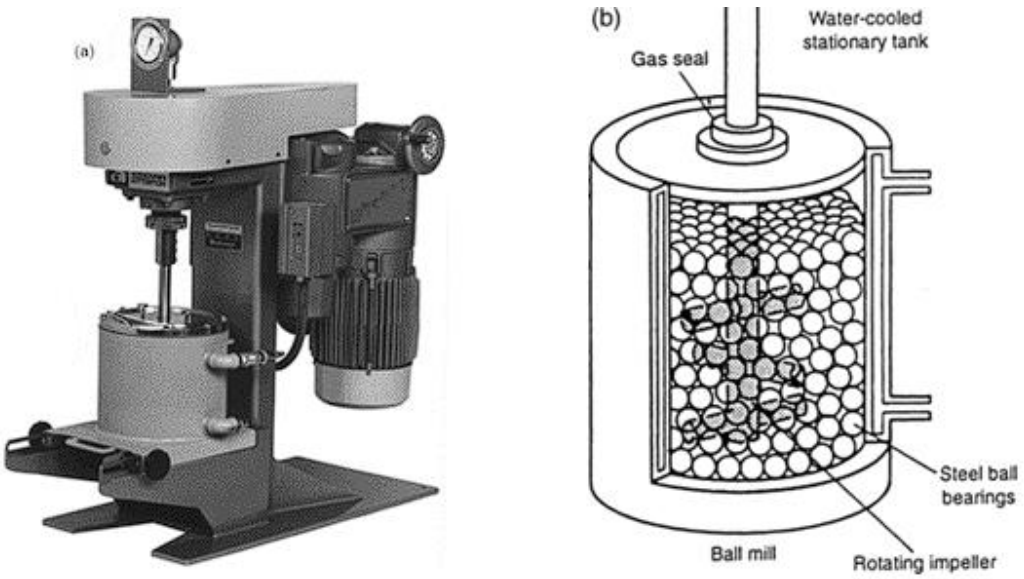

Figure 1.12. (a) Model 1-S attritor. (b) Configuration of spinning arms on a shaft within an attrition ball mill. Courtesy of Union Process, Akron, OH [108].

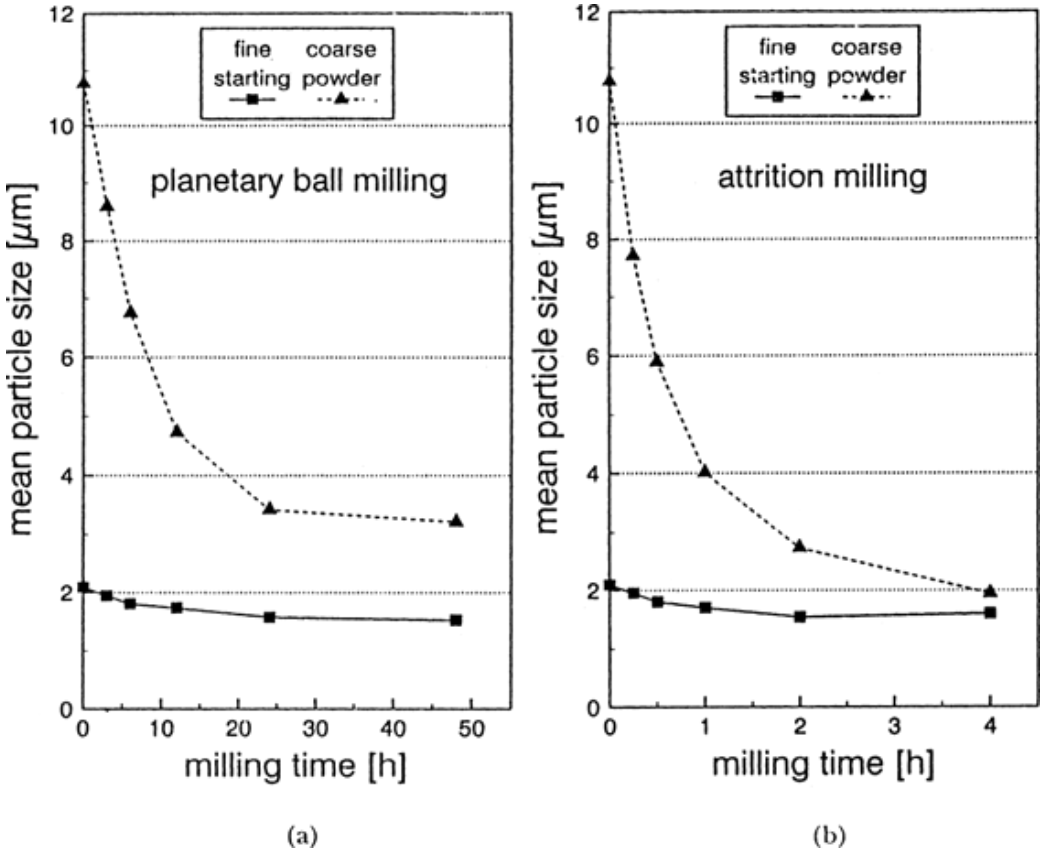

Figure 1.13. Grinding of TiB_2 powder to achieve comparable particle sizes in (a) planetary ball mill and (b) attritor [108].

According to Table 1.4, which compares different mills, attritor mills have the highest capacity, but these mills can be used only for basic mechanochemical operations or some high amount of grinding operations like more than 1 kg of powder. When compared according to mechanical impact effect and volume comparison, planetary ball mills appear as the best choice.

Table 1.4. Conventional capacities of various kinds of mills.

Typical capacities of the different types of mills	
Mill type	Sample weight
Mixer mills	Up to 2 x 20 g
Planetary mills	Up to 4 x 250 g
Attritors	0.5−100 kg
Uni-ball mill	Up to 4 x 2000 g

The planetary ball and mixer mills are preferred due to their ability to accommodate greater energy loads. However, when both of these mills are compared, the planetary ball mills are more beneficial for MA as a great amount of powder can be contained in them [115], which enables the mills to make an even large portion of the production of powder during the subsequent production stages. Another advantage of a planetary ball mill over a mixer mill is that the chamber's huge size affords the possibility of carrying out a rapid response with increased BPR rates [108].

1.5.2 Milling Container and Material

The grinding container is also known as vial, bowl, jar, chamber, or grinding vessel. The container's material is critical due to the effects the container's inner walls receive from the milling medium. The material of the container vessel is sometimes displaced and mixed with the powder, which can modify the powder by contaminating it. It is worth noting that the powder will only be contaminated if the vial's material is different from the powder's material. Alternatively, if the material of the container and powder is the same, the chemistry will be modified unless appropriate precautions are considered to make amendments for the additionally mixed material in the substance being ground. Some of the most commonly used materials for vials are bearing steel, hardened chromium steel, hardened steel, stainless steel, WC-lined steel [116], tool steel, WC-Co, and tempered steel.

However, some particular materials are utilized for specific objectives. Special chamber selections are made according to the materials that are desired or undesirable to react. In addition, special designs can be made for substances that are not required to be mixed with the final product. For example, the specific materials used are yttria-stabilized zirconia (YSZ) [117], sintered corundum, titanium [118], sapphire [119], [120], Cu−Be [121]–[125], copper [126], hard porcelain, Si_3N_4 partially stabilized zirconia+yttria [127], [128], and agate [105], [129], [130].

Moreover, the container's shape is also significant, particularly regarding the vial's inner design. Both types of SPEX mill jars are employed, such as round ended and flat-ended. Studies showed that the rate of alloying was much higher in the vial with a flat end than in the vessel with a round end [131]. For example, the Si-Ge mixture was needed to be ground for 15 hours in the vial with a round end so that the indicator peak of the desired phase could be reached to a constant intensity in X-ray diffraction pattern, while for the same result and mixture, this time was 9 hours in the vial with a flat end [60].

1.5.3 Milling Speed

The milling speed is also important because the energy incorporated into the powder depends on the rotation. However, the milling speed cannot be increased exponentially due to the limitations of the different designs of the containers. For instance, the greater rotation speed will result in a high-speed movement of the balls in a traditional mill. When the speed of the balls exceeds the critical speed, the balls are stuck with the vial's inner walls; therefore, they do not fall on the powder being ground with impact force. Hence, the rotation speed of balls should be below the critical value. This way, balls will fall on the material being ground from a reasonable height, producing optimum impact energy [108].

A further restriction on the higher speed is high velocities (or milling intensities) generating high vial temperature. This may be useful when diffusion is needed to boost powder homogeneity and alloying. In certain instances, however,

this elevated temperature may be detrimental since it intensifies the transformation process and causes the dissolution of supersaturated solutions or other metastable stages generated during grinding [132]. In addition, the powder may be contaminated due to high temperatures. During the development of nanocrystals, it has been investigated that the internal strain and size of crystals are decreased and increased, respectively, by high velocities due to improved dynamical recrystallization [133].

It has been demonstrated by Calka et al. [134] that the resultant powder's constituents are different when carbon and vanadium powders are ground together by employing different levels of energy. The different energy levels are generated by adjusting the positions of the magnets present in the unit ball mill. VC was observed to form at high velocities during grinding, whereas, at a low speed, a powder made up of micrometer scale particles of amorphous carbon and vanadium, a V+VC mixture, or V_2C were observed at lower speeds upon annealing. On the other hand, at a moderate speed, the VC was formed. Another example is that of fully amorphous powder, which transformed into a Ni-Zr mixture at a maximum velocity of grinding speeds, while at the moderate and low grinding, amorphous and crystalline mixture stages were formed [135].

1.5.4 Milling Time

One of the most critical factors is milling time. Usually, the time is selected to attain a stable condition between cold welding and the fracturing of powder particles. Different factors determine the time required for grinding, such as milling intensity, type, temperature, and ball-to-powder ratio. The duration must be determined for combinations of the specific powder system and aforementioned parameters. However, it needs to be noted that undesired phases may occur, and the contamination level rises if the powder is ground for more time than necessary [136]. Thus, it is preferable that grinding time should not exceed the required time.

1.5.5 Grinding Medium Material and Size

The most common grinding medium and ball materials are hardened chromium steel, hardened steel, stainless steel, tool steel, bearing steel, WC-Co, and tempered steel. The balls create impact force on the powder because of the milling medium's density; therefore, it should be sufficient to create impact force.

The grinding efficiency is also affected by the size of the grinding medium. As a rule of thumb, a large grinding medium has high density, which will be advantageous as more impact will be incorporated in the powder particles due to the larger weight of the balls. Moreover, it has been investigated that the final constituent of the powder depends on the grinding medium's size. For instance, an Al-Ti solid solution was formed when balls of 15 mm diameter were utilized to grind a mixture of blended elemental Ti-Al powder [137].

It has also been shown that employing steel balls of 3/16” diameter resulted in the formation of an amorphous phase in Ti-Al alloys than employing balls of 3/4” diameter [136]. However, there are contradicting findings; for example, when grinding was carried out using larger steel balls, the stable crystalline compound was generated instead of the amorphous stage. Another study reported that an amorphous phase is developed when the Ti-Al mixture is ground using 8- or 5-mm diameter steel balls; however, when 12-mm diameter balls are used, the amorphous phase is not developed by grinding [138], [139]. One study of similar nature reported in the Pd-Si system that small size of balls helps in the development of the amorphous phase development [140]. The amorphous phase is produced by intense frictional action, which is possible by using smaller balls. Different studies also report that "soft" grinding parameters, with characteristically low energies, the small size of balls, and a low ratio of ball-to-powder [126], [139], [141], [142], results in the formation of metastable or amorphous phases.

Many researchers used only single grinding medium size; however, different cases advocate using different ball sizes in the same study [143]. The highest

collision energy is attained by using balls of different sizes [143]. When the process of grinding begins, the powders are ground by the pins on the grinding medium's surface, and they are also cold welded. In this way, the wear of the grinding medium is prevented; hence, the contamination of the final product is also avoided. Still, the coating thickness of the ground material should be minimum so that the resultant final product is not compositionally heterogeneous [144]. A major disadvantage of the smearing of powder is lower yield due to the difficulty of separating powder from the ball surface. The solution to this problem is using small and large ball sizes together during grinding. As reported in Ref. [145], using large and small balls will result in less powder coating on the ball surfaces and cold welding. The investigation did not reveal any specific reason for better yield by following these parameters; however, a possible explanation can be the shearing force produced by different ball sizes, which helps in separating powder from balls' surfaces [60].

Furthermore, tracks are produced when the identical size of balls is used with round or flat-ended container vessels. It results in rolling balls in a predefined trajectory instead of randomly hitting the surface's bottom. Thus, different balls should be used to 'randomize' the balls' motion [90, including a combination of large and small-sized balls.

1.5.6 Ball-to-powder weight ratio

The ball-to-powder weight ratio (BPR), describing the ratio of balls' weight to powder, is a significant parameter. It is also known as the charge ratio (CR). There is an inverse relationship between BPR, and the time needed for the reduction process. In other words, the required time for the reduction process decreases when the BPR increases. For example, it has been observed that the time required to form Ti; when the Ti is formed by reducing $TiCl_4$ with Mg at the temperature of 208°C at BPR 2:1, the time required for this process is 48 hours. On the other hand, the same process can be completed within 18 hours when BPR is 12:1 [108].

Various researchers have studied this ratio to be anything from 1:1 [146] to 220:1 [147]. In most cases, a ratio of 10:1 is utilized when grinding powder in a limited-capacity grinder, such as a SPEX. However, when milling is performed in a high-capacity mill, such as an attritor, a BPR of 50:1 or even 100:1 is used. There is a substantial effect of the ball-to-powder weight ratio on the grinding time necessary to obtain a specific powder phase. The time required decreases as the BPR increases [98].

Using a stirring ball mill, Xi et al. [148] investigated how BPR affected the CuO reduction by Si during MA. They found CuO was entirely converted to pure metal Cu when the ball-to-powder weight ratio was 80:1. When the BPR was lower than 60:1, CuO was only partially transformed to Cu_2O and Cu, and when the BPR was less than 30:1, no Cu was recovered from the CuO reduction. The findings have been rationalized on the grounds that complete conversion to pure metal is possible with a high BPR due to the high collision energy.

The influence of BPR on time and ignition temperature was systematically investigated by Schaffer and McCormick [96]. Also, they found that the combustion reaction was absent with smaller grinding media (1 and 3 g balls) but took place with larger ones (8 g balls) [149].

1.5.7 The extent of filling the vial

After filling it with material to be ground, the remaining space in the vial is important as it ensures that an appropriate impact force is exerted on the powder during the milling process, which then results in alloying of the powder particle. Consequently, the volume of powder and balls used to fill the vial is crucial. If the volume of balls and powder is very small, the production rate will also be relatively low. Conversely, if it is very large, there is little area for the balls to move; hence, the impact energy is diminished [98].

1.5.8 Milling atmosphere

The purity of the final product also depends on the milling atmosphere. Hence, container vessels that are filled or evacuated with an inert gas like helium or argon are required to avoid contamination. Nitrogen has been discovered to react with metal powders; hence, it cannot be utilized to safeguard against contamination during the grinding process, except if the goal is to create nitrides[60]. Highly pure argon is the most widely used ambient gas to prevent oxidation and corrosion.

Various milling atmospheres have been utilized for specific reasons. Nitrides are produced in an environment of nitrogen or ammonia [150], [151]. Hydrides were produced in an environment of hydrogen [152]. It has been proven that the existence of air in the container produces nitride and oxides in the powder, particularly if the powder is reactive. Additionally, the type of environment appears to influence the type of the final stage. For instance, when Cr-Fe powder mixes were ground in different atmospheres, the resulting powder had a varied composition [153]. No amorphous stage emerged when the powder was ground in an argon environment, and Cr peaks persisted in the X-ray results. In contrast, when the powder was ground in argon-containing air or nitrogen-containing air, it became entirely amorphous. Furthermore, it has been observed for some systems that amorphization kinetics are faster under air due to oxygen [154], [155].

1.6 Acid Leaching

Leaching is a procedure commonly used in extractive metallurgy in which ore is processed with chemicals to transform the precious metals into soluble salts while the impurities remain insoluble. The remaining materials, termed tailings, can be drained and refined to recover the pure metal [156]. In the MA, it is applied to remove the by-products, unreacted raw materials, and contamination from the milling container and the media.

Several issues arise while processing metal powders using MA. One of those major issues is the amount and nature of impurities. These impurities contaminate the resultant product. The contamination of powder is caused by several reasons, such as the development of fresh and new surfaces, powder particles' small sizes, and the accessibility of a wide surface area. As a result, it appears that powder particle contamination is an innate disadvantage of the process unless extreme efforts are made to minimize or eliminate it.

Different types of factors play a vital role in contaminating metal powders: 1) process control agents that are added in powders, 2) the purity of chemicals of original elements used in powders, 3) grinding equipment (grinding medium and vial) and 4) grinding environment. Also the existence of interstitial contaminants such as nitrogen and oxygen is detrimental to reactive metals such as zirconium and titanium, optimum contaminant limits are often prescribed for tolerable mechanical and microstructural qualities [157]–[159].

When the mechanical alloying starts, powder particles are stuck in the grinding medium, and these particles have to go through various plastic deformation. The fracture of particles of powder creates fresh surfaces. Moreover, collisions take place among grinding balls and between container vessels and grinding mediums. Due to the various collisions, the vial and grinding medium's wear and tear are caused, which in turn introduce contaminants in the powder particles. Therefore, the contamination extent or magnitude is dependent on a variety of factors such as milling intensity, grinding medium, milling time, powder's hardness/strength differences, and milling environment [60], [160].

As stated above, the metal powder covers the inner container walls as well as the grinding medium during mechanical alloying. No particular attention was paid to the coating of surfaces with powder since was believed to avoid contamination. However, the studies on various alloy systems indicated the presence of contamination. One example of contamination is the presence of 1-4wt% Fe in most of the powder particles, in which a grinding medium made of steel is used regardless

of the system milled. Similarly, the W-C mixture showed the presence of 20 % Fe when it was ground for 310 hours, whereas the presence of 33 % Fe was also reported in pure U ground for 50 hours using the SPEX mill [161]. Additionally, the grinding of U-5Ni alloy was also contaminated by the presence of 60 % Fe; the grinding process took place in the SPEX mill [162]. The contamination percentages presented above are considered high.

Another such example is the presence of a large quantity of nitrogen (up to 33%) and oxygen (up to 44.8 %) [163] in Ti-5Al powder processed in a SPEX mill for 30 hours [164] and in the Al−6Ti powder particles which are ground for 1300 hours using a low energy mill, respectively. The iron contamination increased and resulted in up to 10.5% in planetary ball mill-based systems due to steel containers and grinding medium [165]. In addition, primary contaminants are nitrogen and oxygen caused due to environment [163]. However, other contaminants, such as Cr, are also mentioned in some cases[166]. The oxides of the reducing agents are also formed as a by-product. At this point, if by-products are not desired to remain in the system, they must be removed from the system by acid leaching.

Also, intermixing of the phases because of the metal phase's high reactivity related to nanocrystalline particle size caused by the mechanical alloying, the elimination of undesired reaction by-products can be challenging. The by-product phase can be eliminated by leaching in hot water or distillation under vacuum or dilute acid.

As reported by P. Amin, when B_2O_3, C, and Mg are mixed with 1:1.5:12 ratio for magnesiothermic reduction of B_2O_3 with milling and furnaces about 650 °C after the grinding process of B_4C for the partcile size reduction, the resultant product is washed away with hot water in order to extract B_2O_3. After that, the product is leached in 2M HCl to attain the B_4C phase. The B_4C peaks are clearly identified after the HCl acid-leaching process [167].

Alkan et al. demonstrated that when Mg was the reducing agent and the main raw materials was B_2O_3 and C with ratio of (B_2O_3/Mg/C, 2/6/1). Final product are %

70.4 MgO, % 22.3 $Mg_3B_2O_6$ and % 6.3 B_4C. According to this, B_4C production with SHS methods forms a different by-product. $Mg_3B_2O_6$ is a by-product relatively hard to dissolve in weak acids. For producing pure B_4C, an acid leaching operation using stronger acids was required. The possible by-products, $Mg_2B_2O_5$, $Mg_3B_2O_6$, and MgO, can be dissolved in aqueous HCl solutions. The investigators maintained a constant 400 RPM for the solution stirring speed and 20 g for the SHS product starting weight. A touch thermometer was employed to track the shifting temperatures of the liquids. 150% of the stoichiometric concentration of hydrogen chloride was used to conduct the leaching trials. At last, XRD analysis showed distinct B_4C peaks [168].

Furthermore, a sample ground for 10 hours was acid leached in 1M HCl at 80 ℃ for 1 hour [84]. Centrifuged, filtered, and rinsed multiple times with purified water, the leached solution finally had a pH of around 7. Lastly, after 1 hour in an 80 ℃ vacuum oven, the sample was dried. So, it can be concluded from the XRD data that the B_4C peaks are very distinct [84].

According to the results obtained from the results of these studies, excessive energy input is required for B_4C production. In order not to realize very high energy inputs, more active reducing materials such as Mg are used. In this way, reactions take place. Especially since one of the main raw materials used for B_4C production is B_2O_3, by-products are formed. In many production methods using Mg, the main by-product is MgO. Magnesium borates can be formed in some methods where more active combustion reactions occur. These formations can be easily removed from the system by acid leaching operation. When we look at the studies in general, HCl is used because of the stable structure of B_4C and the possibility of deterioration.

1.7 Kinetic Modelling of the System

In order to perform the kinetic modeling of the system, the value of n can be found by using the Avrami equation. With the n value found, it is possible to make interpretations about the system.

For a constant temperature, phase transformation and phase change calculations can be made with the Avrami (Johnson–Mehl–Avrami–Kolmogorov (JMAK)) equation. It also can be used for chemical reaction rates and modelling of these systems and crystallization kinetics. Mechanochemical milling is an operation that does not have a specific temperature input and is characterized as constant temperature in terms of kinetic models [169], [170]–[172].

It is aimed to obtain the N value, which is the most important value for the kinetic modeling and interpretation of the system. For this hand, calculations were made based on the Avrami equation as seen below. Also, k and n are time-independent constants for the particular reaction. This expression is often referred to as the Avrami equation.

According to N value calculation results, Originally, N was held to have an integer value between 1 and 4, which reflected the nature of the transformation in question. In the derivation above, for example, the value of 4 can be said to have contributions from three dimensions of growth and one representing a constant nucleation rate. Alternative derivations exist, where n has a different value [173].

If the nuclei are preformed, and so all present from the beginning, the transformation is only due to the 3-dimensional growth of the nuclei, and n has a value of 3.

An interesting condition occurs when nucleation occurs on specific sites (such as grain boundaries or impurities) that rapidly saturate soon after the transformation begins. Initially, nucleation may be random, and growth unhindered, leading to high values for n (3 or 4). Once the nucleation sites are consumed, the formation of new particles will stop.

Furthermore, if the distribution of nucleation sites is non-random, then the growth may be restricted to 1 or 2 dimensions. Site saturation may lead to n values of 1, 2 or 3 for surface, edge, and point sites respectively [174].

CHAPTER 2

EXPERIMENTAL PROCEDURE

In this study, the boron carbide powders were produced by mechanochemical milling. The characterization has been made for the optimization of process parameters and the determination of the properties of the final product.

The relative Gibbs Free Energy (ΔG) of the reactions has been calculated to gain insights on the thermodynamics of the mechanochemical alloying. Reaction kinetics have been studied and the mechanism of the transformation has been explained by the analysis of the transformation exponent.

2.1 Steps of Mechanochemical Synthesis

In this study, the mechanochemical production of B_4C has been optimized. The steps in mechanochemical milling are mixing the powders, loading the powder mixture into the mill with the balls, and milling. The milling should be conducted for a duration that is long enough to reach the steady state where every powder particle is at the desired composition[175], [176].

The critical factors for the milling process are the jar and mill design, raw materials and their proportions, and the milling parameters. The process parameters that require optimization are the ball-to-powder ratio (BPR), ball material and size, planetary mill speed per minute (RPM), milling time, and inert atmosphere gas. This operation requires unique milling jars made from materials with high abrasions and high-pressure strength. The milling jar design is detailed below.

Unwanted by-products that are usually not in controllable variety or quantity form during the milling. The acid leaching was applied following milling to remove these.

Acid leaching was followed by drying to improve the quality of the product. The product remaining after an acid wash is highly wet with weak and strong agglomerations. So, optimizing the drying parameters and using anti-agglomeration methods is necessary.

The steps of the operation and the parameters optimized at each step are shown in Figure 2.1.

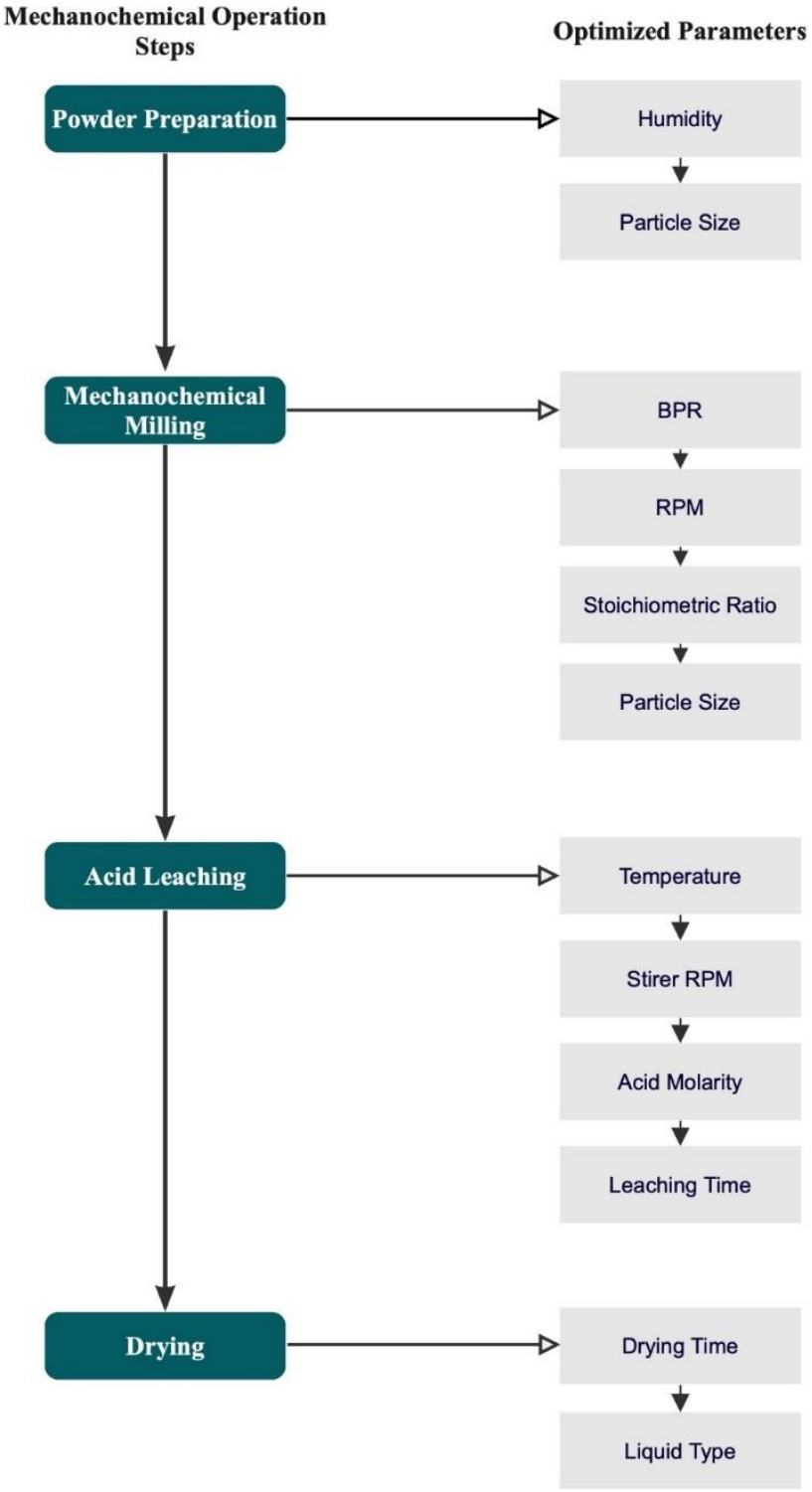

Figure 2.1. Summary of the production steps and the optimized parameters in this study.

2.2 Mechanical Jar Design

The low-temperature synthesis of B_4C by mechanical alloying is only possible by applying high mechanical forces requiring unique milling jars. The most important criteria for jar materials are high abrasion and high compressive strength. The jars with the required abrasion and high-pressure strength to produce B_4C are not commercially available. So, the jars are specially designed and manufactured for this study.

The design and production of the milling jar involve material selection, optimization of reservoir structure parameters such as volume, wall thickness, internal diameter, locking mechanism, sealing material, and design of a safe, ventilated, inert atmosphere cover.

The main criterion for the jar design is obtaining a structure that can withstand strong mechanical forces. The most fundamental ones of these forces are the moment of inertia, friction, action and reaction force. Due to the high friction force involved, abrasion resistance is the most critical design criterion. The contamination or deviation from the targeted chemistry can occur due to the interactions between the powder and the jar wall. The most commonly used materials for ball milling jars are hardened steel, tool steel, hardened chromium steel, tempered steel, stainless steel, ZrO2, WC-Co, and WC-lined steel [177]–[182]. Among these, the best candidates for this study are traditional steels, namely SS314 and SS316, and tool steel 2379 (X153CrMoV12). These are the most frequently used steels in this industry. The main reason for this is that it is easily accessible and cheaper than other special types. As detailed in the results and discussion section, since the iron contamination was higher with traditional SS314 and SS316 due to lower abrasion resistance, tool steel 2379 (X153CrMoV12) was chosen as the jar material. In order to reach the necessary strength heat treatment is applied. The austenitization took place at 830 ℃ under vacuum. The steel was then air-cooled. After this operation, hardness measurements were made from four different points. The difference between these measurements

is less than 0.5 Hardness Rockwell C (HRC). The average hardness value obtained was 60.2±1.1 HRC.

The jar size should also be chosen carefully because 300 ml and below jars yield a very small amount of product. While jars larger than 450 ml can be used for production with already optimized parameters, it would be wasteful for an optimization study like this one since the amount of required raw materials' increase with increasing jar size. So, the trials have been limited to 300 ml and 450 ml. The 450 ml jar is preferred because the powders obtained in the trials with this size yield enough product to be characterized by several different methods.

The inner diameter and wall thickness are other parameters to be decided for this system. The inner diameter should be large enough to allow the balls to sweep the system. At the same time, it is beneficial to maximize the wall thickness since many experiments will be carried out with the same jar and excessive wear causing thinning of the jar wall may occur. So, a large wall thickness should be chosen while allowing a large inside diameter. At the same time, the diameter of the bottom jar was kept large so that unwanted accumulation of powder at the bottom does not occur. Tried inner jar radiuses are 0-5 mm and 20 mm as detailed in results and discussion section.

The next step was the design of the cover. There are two design requirements. The cover should be ventilated to release the produced gases and keep the inert atmosphere. For this, a ventilation valve was designed. The process parameters mentioned above were kept constant for the design of the ventilation valve. Based on the experiments, a 9-bar-pressure valve design was found to be sufficient for the system to operate safely. The cover has been sealed with Viton gaskets with two specially opened gasket channels to keep the inert atmosphere pressure constant.

2.3 Mechanochemical Synthesis Parameters

After jar design and production were completed, mechanochemical synthesis experiments were conducted using RETSCH ball mill PM 100. The drive power of this mill is 750 W and the sample/batch volume is 350 ml.

Optimizing the milling process requires selecting a reducing agent, the proportions of the reactants, and the milling atmosphere. In addition, the process parameters, namely milling speed (revolutions per minute- RPM), milling duration, ball-to-powder weight ratio (BPR), ball material, and size, should be optimized to guarantee the purity and quality of the resultant powders. The optimization of the parameters has been based on the yield and safety of the process. Different parameters that were tested are given in Table 2.1.

The best candidates for the primary reducing agent were selected as magnesium (Mg) and aluminum (Al) 325 mesh and 99.5% and more purity, based on literature [60]. Other raw materials are boron oxide powder (98.9% purity, 300-325 mesh by Eti Maden) and activated charcoal (99.5% purity, 325 mesh by Nanografi).

The selection of the reducing agent was based on efficiency. Although Al is advantageous over Mg concerning cost and availability, it is not as reactive as Mg. Hence, it has the potential to limit efficiency. The jar size, milling speed, and BPR have been kept constant at 300 ml, 300 RPM, and 15:1, respectively, for selecting the reducing agent. Aluminum was found ineffective in reducing B_2O_3 due to its high stability. For example, when Al was used as a reducing agent, the yield was minimal even after 10 hours, as characterized by phase analysis. On the other hand, experiments using Mg powder yielded two times more B_4C than the experiments that used Al with the same process parameters.

The milling speed, characterized by the revolutions per minute (RPM), increases the energy input into the powder. However, there are some limitations to the maximum milling speed. Above a critical value, the balls are pinned to the walls;

hence milling cannot take place. Furthermore, the higher speeds may increase the temperature or the pressure beyond safety limits [183]–[186].

The milling duration was chosen so that a steady-state between different mechanisms, fracturing and cold welding of the powder particles, can be reached. The time required for reaching steady-state changes according to the milling speed, the ball-to-powder ratio, and the temperature of milling [187]–[189].

In this study, five different durations have been tested. These are 3, 5, 8, 10, and 14 hours. As detailed in the results and discussion section, the yield of the products was insufficient in experiments below 8 hours, while longer durations caused distortions in the crystalline structure, as characterized by peak broadening in the X-ray diffraction pattern without improving yield. So, the optimum duration was chosen as 8 hours.

Ball size is also an important parameter. It has been shown that a large ball size can increase the milling efficiency because the larger weight of the balls transfers higher impact energy. It has also been shown that ball size may affect the phases forming [190], [191]. However, there are also reports suggesting the highest collision energy is provided when balls of different sizes are used. [108] So, mixed ball sizes ranging from 5 mm and 15 mm have been used in this study. The minimum ball size has been decided based on the fact that balls smaller than 5 mm have a very long life as they deform much slower, so 5 mm was chosen. While deciding the maximum ball size, the inner radius and the bottom fraction effect have been considered. As the requirements are met by 15 mm, it has been chosen as the maximum ball diameter. These will be detailed in the results and discussion.

As in the case of ball size, an increase in the ball-to-powder weight ratio (BPR) increases the transferred energy and hence decreases the time required to form the targeted phases [187], [192]–[194]. In this study, the ratios 10:1, 15.1, and 25:1 have been tested. The experiment with 15:1 showed the most successful result. The kinetic is much slower to load energy with lower ratios, which reduces overall

efficiency. If higher ratios than 15:1 were used, the system was energized beyond the safety limits leading to opening the safety valve earlier.

Another critical parameter is the proportions of the raw materials [189], [195]. In this study, the proportions corresponding to the stoichiometric ratio of B_4C formation by reactions of Mg and B_2O_3 and lower and higher than the stoichiometric Mg amount have been used. It has been found that the stoichiometric ratio yields a higher efficiency than the under-stoichiometric amount. The system worked beyond the safety limits when the Mg amount was higher than the stoichiometric amount. As detailed in the discussion section, production yields were not improved if more Mg than stoichiometric amounts were used.

Table 2.1. Experimental conditions used in this study.

Reductive Material	RPM	Duration (hrs)	Ball Size (mm)	BPR	Stoichiometric Ratio (B_2O_3:C:Mg)
Magnesium	250	10	10	15:1	10:01:11
Aluminium	250	10	10	15:1	10:01:11
Magnesium	250	10	10	15:1	10:01:11
Magnesium	250	10	10	15:1	10:1:13 (OVER)
Magnesium	250	10	10	15:1	10:1:9 (UNDER)
Magnesium	100	10	10	15:1	10:01:11
Magnesium	250	10	10	15:1	10:01:11
Magnesium	450	10	10	10:1	10:01:11
Magnesium	500	10	10	15:1	10:01:11
Magnesium	intermittent	10	10	15:1	10:01:11
Magnesium	450	3	10	15:1	10:01:11
Magnesium	450	5	10	15:1	10:01:11
Magnesium	450	8	10	15:1	10:01:11
Magnesium	450	10	10	20:1	10:01:11
Magnesium	450	14	10	15:1	10:01:11
Magnesium	450	8	10	10:1	10:01:11
Magnesium	450	8	5	15:1	10:01:11
Magnesium	450	8	5,15	15:1	10:01:11
Magnesium	450	8	10	20:1	10:01:11

When the system was first switched on, there was a noticeable amount of moisture. The reason for this is that the system is equipped with desiccant materials. The materials used in the system are known for their magnesium and boron oxide desiccant properties. Therefore, as a result of the combustion reaction, moisture was produced in the system. This moisture stays in the system and dramatically reduces efficiency by sticking to the balls and the reservoir. It is therefore required to pre-process the raw materials. All powders were pre-cleaned and dried at 40 ℃ for 6-8 hours in an oven with silica gel. Weight measurement before and after this operation showed a decrease in weight upon drying, indicating excess moisture in the powders. The drying process was repeated before each experiment to avoid the effect of moisture, such as agglomeration.

2.4 Acid Leaching and Obtaining Final Powder

2.4.1 Acid Leaching

Acid leaching is the second stage in the production of the B_4C by mechanochemical milling. At this stage, all contamination and by-products in the system, such as MgO and other magnesium borates, are disposed of from the system. The most important parameters in this process are the acid type, stirring speed and temperature, and centrifugal speed and time. The drying process is also a part of acid leaching and is required to obtain a high-quality product without agglomeration.

In this study, Sigma Aldrich brand 37% hydrochloric acid used for acid leaching operations. Also, the magnetic stirring temperature has been varied. Testes have been carried out at 40 ℃ and 70 ℃. Furthermore, the magnetic stirrer speed was tested between 100 and 1000 RPM.

During the trials, the addition interval and rate of the powders were kept the same. When powders were first introduced into acid, a slight foaming and gas output occurred. Afterward, an orange-colored smoke was observed. All the overflow and

smoke release only lasted for a few seconds. After this, no overflow was observed. Then, with the magnetic fish continuing to stir the system, the system reached equilibrium and continued to mix homogeneously again. Under these conditions, leaching continued.

Also, a curved magnetic stirrer wish was chosen for maximum vorticity to avoid powder accumulation at the bottom of the beaker. Also, care was taken to ensure that the fish moved in such a way as to prevent the powder from settling to the bottom by creating vorticity in the system. These experiments were carried out in a fume hood suitable for chemical operations with a lid due to the danger of gas outgassing and overflows.

Purified powders were washed several times with pure water to remove the acid until the pH of the aqueous solution equaled that of the pure water. The products were washed and precipitated under centrifugal force. The precipitation operation was carried out in Hanil Fleta5 centrifuge in centrifuge tubes.. At the stage of deciding the RPM and duration of the procedure, after several trials at 1000 and 2000 RPM, 5 and 10 minutes, it was seen that most of the powders precipitated and the solution became very clear after precipitation at 3000 RPM for 20 minutes.

After testing these parameters, hydrochloric acid used. The magnetic stirrer speed and temperature were chosen as 250 RPM and 70 ℃, respectively.

2.4.2 Powder Extraction

After the completion of the precipitation process, the acid solution is safely poured out, which leaves the settled powders at the bottom. All powders must be collected from the bottom of the tubes, as it will increase the amount of product obtained. A micro spoon was used directly to collect the powders, which adhered to the bottom due to the effect of the RPM. Furthermore, to remove the powders remaining at the bottom of the tubes, pure water was sprayed at the bottom of the tubes with a fine-tipped nozzle, and the powders were forced to separate from the

tube. With these process steps, all the powders remaining at the bottom of the tube could be collected.

2.4.3 Washing

After collecting the powders from the centrifuge tubes, the powders needed to be washed to remove the acid. The purest water possible should be used for washing the powders. Impurities in the water are not desired in the product. Therefore, 0 TDS (Total Dissolved Solids), Distilled (DI) water suitable for laboratory use was used. In order to test the total conductivity value of the water taken from the pure water purifier, a digital TDS meter was used. This device performs total conductivity control by detecting the substances in the water. After the controls were ensured, it was seen that the water to be used was 0 TDS.

The powders exposed to a single-time acid washing operation were collected in a beaker and 300 ml of pure water was added and mixed with the help of a magnetic stirrer fish. During this process, mixing was performed at 300-400 RPM for 10 minutes at room temperature. In order to determine whether the powders were washed sufficiently or not, a pH meter should be used. The pH value of the aqueous solution containing the powders should be measured. The value to be compared is the TDS value of pure water taken from the pure water purifier before use. This value may vary according to the purity of DI water and the device used. As a result of the measurements, it was observed that the pH value was 6.5. Therefore, the washing operation must be repeated until the pH value of the aqueous solution is 6.5. This measurement process is also carried out with the help of digital pH meters and Sigma brand paper pH meters for verification.

During the washing operationprecipitated powders were collected with the same methodology detailed above and the TDS value of the added water was measured. In almost all experiments, it was observed that a one-time pure water wash was insufficient. For this reason, after the necessary measurements were made, the same procedures were repeated and the powders were washed a second time in a

beaker filled with pure water. After the second washing, the measurement was performed and the result was 6.4 pH indicating that the powders were sufficiently cleaned.

Finally, the drying operation was tried by using two different liquids, water and alcohol, during the drying phase of the powders. As explained in the results and discussion, alcohol provides a more successful drying.

The products have been left to dry in a 40°C oven for 2 hours with desiccant silica gel.

2.5 Characterization

2.5.1 Particle Size Analysis and Optimization

Both raw materials and the products were tested in a Malvern Mastersizer 2000 device in METU Metallurgy and Materials Engineering using an ethyl alcohol solution to obtain their particle size distribution. In 7 different periods, the particle size was analyzed by MasterSizer device using water and alcohol solution.

In addition, as detailed in the results and discussion section 3.2, boron oxide particles were found to be larger than other raw materials. Therefore, an additional milling operation was performed.

The particle reduction operation of boron oxide was applied to a large amount of material. Before applying this process, boron oxide powder sufficient for about 10 experiments was dried and dehumidified for 8 hours at a low temperature of 40 ℃ in the oven using silica gel. A particle size reduction operation was then performed and the prepared material was stored in a glass, airtight container for further experiments.

There are some critical considerations when performing this operation. The energy loaded to the system during the particle size reduction phase should be

controlled to avoid excess mixing of the raw material and hence contamination of the raw material by the chamber and the balls. The two most important parameters to keep the energy supplied to the system under control are the RPM of the device and the BPR used. Generally, in systems using planetary ball mill, higher ratios than 10:1 BPR are preferred. 150 rpm is also used for this BPR [203]. However, taking into account that this is not mechanical alloying, but size reduction, safe grinding was achieved with lower values. The rpm value was kept at 120 rpm, which can be considered low. Although the BPR value is 15:1 in mechanical milling operations, it was kept at 2:1 to generate a stable and low energy load during particle size reduction. In this way, the particle size of 216 microns was reduced to 63 microns.

2.5.2 Phase Analysis

After milling and acid leaching, the products have been subjected to phase analysis by XRD. XRD was carried out on a Rigaku MiniFlex 600 W High-speed detector (D/teX Ultra, 1D) device with a scanning speed of 0.8^{o}/min located in the METU central laboratory within the range of 10-80^{o}. Rietveld analysis has been conducted by using GSASII software to obtain the phase amoun

2.5.3 Morphological Characterization

Morhological characterization has been conducted by scanning electron microscopy (SEM). Raw, milled, and acid-leached powders have been examined. Scanning electron microscopy (SEM). In SEM, two types of electrons are used, backscattered electrons (BSE), secondary electrons (SE) for different zoom values.

Prior to morphological characterzation by SEM, the insulating powders were gold plated. Also The JXA-8230 Electron Probe Microanalyzer used for SEM which has 6nm resulation.

2.6 Kinetics modelling

For the kinetic modelling of the system, the N value must be calculated. The equation is also known as the Johnson–Mehl–Avrami–Kolmogorov (JMAK) equation. At this stage, calculations were made based on the $y = 1 - \exp(-kt^n)$ formula [196], [197]. The graphs created depending on the t and k values and the interpretation of the N value are mentioned in detail in the result and discussion section. To find the order of reaction, n, we need to calculate rate constant, k and time period $t_{0.5}$ from the graph plotted between percentage transformation values of B_4C and MgO. As the details can be seen in the results and discussion section, with the help of the graphics and the n value obtained after these calculations, interpretations were made by performing a literature review.

CHAPTER 3

RESULTS AND DISCUSSION

3.1 Mechanical Design

3.1.1 Mechanical Jar Design

In the previous section, it was mentioned that one of the most important steps to synthesize B_4C at low temperatures is to design a high-pressure and abrasion-resistant jar. The jar consists of two primary components. One is the lid and the other is the base.

The basic components of the jar design are chamber cover design with sealing for inert gas pressurization and high-pressure protection. Locking mechanism compatibility is another design criterion. Relief valve design and optimization support are required to avoid explosions in case of high pressure and temperature.

The first step was the design of the cover. The cover material should be the same as the chamber material so that both the base and the cover would have the same resilience and toughness along with the thermal conductivity and the thermal expansion coefficient.

A lock mechanism that would be completely locked by tightening with imbus Metric 4 size bolts from 6 different points was found to stand to the pressure inside the chamber. There were three different holes in the cover. Two of them would be used for the inlet and outlet of the inert gas. Ball valves that could withstand high temperature and pressure values were used on these holes. As a result of the first experiments, the plastic valve handles either lost their structural integrity or melted due to the high temperature and the effect of G-force. It is important to state that this production route is carried out at room temperature without any energy input, but

the temperature of the system rises due to friction force or chemical reaction. Upon observing the plastic ball valve failure, the plastic valve handles were replaced with stainless steel ones. The valves had two sides, one with a male and one with a female thread. The male thread was used for mounting to the chamber and the female thread was used for inert gas sweeping operation. In addition, when performing the inert gas pressurization process, using a structure similar to a high-pressure filling port with a valve resulted in a more successful sweeping operation. Also, the mentioned port was able to keep the pressure inside the chamber constant. The importance of using a high-pressure filling becomes apparent when it is compared to a traditional threaded structure. For example, in the case of a traditional threaded structure, if 3 bar argon or nitrogen gas is supplied inside, the pressure may drop to 1-2 bar while trying to remove the conventional connection apparatus, and it may become impossible to control it again. Upon this consideration, a high-pressure filling port was used in this study. It has been observed that cleaning the valves after several uses is also important since the powder might build up in the valve and affect the sweeping operation negatively.

The third hole on the chamber cover was for the safety valve required for high-pressure and temperature applications. This inlet should be larger than the inlet of the valves. A spring assistant relief valve with spherical support as a spring buffer was used as the safety valve. Relief valve design details and optimization are given in the following section.

The geometry of the chamber was also critical for high-yield production. The geometry should be designed so that the mechanical forces in action do not deform the chamber. These forces are basic mechanical forces such as centrifugal, friction, impact, and reaction. With the effect of the circular acceleration of the jar, the balls hit the opposite wall, each other, and the powder at high speeds. As mentioned in the literature review, with this impact, very high temperatures can be reached at the contact points.

Initially, the inner bottom diameter was kept low to keep the inner volume as large as possible. However, after the initial experiments, it was observed that powder accumulation took place due to the small inner diameter at the bottom of the jar and limited the reaction forming B_4C. Firstly, the inner diameter was kept at 5 mm; this diameter should have let a 10mm-diameter ball sweep the bottom of the jar completely. However, as seen in Figure 3.1, with the complexity of the system, this situation was not realized. Even in the case of using balls smaller than 10 mm, powder accumulations were observed at the bottom. In addition, the small radius, as in Figure 3.2(a), is also a hindering factor for the balls getting mixed up in the system.

Consequently, visual observations and the XRD analysis showed that the yield of B_4C was minimal and a new design with a larger bottom diameter was required. If the jar bottom radius is larger, as in Figure 3.2(b), the balls hitting from one wall to the other wall accelerate with the help of this radius. Therefore, the inner diameter was increased to 20 mm. In the trials carried out after design revisions, it was observed that there was no accumulation at the bottom of the chamber. Therefore, the blind spots at the bottom were eliminated with a larger diameter.

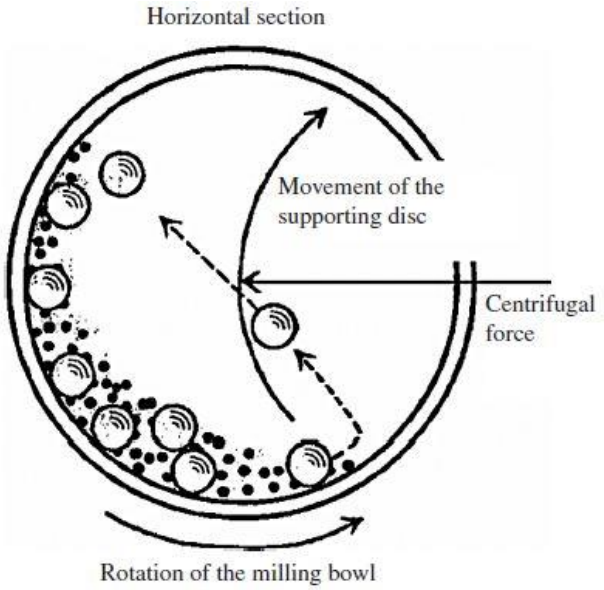

Figure 3.1. A simple schematic of milling operation[60].

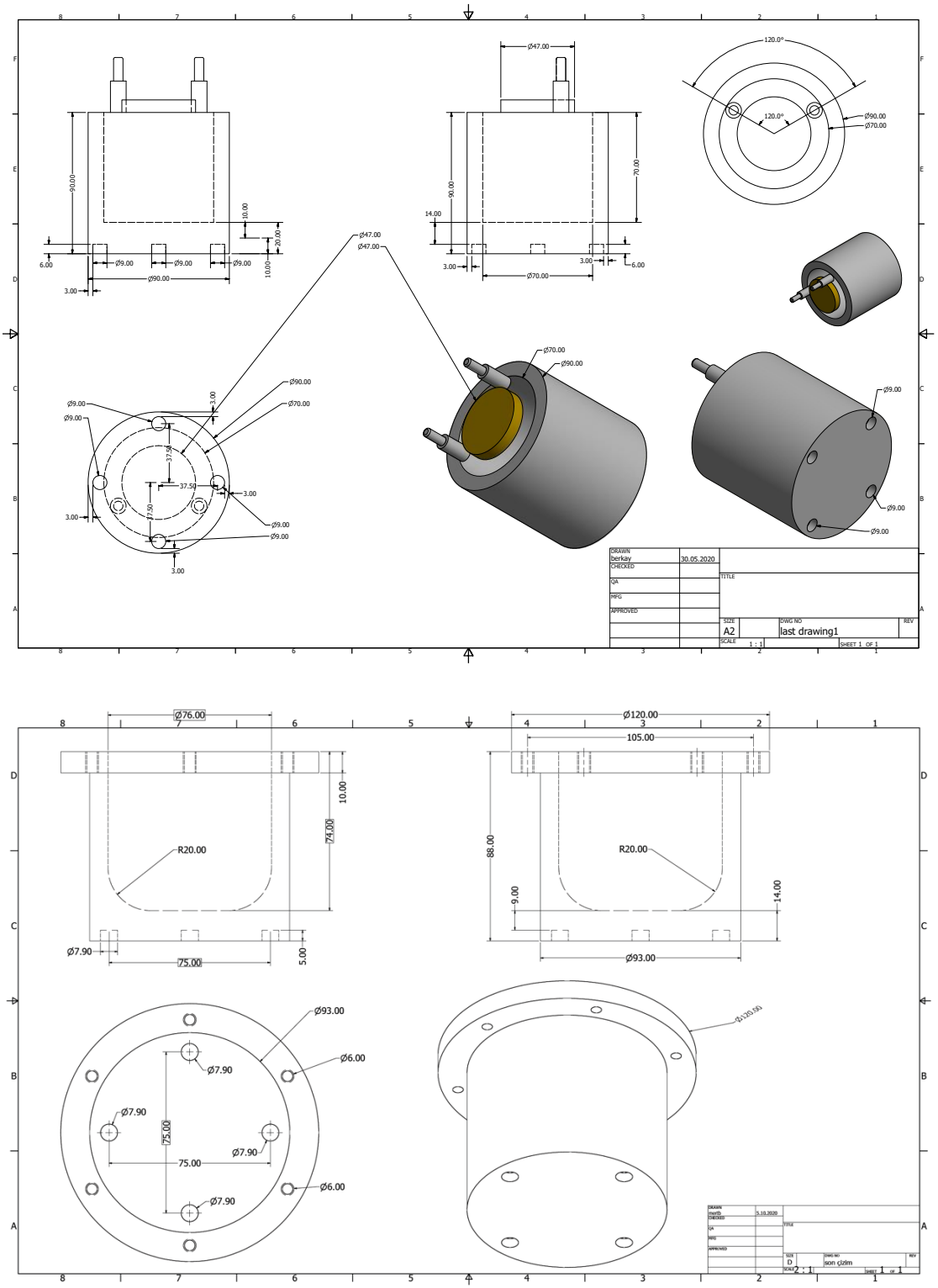

Figure 3.2. Jar technical drawing without bottom jar Radius (upper), jar technical drawing with 20 mm jar bottom radius (bottom).

3.1.2 Relief Valve Design and Optimization

The safety valve is the component that will prevent a major explosion in the entire system in case of unexpected acceleration of the reaction or an increase in the temperature of the system. In any unexpected situation, the valve opens and helps the system to stop safely by releasing excess pressure. During mechanical alloying, energy loading occurs in the system due to the mechanical effects of impact and reaction. When all these forces are combined with the highly flammable magnesium powder, which is the reducing agent used in this study, the tendency of the system towards flashing and even explosion increases. Even if the inert gas sweeping has been successfully performed in the system, some gases are present due to both the trace amount of oxygen remaining in the system and the nature of the chemical reactions. The reaction releases a high amount of carbon monoxide (CO) and it builds up in the system. All these require a safety valve to minimize the risk of an explosion so that when the determined safe pressure range is exceeded, the system opens itself, releases, and brings the pressure back to the safe range.

The valve was mounted to the system using a male thread, as shown in Figure 3.3. The inner valve body mechanism material was chosen as polytetrafluoroethylene (PTFE). since its melting temperature is higher than 200 ℃, which is the maximum temperature that the lid could reach. The materials such as nylon with melting temperatures lower than this threshold might melt and cause an explosion due to the inability of the safety valve to function. There is a variety of safety valves with respect to shape and size. Our main selection and design criterion was the locking mechanism of the RETSCH brand planetary ball mill. This mechanism has a three-lever design. The mechanochemical system needs two valves and one relieve valve.

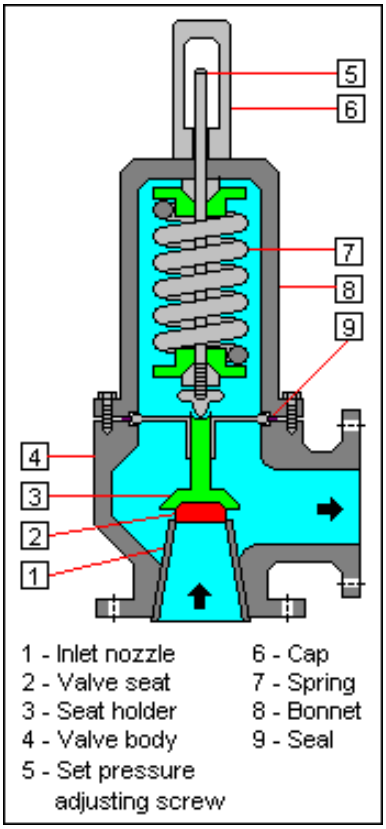

Figure 3.3. Relief valve.

After testing different sizes of safety valves, trials were carried out with the smallest one. It is possible to find safety valves as small as 1.5 cm in length and 1 cm in diameter. Springs have a dynamic working mechanism, the force that should be applied according to the compression ratio of the spring is also variable. Therefore, it is impossible to calculate the pressure in the system to find the force value at which the spring will open and these should be determined experimentally. In order to determine the characteristic of the system, the first trial was made with the safety valve with the smallest bar value of 0.1 bar. This value has been gradually increased, as shown in Figure 3.4.

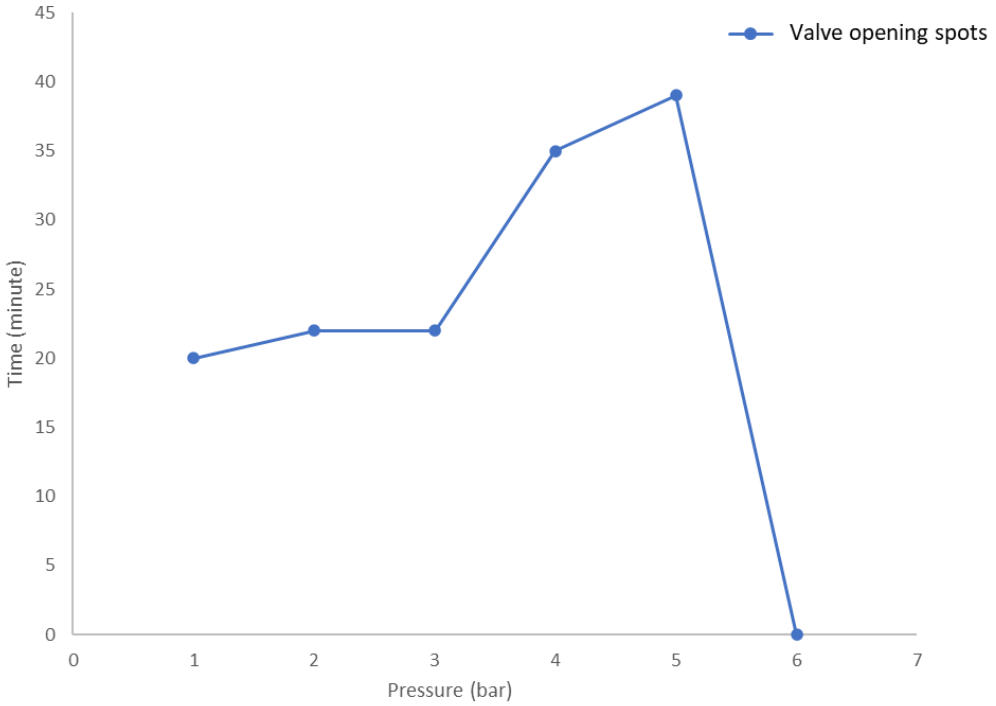

Figure 3.4. Relief valve opening pressures.

The aim of testing different safety valve spring values was to find a pressure that could provide safety and was also not too conservative so that experiments could still be conducted without valve opening. The important point was to find a safe interval to perform the experiment before the safety valve was activated. Because opening the system for safety reasons may change the experimental parameters that are carefully chosen. For example, if the system is opened, it discharges the compressed air into the atmosphere. During the mechanochemical activation period, there is a powder cloud in the chamber. As a result, along with the compressed air discharged to the outside, some of the powders could be discharged, too. This would cause the raw material ratios loaded to the system for the maximum yield would change.

The first test was carried out with a safety interval of 0.1 bar. The safety valve was opened 20 minutes after the experiment started. It was not expected for

mechanochemical activation to take place in the first 20 minutes at a degree of increasing pressure enough to cause valve opening. Considering that Mg powders are flammable even at high humidity in the open air and become more active as the particle size gets smaller, premature valve opening was hypothesized to be about increased activity of the Mg powder with reduced size. According to our hypothesis, the particle size reduction took place in this period and the 20-minute mark corresponded to the sudden increase in the pressure with the ignition of reduced-size Mg powder due to changes in temperature during the milling operation. In order to test this, the safety valve spring value changed to 0.8 bar. However, no increase in the duration of valve opening was observed. Increasing the safety valve spring valve to 1 bar also did not lengthen the time passed until the valve opening, verifying the hypothesis.

In order to test the limits of the system or the existence of a pressure that can lengthen the duration of safety valve opening, the safety valve spring value increased to 2 bars and the duration of valve opening became 35 minutes. Although it was almost double the previous trials, it was still not enough for mechanical alloying to take place. The fifth trial, with a 4 bars threshold, lengthened the valve opening duration to 40 minutes. These trials showed the requirement for a stiffer spring so that the pressure threshold was chosen as 9 bars.

After several trials, it was observed that a successful experiment could be conducted without the safety valve opening with the 9-bar threshold. In case of higher magnesium or reactive substance increase, this valve value may not be enough, but under these system conditions, the process was completed without opening the relief valve.

3.1.3 Material Selection

Materials with higher hardness should be preferred to reduce the amount of wear and perform more experiments with the same jars. Furthermore, the contamination from the interaction of the jar and powder should be minimized, and

also the contamination should be leachable from the product. Firstly, SAE304 stainless steel was used. Iron contamination reaching up to 10% was observed due to the low friction resistance of the material when SAE316 and SAE316L were used. Furthermore, even with a single use, surface abrasion is visible, proving the requirement of a material with a higher wear resistance. Here, tool steels, due to their high wear resistance, appeared as promising candidates along with Ti and ceramic. The hardness of the tool steel is in the lower range among these materials. However, considering the contamination should be easily removable from the system, titanium chambers were not preferred since titanium contamination could not be leached away. Similar discussions are also valid for ceramic materials such as alumina. So, instead of selecting Ti or ceramics, increasing the hardness of the tool steel by heat treatment was chosen. The material selected was AISI D2 cold work tool with an average composition of 1.55 wt.% C, 12.00 wt.% Cr, 0.80 wt.% Mo, and 0.90 wt.% V. Also stainless steel balls from Retsch were used.

The hardness of this steel can be increased up to 60 HRC by heat treatment. It was observed that definite heat treatments, such as conventional baking and hot brine hardening, can cause distortions in the chamber holes, diameter, and critical dimensions. This would cause the lid not to fit properly or deviations from linearity in the chamber walls. A hardening operation starting with austenitization at 830 ℃ under vacuum was conducted to avoid distortions in the structure. Following the austenitization, the jar was normalized. After the process, the stains on the surface were cleaned with 0.1 mm CNC wiping and a successful surface tolerance was obtained. A hardness value of 60.2±1.1 HRC was obtained, showing that this route of chamber production was suitable for mechanochemical milling operations. After the first trial, it was observed that the amount of wear in the chamber was lessened.

When other materials were used, physical defects occurred with the effect of friction even after a single use. These defects were almost absent in this trial. At the same time, by visual examination, it was determined that the iron mixing with the powder was much more limited. Likewise, it was seen that the wear rate in the jar decreased by almost three times. While the deformation of the balls in the jar could

be clearly seen even in a single use in the experiments carried out with the jar made of other materials, almost no deformation occurs until 2-3 uses in the experiments carried out with the new material.

3.1.4 Inert Gas Selection

After chamber design and relief valve optimization, one of the parameters that were required to be decided was the type of inert gas. Inert gases are generally used to avoid unwanted chemical reactions such as oxidation and hydrolysis. The most commonly used inert gases in mechanical alloying systems are purified argon and nitrogen due to their abundance and low cost. Here, inert gases are used for sweeping in addition to avoiding unwanted chemical reactions.

In the systems where an active material such as Mg is used, even 5% oxygen may cause problems in the experiments. It is important to choose a gas heavier than air. Argon is 38% denser than air. As a result, after argon is introduced into the system, it settles to the bottom and replaces oxygen. When the system is filled with balls and powders, argon can enter between these components and provide a successful inert atmosphere. First, argon was swept into the system at low pressure for about 1 minute and the lid was closed. Argon was allowed to replace oxygen for a certain period. The oxygen was carried to the top of the system; no oxygen was expected to be left after one more sweep. This operation was repeated 2 or 3 times before the mechanical alloying was initiated.

The design of the jar and selection of the inert gas atmosphere were followed by raw material characterization so that process parameter optimization studies could be conducted.

3.2 Raw Material Characterization

3.2.1 Particle Size Analysis and Optimization

The raw materials used in this study are magnesium powder from Merck with 99.5% purity and mesh size of 325, boron oxide from Eti Maden with 98.9% purity and mesh size of 200-325, and activated charcoal from Nanografi with 99.5% purity and mesh size of 325. The raw material particle size affects the particle size of the final product. Furthermore, particle size is an important parameter for initiating chemical activation in the mechanical milling operation. The large particles may require longer milling times. Also, the particle size of one product being 2-3 times larger or smaller than the others may cause fluctuations in the particle of the final product. As seen in Table 3.1, the median particle size of B_2O_3 was 216 μm. It was also observed that the range of the particle size distribution was very large. On the other hand, as seen in Figure 3.5, activated carbon has a median particle size of 49 μms and that of magnesium is 57 μm. The fact that boron oxide is more than 4 times larger than the others had the potential to cause a nonuniform particle size distribution in the final product [60].

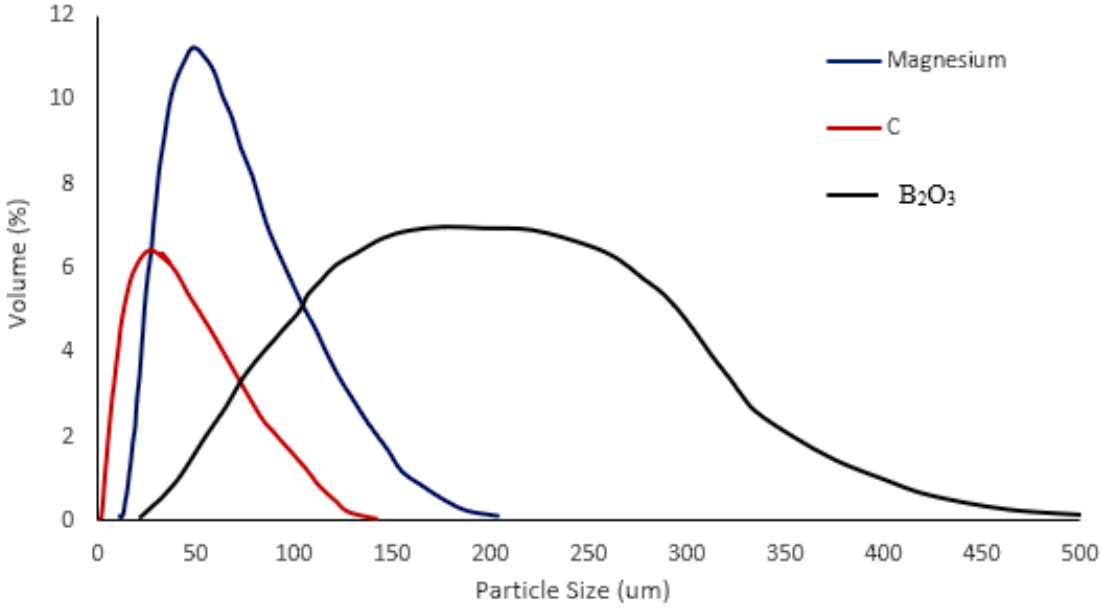

Figure 3.5. Particle size analysis results from Mastersizer

Table 3.1. Raw material particle size before and after an additional milling operation.

Raw Materials	Average Particle Sizes Without Operation (µm)	Average Particle Sizes After Milling Operation (µm)
C	49	-
Mg	57	-
B_2O_3	216	63

Due to the nature of mechanical alloying, the particle size reduction is expected to occur approximately during the first 2 hours. This is followed by the chemical reaction. During the chemical reaction, the targeted product formation starts with the help of a reducing agent through point combustion operations. This takes place by reducing similar size materials and entering them into the chemical reaction. In the mechanical alloying stage, some particles can be much larger or smaller than others, but differences up to 10-15 times cause reaction delays in the system. For example, mechanochemically, it is not desirable to have both 45 and 270

μm-sized particles in the system since small particles tend to react with small particles and large ones with large ones. As a result, there will be unreacted powders at the end of the experiment and the efficiency of the system will decrease.

In our system, the powders that would go into chemical reaction had the sizes of 49 and 216 μm, and since the reaction is expected to take place between powders with similar sizes following their reduction by the Mg powder. As a result, if mechanical alloying is performed with the initial particle sizes of the raw materials, the difference between the smallest and the largest value in the final particle size becomes high. The easiest way to prevent this is to keep the initial particle sizes similar. Therefore, a particle size reduction was applied to the boron oxide powders prior to mechanochemical milling and the particle size was reduced from 216 μm to 63 μm. The particle size analysis results of the B_2O_3 powder before and after the milling operation can be seen in Figure 3.6.

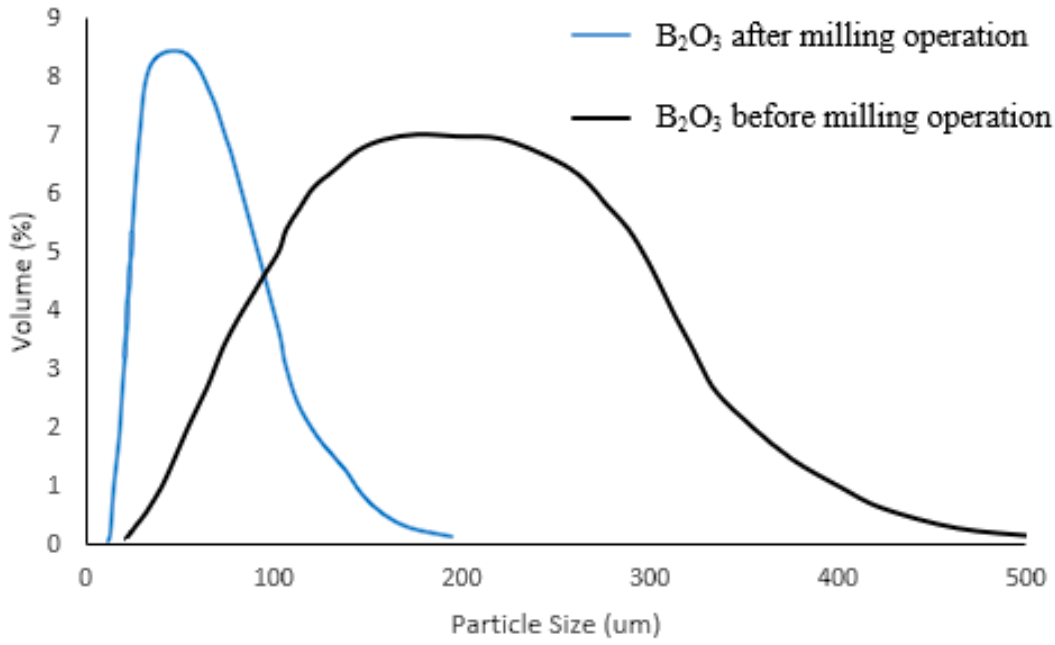

Figure 3.6. Particle size analysis results before and after B_2O_3 milling operation.

3.3 Mechanochemical Operation Parameters

3.3.1 BPR (Ball to Powder Ratio) Optimization

Ball to powder ratio (BPR) is one of the most critical parameters to achieve an efficient experiment. In this study, experiments were performed using different BPR ratios, as seen in Table 3.2.

Table 3.2. Summary of BPR optimization studies.

BPR(Ball to Powder Ratio)	Result
Under 10:1	Requires a long time interval
15:01	Effective
Above 20:1	Insufficient volume

The trials with different BPR are grouped like that, the BPR ratios under 10:1 include 5:1 and 10:1, and above 20:1 include 20:1 and 30:1. As it is summarized in Table 3.2, the chemical reaction process was very long, up to 12 hours boron carbide formation continues effectively. So the overall experiment could be characterized as inefficient in the trials with the BPR below 10:1. In trials above 20:1, the amount of raw material that can be used was greatly reduced to leave 40% free space with the large volume of balls required, even if this leads to a fast reaction, the yield of the production was very low. Because this study aimed to increase the amount that can be obtained with a mechanochemical operation run, this BPR ratio was not chosen. The BPR 15:1 provided both a relatively fast reaction and an acceptable yield. Therefore, the experiments continued with a BPR ratio of 15:1.

3.3.2 RPM Optimization

RPM is important for determining the rate of production. It is necessary to determine an optimum value. Table 3.3 shows the different RPM values tested in this study. In the experiments carried out for the optimization studies of the RPM, the previously optimized parameters, such as 15:1 BPR, inert gas, and raw material particle sizes, were kept constant. The RPM values to be tested values were based on the scientific literature [60]. In Table 3.3, the RPM values labeled as below 300 RPM are 100 and 200 RPMs, between 300-450 RPM corresponds to 350 and 450 RPMs, and above 450 RPM is 550 RPM.

Table 3.3. RPM Optimization results.

RPM	Result
Under 300 RPM	Inefficient-long time period
300-450 RPM	Effective
550 RPM	Deformation in the lattice of B_4C

In order to produce boron carbide at 300 RPM, a test period of at least 12 hours was required. While it is possible to produce B_4C efficiently with long milling times, it was not preferred due to the risks posed. The system must operate in the most inert environment possible. However, since the system has gaskets and valves, it has the risk of gradually losing its inert environment under the influence of highly activated mechanical movements like the angular velocity of revolution and angular velocity of rotation. That affects the final efficiency of the production and quality of the final product in an unrepeatable and controlled manner.

The RPMs higher than 450 resulted in the loading of excess energy to the system. Excess energy in the system also has drawbacks. Since the forces mentioned above are directly proportional to the impact speed and angular velocity, the

chemical reaction energy of the system increases with increasing RPM. Too high impact speeds cause the energy level to go above the optimum level and result in the distortion of the crystal structure and that causes peak broadening in the XRD results. While the lattice distortions in the structure are not desirable due to deviation from the properties in of th product, it also makes the analysis of XRD for determination of the amount of the phases in the structure very challenging, if not impossible. The examination of the XRD patterns of the product after experiments with RPMs above 450 shows the distortions in the structure with peak broadening as can be seen in Figure 3.7.

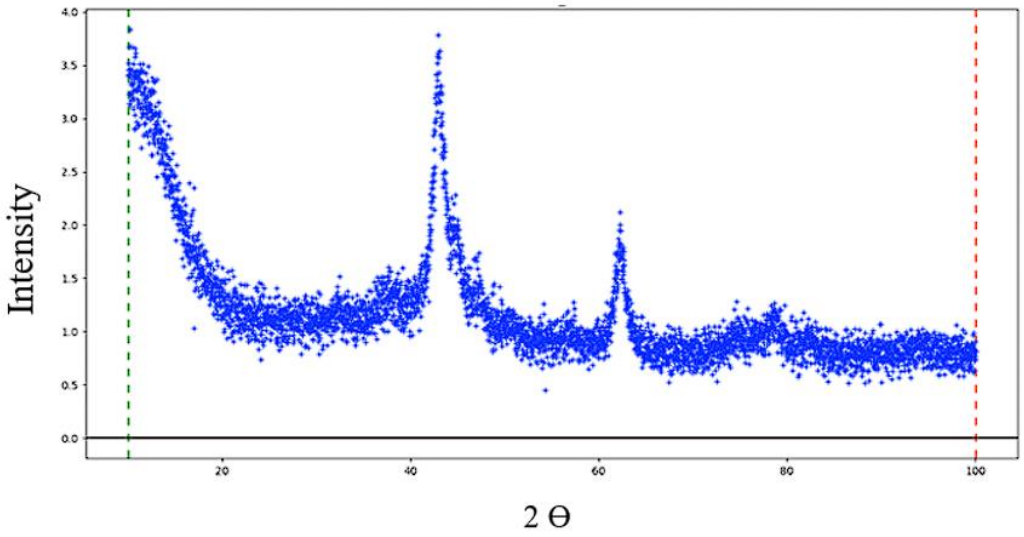

Figure 3.7. 550 RPM and more than 12 hours of mechanochemical milled powder.

Successful productions were achieved in the experiments carried out at 350 and 450 RPM. Prolonging the process at 300 RPM and below causes other problems and moves away from efficient production. The 550 RPM causes a more uncontrolled experiment due to being too fast. High RPM values caused undesirable lattice distortions. It was decided to continue with 450 RPM for a controlled and efficient process.

3.3.3 Milling Time Optimization

For boron carbide to be used in high-value-added applications, it must be reduced to the smallest possible particle size. After optimizing some of the parameters mentioned above, particle size analysis of the product and optimization of the milling duration were performed. In order to observe the effect of milling time on the particle size of the B_4C produced by mechanical alloying, the experiments with varying milling times were conducted while keeping BPR, RPM, ball size, inert atmosphere, jar size constant. The values of the constant parameters are given in Table 3.4. The particle size was analyzed for seven different duration ranging from 1 hour to 17 hours. Figure 3.8 illustrates the change in the particle size with increasing milling time. The plot shows that the fastest particle size decrease occurs within the first 3 hours. In this period, a 66% decrease in particle size was observed. It can be seen that the particle size reduction continues regularly in the milling processes for up to 8 hours. However, the particle size reduction did not progress rapidly at later milling times and almost stopped at 15 hours. The particle size of 1.41 μm at the end of 8 hours decreased to 1.15 μm at the end of 17 hours. A decrease of only 0.26 microns after 9 hours of milling shows that the efficiency of the system reached saturation after 8 hours of milling.

Table 3.4. Fixed mechanochemical milling parameters.

Parameters	
BPR	15:01
RPM	450
Ball Size	8 and 10
Atmosphere	99.99% argon
Jar Size	300 ml

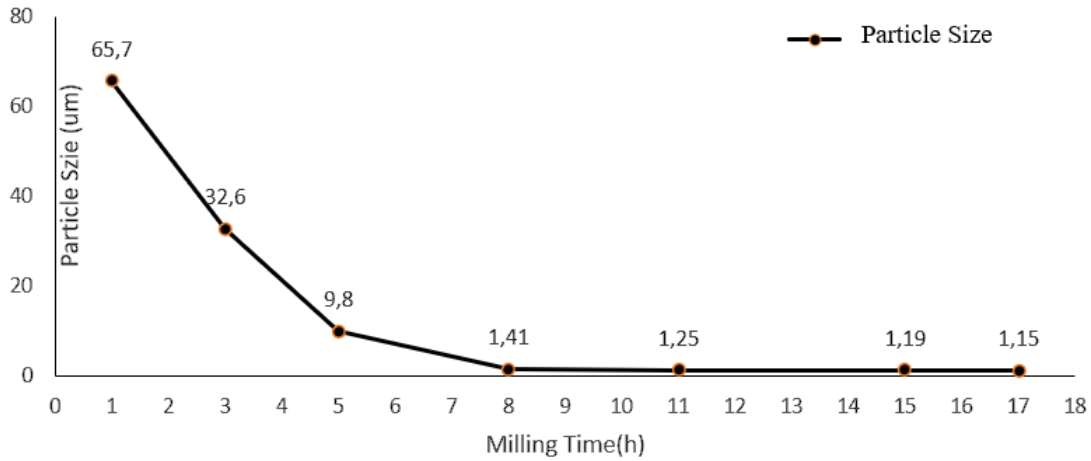

Figure 3.8. Particle size change with the milling time.

For the production method that is optimized here, that is the smallest particle size that can be achieved without causing problems in the system. As mentioned in the literature review, it is better to choose bigger ball sizes that will create a higher degree of crushing for larger particle size reduction. In addition, in order to reach particle sizes of 100 nm and lower, it is necessary to load more energy into the system by increasing RPM. However, starting or continuing the experiment with a higher RPM speed causes the problems mentioned earlier, such as more contamination from the materials used, more energy consumption, and the risk of crystal structure deterioration.

Figure 3.9 shows the results of XRD analysis after 3 hours, 5 hours, and 8 hours. According to these results, from 3 hours to 8 hours, Magnesium decreases, which is the reductant in the system, the increase of MgO, the main by-product, and the increase of B_4C peaks in the 8-hour XRD result, despite the highly dominant MgO.

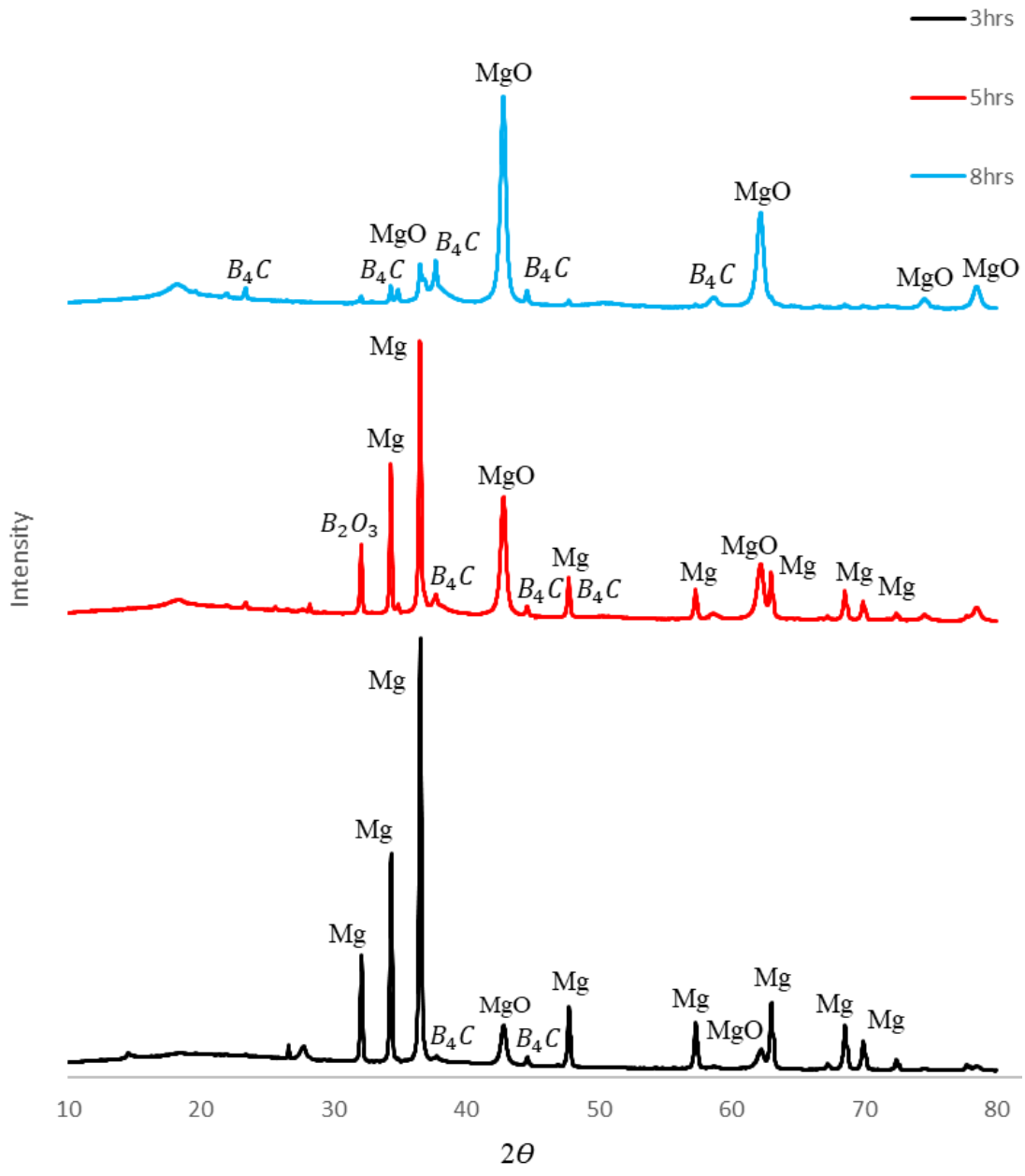

Figure 3.9. 3 hour, 5 hours and 8 hour XRD results.

In Figure 3.10, particle sizes and morphologies are shown for 3, 5, and 8 hours of the mechanochemical milling operation. It can be seen in the 3-hour SEM image that the particle size was smaller than the initial particle sizes, but still, a wide

range of particle size distribution could be observed. On the other hand, after 5 hours of milling, the amount of smaller size particles was increased and these small particles were wrapped around the larger particles. Finally, looking at the 8-hour milling result, the particle size distribution is narrowed and the majority of particles are in the range of 2 μm. At this point, the particle size cannot be reduced further with the determined parameters of the system. For smaller particle size results, it is necessary to change the parameters such as BPR and ball size towards increasing the crushing effect in the system.

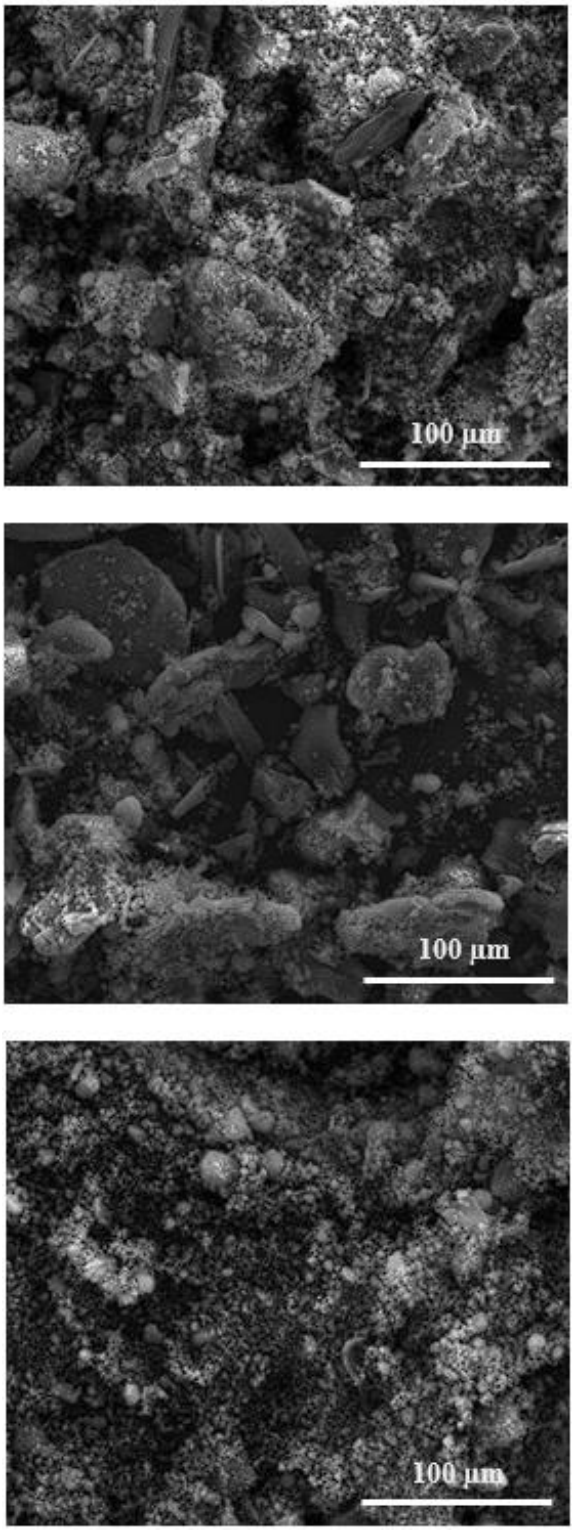

Figure 3.10. SEM images of the samples taken at different time intervals in the mechanochemical operation, 3 hours milling (upper), 5 hours milling (middle), and 8 hours milling (below).

3.4 Acid Leaching

The step following mechanical alloying for the production of boron carbide by the mechanochemical operation is acid leaching. The mechanical reduction yields a product with a large amount of contamination from the grinding medium and the jar. Removing not only the contamination but also the unreacted raw material and by-products from the system is critical for the purity of the final product. The reducing agent determines the type of the main by-product. In the case of using magnesium as a reducing material, magnesium oxide formation occurs in the system. In addition, different impurities are mixed into the system apart from the reducing agent. These can be things such as iron mixed with the system and ambient dust in the production stages. Obtaining a completely pure product due to the by-products formed in the system is only possible with acid leaching for mechanochemical milling operation.

Besides the fact that acid leaching is critical for obtaining a quality product, one of the main issues to be considered when performing acid leaching is not to damage the main product.

The powders used in acid leaching optimization were produced with milling parameters, the optimized values of which were presented in the previous sections. Some parameters were optimized according to information gathered from the scientific literature, while experiments optimized others. The optimization criteria are based on the amount and quality of the final products. Following leaching, the collection and separation of powders by centrifuge, extraction, and washing and drying of powders are required.

After determining the important parameters for acid leaching, studies were carried out to optimize the basic parameters important for acid leaching. These important parameters are acid type and molarity, leaching temperature, magnetic stirrer RPM, leaching time, and final results.

3.4.1 Acid Molarity

Since nitric and some other acids are much weaker than hydrochloric acid for the successful removal of iron, magnesium oxide, and unreacted raw materials remaining in the system, hydrochloric acid was used [187], [200].

Another important parameter is the acid concentration. While optimizing the acid molarity, the leaching time, table temperature, and stirring speed were kept at 30 minutes, 40 ℃, and 500 RPMs, respectively, based on the scientific literature.

According to equation 10 and equation 11 given below, the experiments carried out for acid concentrations that can be seen in Table 3.5, with three different levels as under 1 M,1 M, and over 1 M.

$$M1 \times V1 = M2 \times V2 \quad (10)$$

$$M = \frac{\% \text{ x. d. } 10\ MA}{MA} \quad (11)$$

The visual results were very helpful for optimizing the acid molarity. As summarized in Table 3.5, conditions such as overflow, foaming, or insufficiency of mixing can be observed in the system.

Table 3.5. Acid molarity optimization results.

Molarity	Result
Under 1M	Low solvent effect
1M	Effective
Above 1M	Overflow and uncontrolled reaction

The first trial was made with under 1M in order to reveal the effect of the procedure on the product and safety limits. Then, it was continued with a trial at 1M. Finally, above 1M trials were performed and the results were compared. The dilute mixture was placed in a 500 ml borosilicate beaker during this process. Then, the powders obtained after mechanochemical milling were collected and added slowly. Discharging all the powder at once caused foaming and a sudden reaction in the system, resulting in an overflow of the acid solution and the powder. It was decided to slowly add the powders to the stabilized mixture until the entire amount of powder was added. Furthermore, the size of the beaker was changed to 1.5 L as a further precaution against overflow.

During the slow addition of the powders to the system with the help of a spatula, a slight foaming and reaction started with the effect of the powders mixed into the system. The system became stable again by absorbing the foam within 8 to 10 seconds and new powders were added. 2 minutes after adding all powders, the reaction accelerated after the system continued to mix with the magnetic stirrer and the temperature of the system increased by 10℃ and started to emit smoke close to orange color. This process continues for about 2 minutes. At this stage, it was observed that chemical dissolution starts. At the same time, it was also observed that the leaching operation starts in the system.

The final product, which was acid leached with a solution of molarity less than 1M, was analyzed visually and by Rietveld analysis. The analysis showed that the iron and magnesium by-products in the system had not yet been completely dissolved. This result did not change even though the time was extended. Even in the 30-minute acid leaching period, the solution did not foam and react as much as with other molarities at the time of adding the powders. The dissolution of the iron observed in the 1M portion did not occur either. Therefore, regardless of the duration, leaching cannot be performed in less than 1M.

After unsuccessful attempts with acid molarity under 1M, trials were carried out with acid molarity of 1 M. The experiment with 1M acidic solution was

completed visually and experimentally without any problems, Rietveld Analysis (Table 3.8) was performed, and it was observed that the leaching process was successful.

In order to test if, with higher acid molarity, the leaching can be completed in a shorter duration, the test was performed with the same parameters that were used for 1M acidity trials with acid molarity higher than 1M. Although the powders were slowly introduced into the system, foaming and overflowing occurred. Even addition of 0.5 grams of powder, foam accumulated on the upper surface and slowly overflowed, and with the overflow, a large amount of gas was released. The stirring speed was the first parameter changed to slow the reaction, but lower stirring speeds were ineffective in preventing overflow.

Increasing the acid molarity resulted in an uncontrollable reaction, overflow, foaming, and dissolving of the targeted product, B_4C. Therefore, acid molarity is chosen as 1 M.

3.4.2 Leaching Temperature

After optimizing the molarity of the acid, the leaching temperature was varied to observe its effect on the purity of the product. The tests were conducted at two different temperatures, as shown in Table 3.6, namely 40 ℃ and 70 ℃.

Table 3.6. Leaching temperature optimization results.

Leaching Temperature	Result
40°C	Dissolution of by-products started, but not all of them were dissolved
70°C	All unwanted products are dissolved

Firstly, the leaching temperature was set to 40 ℃. It could be observed that the chemical reaction, foaming, and orange smoke output in the system occurred slowly. However, visually, it was observed that iron in the form of shiny pieces large enough to be seen with the naked eye remained in the system. Likewise, even if magnesium oxide started to dissolve, it was not completely removed from the system. Therefore, it was decided to use a higher leaching temperature of 70 ℃.

In the experiments carried out at 70 ℃, it could be observed that the chemical reaction, foaming, and orange smoke output in the system during the addition of the powders to the system was higher in comparison to those at 40 ℃. It is seen that the value in the thermometer approaches around 75 °C during the instantaneous addition of powders. After the temperature increase in the system, the system was measured to be 70 ℃ again with a thermometer immersed in the beaker. The temperature increase during the first introduction of powder to the acid solution did not stay constant during the whole process of the powder addition. A hot plate was used to keep this temperature constant at 70 ℃. During leaching at 70 ℃, the formation of an iron layer was observed on the surface of the acid solution, proving that the iron residue was dissolved and floated on the surface. Based on these findings, the acid leaching temperature was chosen as 70 ℃.

3.4.3 Magnetic Stirrer RPM

Experiments between 100 and 1000 RPM were performed. As shown in Table 3.7, the following results were obtained.

Table 3.7. Stirrer RPM optimization.

Stirrer RPM	Result
Under 200 RPM	Balancing problem
200-300 RPM	Effective stirring
Above 300 RPM	Magnetic connection lost

If the fish was too slow (200 RPM and below), it could not create enough flow and stirrer effect in a solution containing powder, and the inertia of the water overcame the fish's mobility and caused balance problems.

If the experiment was carried out too fast (300 RPM and above), the required vorticity was provided in the solution, but in some physical situations, such as powder becoming stationary at a point and starting to accumulate. Higher speeds increased the effect of the position of the fish and prepared the ground for the magnetic connection to break. Even if a visually efficient vorticity was observed, usually within 1-3 minutes the fish slipped out of position and started to hit the beaker uncontrollably. Therefore, leaching operations were continued at 250 RPM for optimum efficiency.

3.4.4 Leaching Time and Final Results

Leaching time is an important parameter in terms of the complete removal of the by-products. The duration is required to be optimized so that all the by-products are removed without any deterioration of the targeted product.

In this study, two different durations were tried, namely 10 minutes and 20 minutes. After the 10-minute experiment, the iron residue did not dissolve completely and did not rise to the surface, as described in the previous section. It could also be observed by visual examination that the reaction continued at a certain rate upon completion of the 10 minutes. The 20-minute experiment resulted in the deposition of a glossy iron layer on the upper surface of the solution, showing that the reaction was largely successful. Observationally, after the reaction reached saturation, the system was stopped at the twentieth minute, and the powders were collected and prepared for the test.

Figure 3.11 illustrates the Rietveld analysis results from GSAS-II software. According to this result, it was seen that the sample was extremely rich in the main by-product, MgO, after milling (Figure 3.11(a)). However, in the second image (b),

it can be observed that all the main peaks of boron carbide settled after the acid-leaching operation. According to the analysis, the acid-leaching effectively removed the by-products and the contamination. After leaching, there were only B_4C and some free carbon in the powder.

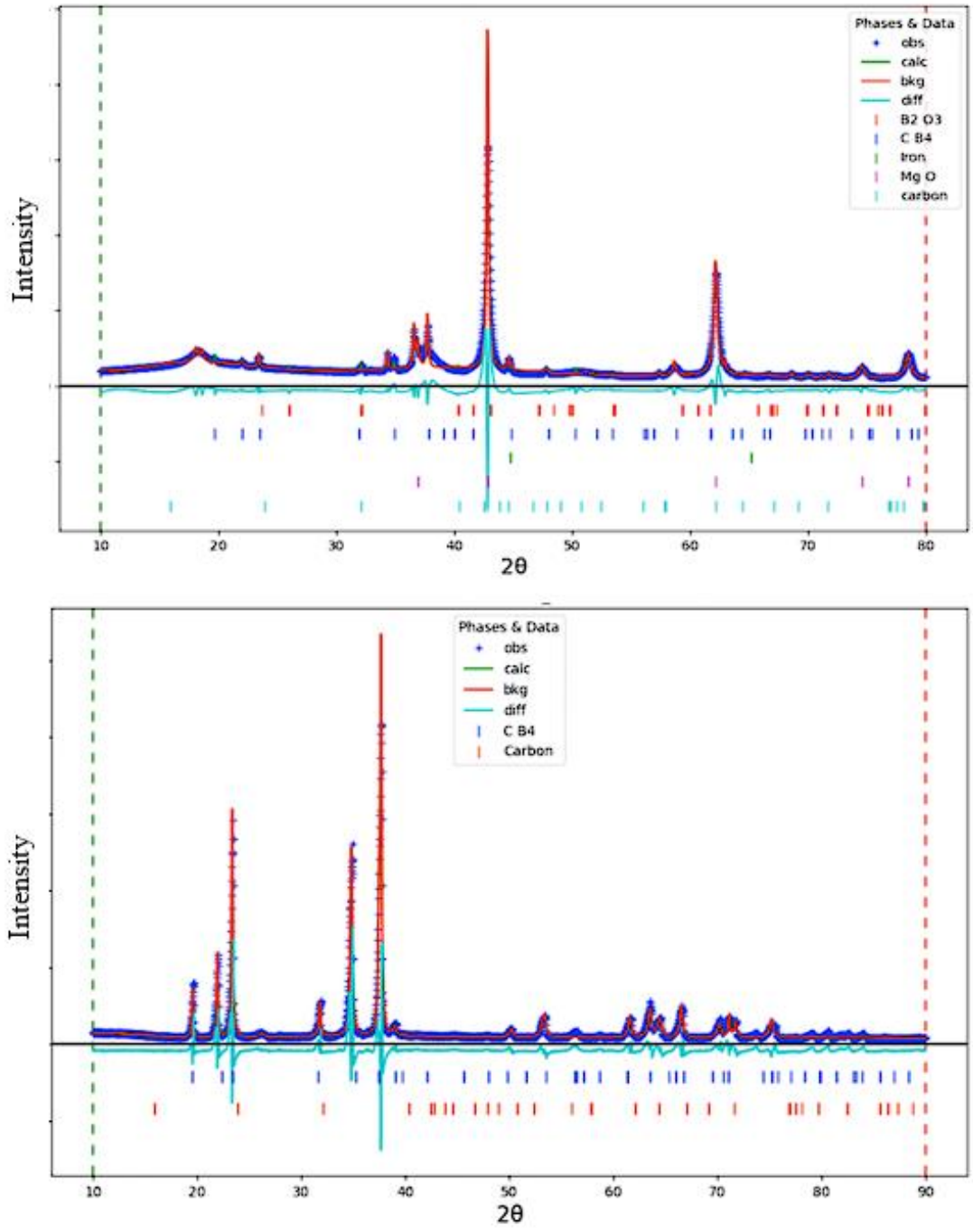

Figure 3.11. GSAS-II software Rietveld analysis, (a) 8 hour milled sample, and (b) acid leached sample.

Table 3.8 shows the phase analysis of the 8-hour milling sample, the most successful sample, before and after acid leaching, and the Rietveld results of the acid leaching operation performed for this sample. Also according to results, after successful leaching, there are no any by-products and contamination remained.

Table 3.8. Purity of 8h milled sample and purity of acid leached sample.

	B_4C	MgO	C	Fe	Mg	B_2O_3
Before Leaching (8h)	14.1	74.7	1.2	5.9	3	1.2
After Leaching	98.08	0	1.92	0	0	0

Figure 3.12 shows the powders again before and after acid leaching. Before the acid leaching operation, boron carbide, the targeted main product, was covered with by-products, as seen in Figure 3.12 (a). After the acid leaching operation, the boron carbide particles were visible without residue on them (Figure 3.12 (b)). This point was more evident at higher magnification, as shown in Figure 3.12 (c). In addition, as seen in Figure 3.13, no experimental environment residues other than B and C were found in the EDS image taken after the acid leaching operation. Only Si detected by EDS is thought to come from the coating for conductivity in preparation for the SEM operation.

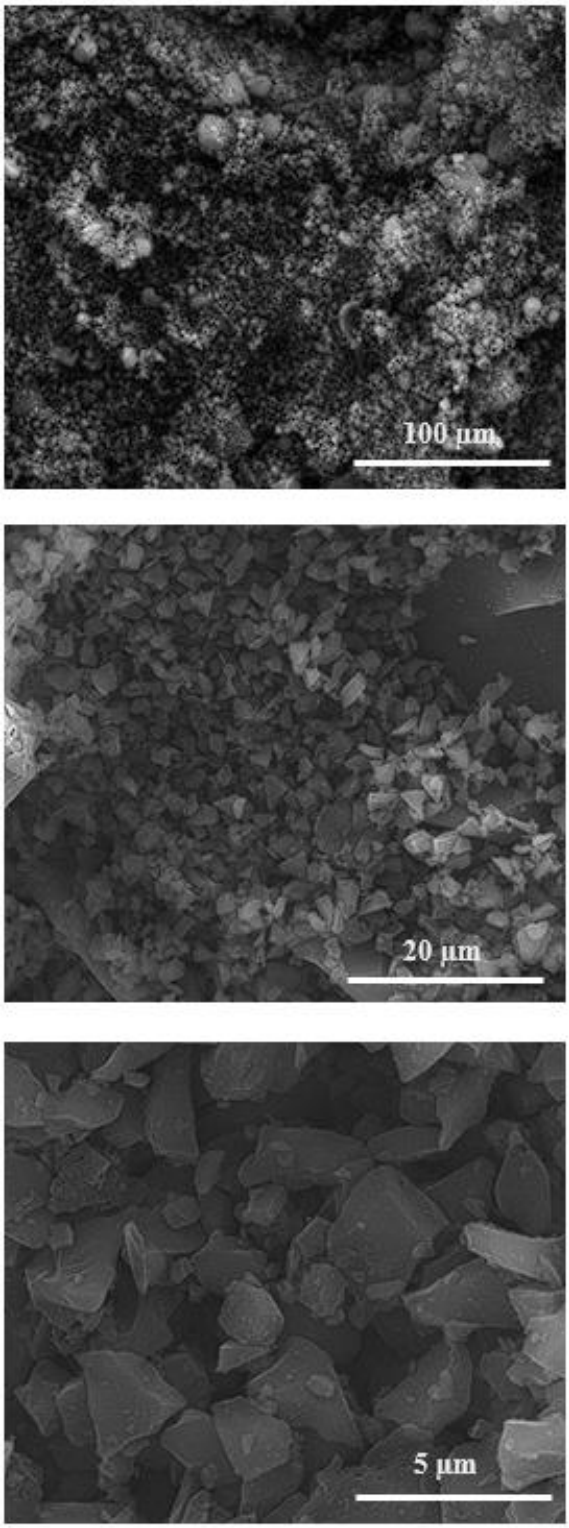

Figure 3.12. Before and after SEM images for acid leaching operation, 8 hours milling (upper), 8 hours milling and after acid leaching (middle), and acid leached 20.000x magnification (below).

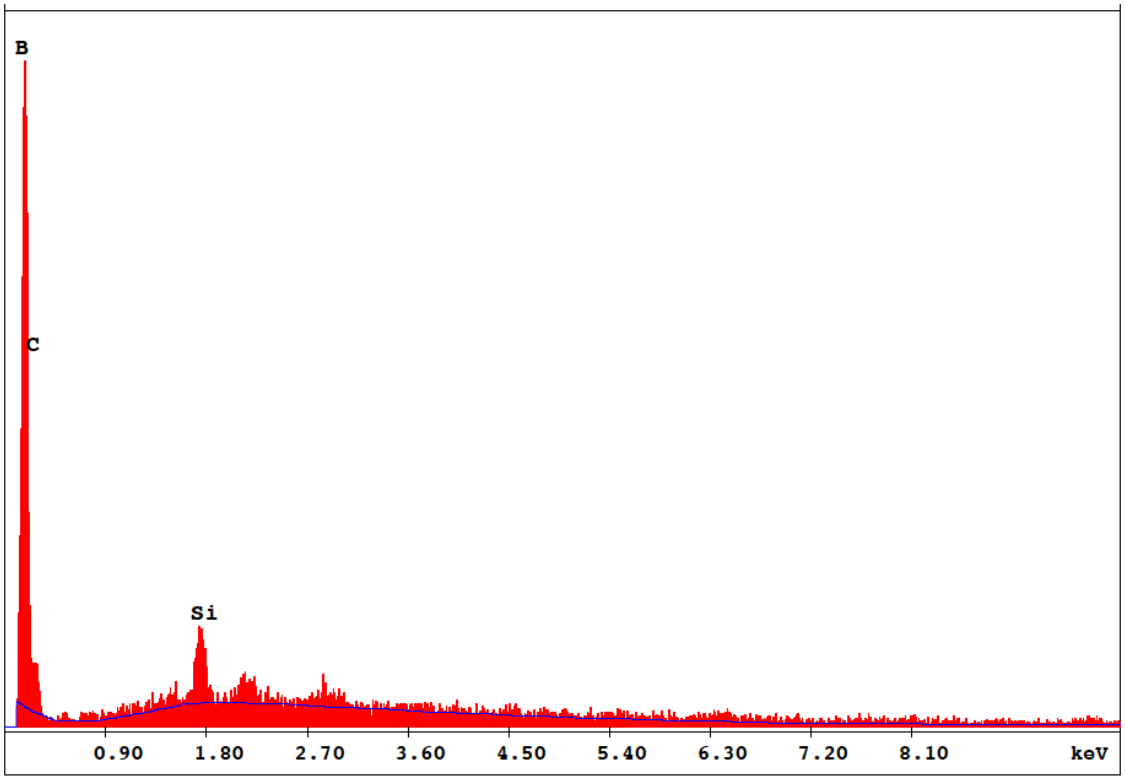

EDAX ZAF Quantification (Standardless)
Element Normalized
SEC Table : Default

Element	Wt %	At %	K-Ratio	Z	A	F
B K	87.40	88.61	0.7336	0.9913	0.8467	1.0000
C K	12.39	11.31	0.0076	1.0618	0.0575	1.0000
SiK	0.21	0.08	0.0022	1.0111	1.0524	1.0000
Total	100.00	100.00				

Element	Net Inte.	Bkgd Inte.	Inte. Error	P/B
B K	268.88	9.75	1.76	27.57
C K	25.83	8.50	7.08	3.04
SiK	52.90	20.68	5.13	2.56

Figure 3.13. EDS result obtained by SEM device after acid leaching operation.

Therefore, for acid leaching operation, a magnetic stirrer of 250 RPM gave the optimum result in 20 minutes at a leaching temperature of 70 ℃.

3.5 Steps Following Acid Leaching and Obtaining Final Powder

3.5.1 Centrifuge Operation Optimization

Successful collection and separation of powders exposed to acid leaching from the leaching solution is very crucial for effective production. At the initial stage of these processes, it was predicted that waiting would be sufficient to collect the purified powders from the acidic solution. However, even after waiting periods of up to 10 hours, the mixture was not sufficiently clarified and particles floating in the solution were observed. Only about 70% of the total powder content was observed to settle. Therefore, it was decided to use a centrifuge. Another important point here is that keeping the product in acid for hours after the milling operation has the potential to damage the product. While performing this operation, the RPM and duration were varied to find the optimum values. After several trials with 1000 and 2000 RPM and 5 and 10 minutes, it was seen that most of the powders precipitated and the solution became very clear after precipitation at 3000 RPM for 20 minutes. However, the solution was not expected to be as transparent as at the beginning of the experiment due to the impurities dissolved from the substances in it. The precipitation operations were performed at 3000 RPM for 20 minutes using 4 units of 50 ml centrifuge tubes.

3.5.2 Drying

Successful drying of powders is as critical as successful test operations. The contamination of the powder by ambient dust should be avoided during drying. The first drying experiments attempted to dry the pure water-mixed material in a borosilicate chamber in an oven at temperatures as low as 50 ℃. However, after this operation, it was observed that most of the powder produced adhered to the bottom of the pot. In addition, the majority of the particles stuck together. This resulted in the formation of an agglomeration-like structure. Early-stage agglomeration could

be observed visually as the particles attracted to each other. In order to get rid of this situation, a small grinding operation might be sufficient, but it was aimed at completing the production process cycle with maximum efficiency since regrinding a product that has already been purified after the grinding process would lead to a loss of efficiency. The inclusion of the third stage of the production method, which already included two stages, would make it extremely difficult to produce high quantities. Therefore, a more successful drying operation was required.

The second drying trial after the oven trial was to keep the powders in a sterile cabinet at room temperature for 24-30 hours. After this process, it was observed that the early stage agglomeration was not as emphasized as in the oven, but the gathering of powders, such as agglomeration still occurred. Therefore, instead of alcohol was decided to be used for the drying operation for better results as it is generally applied for the drying of nanomaterials. The products washed with pure water were placed in a borosilicate chamber and high-purity alcohol was added. 18% of the powder-to-alcohol solution ratio was used. In this way, the alcohol would be able to disperse the powder more efficiently and expose it to drying. Doing so, it was aimed to minimize the surface tensions on the end product, boron carbide. During the drying operation, it was placed in a sterile cabinet and left to dry at room temperature. The main purpose of the drying operation was to evaporate as much of the acid solution as possible. When evaluated in this way, since alcohol evaporates much faster than water, the drying operation that takes 30 hours in pure water was completed in 7-8 hours in alcohol.

After the drying operation with alcohol, although there was a slight adhesion to the surface, it was seen that weak agglomerations occurred much less. Compared to drying with the aqueous solution, agglomeration-like structures were observed in the water-dried samples and additional milling operation might be required to obtain reliable test data. However, after drying with alcohol, this situation disappeared and powder was obtained, at least not visually sticky. Therefore, this drying method was used in all experiments.

3.6 Kinetic Modelling of the System and General Results

There are limited studies on the kinetics of mechanochemical milling in the scientific literature. Interpretations can be made on the kinetic by calculations from evaluation of the percentage transformations of the main products that are expected to form at a constant temperature. Since no additional temperature input is provided to the system during the production of boron carbide by the mechanochemical method, it will be possible to interpret the kinetics of the process by Johnson–Mehl–Avrami–Kolmogorov (JMAK) model.

In order to perform the kinetic modeling of the system, the value of n can be found by using the Avrami equation. With the n value found, it is possible to interpret the kinetics of the system.

The production of the B_4C and the by-products was found to follow the Avrami kinetics in the system studied here. The kinetic behavior of the system was studied by quantitative phase analysis via X-Ray diffraction and Rietveld Analysis. Table 3.9 includes the percentage weight transformations for B_4C and MgO with respect to time as obtained by Rietveld Analysis. Weight transformation values taken with the help of GSAS-II software. Figure 3.14 shows the percentage transformed vs. milling time. The fraction of transformation *y* is a function of time *t* as follows according Avrami eqaution:

$$y = 1 - \exp(-kt^n) \qquad (12)$$

$$\mathrm{n} = \frac{\ln\left(\ln\frac{1}{1-y}\right) - \ln k}{\ln t} \qquad (13)$$

where *k* and *n* are time-independent constants for the particular reaction.

By convention, the rate of a transformation is taken as the reciprocal of time required for the transformation to proceed halfway to completion, $t_{0.5}$, or

$$\text{rate} = 1/\, t_{0.5} \qquad (24)$$

Table 3.9. Weight percentage transformed of B_4C and MgO with respect to milling duration for 450 RPM, 15:1 BPR.

Time (hrs)	B_4C amount (%)	MgO amount (%)	C amount (%)	Fe amount (%)	Mg amount (%)	B_2O_3 amount (%)
1	0	2.9	11.1	0	63.6	22.2
2	1.7	13.7	10.8	1.2	59	18.4
3	3.5	21.2	8.9	2.5	42	13.7
4	5.9	34.6	6.7	3.6	37	9.4
5	8.4	46.8	5.9	4.2	28	5.9
6	11.8	57.2	4.2	4.7	19	3.7
7	13.2	68.8	2.9	5.1	8	2.8
8	14.1	74.7	1.2	5.9	3	1.2
9	14.3	75.8	0.9	6.5	2.8	1.1
10	14.4	76.1	0.8	6.9	2.6	1
12	14.4	76.2	0.8	7.3	2.6	1

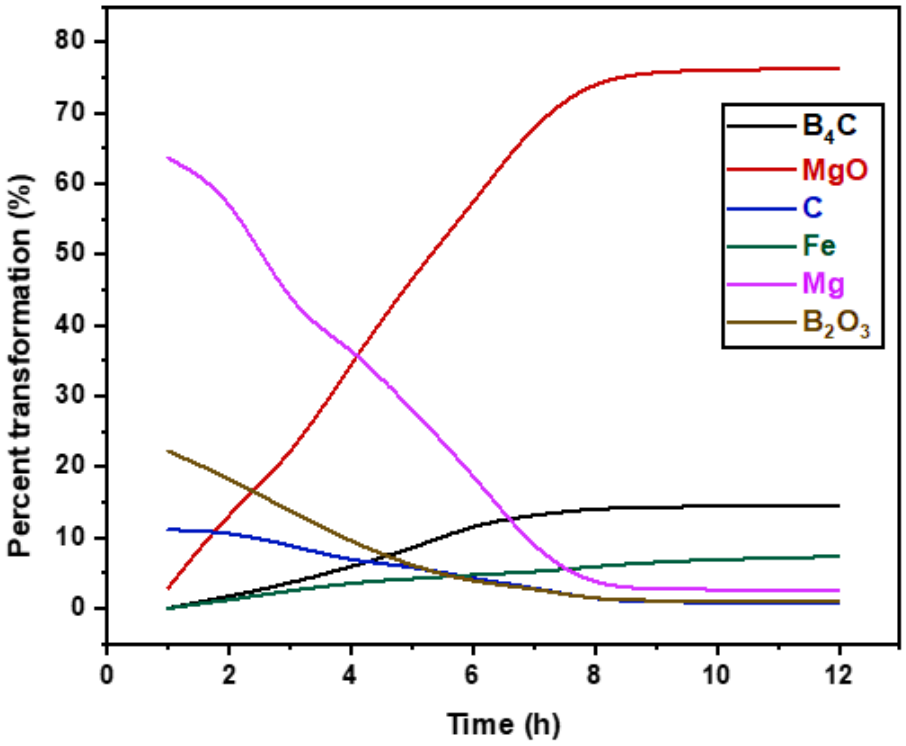

Figure 3.14. (a) Percentage transformed as a function of milling time.

To find the order of reaction, n, we need to calculate rate constant, k, and time $t_{0.5}$ from the graph plotted between percentage transformation values of B_4C and MgO. The value of k, n, and $t_{.0.5}$ was calculated by curve fitting as shown in Figure 3.15. The weight percentage values used in table 3.9, which are obtained from these 2 graphs, are used. In order to see the changes in the ratios more easily, the highest value was set to 1 and the other values were processed at the same rate. The graph that appeared in the form of S in the logarithmic graph obtained afterwards is also seen in the Avrami calculations in the literature. Also, equations (13) and (14) along with transformation percentages of B_4C and MgO were used for calculated Avrami equation constants. That are provided in Table 3.14.

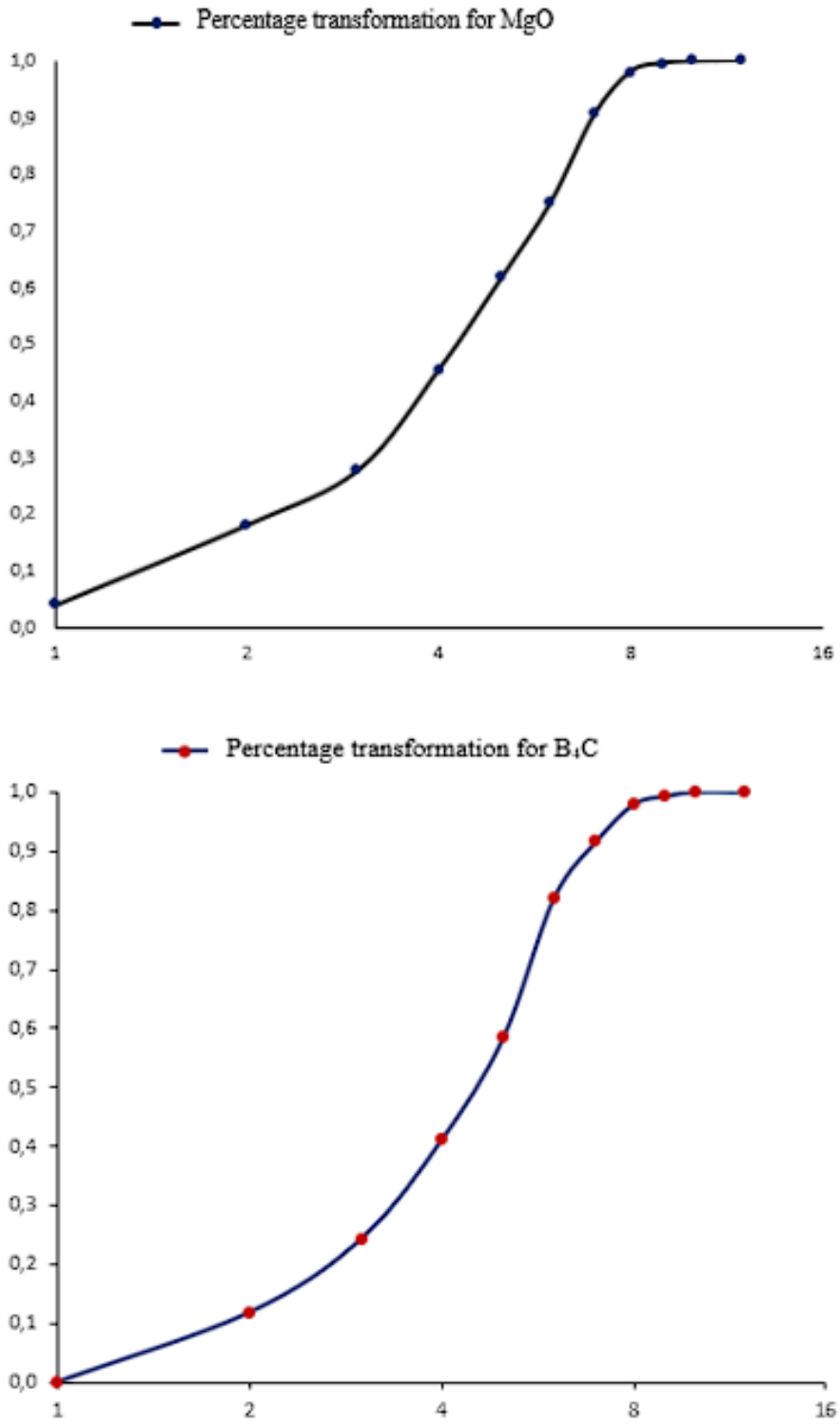

Figure 3.15. Change of percentage transformed for MgO and B_4C as function of time (symbols) and the Avrami equation curve fitting (lines).

Table 3.10. Curve fitting of the B_4C and MgO transformation.

Phase	model	k	n	$t_{0.5}$	r-square	Adjusted r-square
MgO	Y=1-exp(-kt^n)	0.003	1.7	226.08	0.972	0.965
B_4C	Y=1-exp(-kt^n)	0.0025	1.7	234.87	0.962	0.953

Calculated results can be seen in Table 3.10, according to n value results it is understood that there is the transformation is a boundary-controlled process taking place mainly by one dimensional growth.

Also, $t_{0.5}$ calculated from the graph in Figure 3.15. B_4C and MgO formation rates can be interpreted with the help of rate. As mentioned before rate =1/ $t_{0.5.}$ Rate values for MgO is $4.42x10^{-3}$ and for B_4C is $4.26x10^{-3}$. According to these results, it is seen that MgO transformation is faster than the B_4C.

CHAPTER 4

CONCLUSION

In this study, the synthesis of B_4C, the 3rd hardest material, was carried out at room temperature by mechanochemical operation. Since this product is mainly used in critical sectors such as the defense industry, aviation, space, and nuclear sealing, its qualified production is important.

The most common production method of boron carbide is the carbothermic method. With this method, boron carbide synthesis takes place at high temperatures of more than 2000 ℃. The value of energy is increasing due to problems such as global warming, climate change, and polluting production methods in access to electrical energy. Therefore, production methods that consume less energy are gaining importance. One of the most important advantages of mechanochemical operation is the ability to synthesize at room temperature. The same amount of boron carbide produced with 11 dollars of energy consumption, with the mechanochemical method can be produced with 0.66 dollars of energy consumption. On the other hand, the disadvantage of mechanochemical alloying is the low yield. However, with kinetic modeling of the system and scale-up operation, higher production will be possible. A higher amount of boron carbide was produced by designing a reaction chamber that would discharge the friction and dangerous pressure that would be higher in scaled-up operations. One of the most important advantages of this system is that it is possible to produce products with sizes of 2 μm and below without any additional operation. With the carbothermic method, milling is performed as a third operation to obtain the same particle sizes. This results in additional energy costs. In engineering powders used in critical sectors, small particle size is required. Considering that they are used even down to the nanometer level, it will be possible to synthesize this product only with mechanochemical milling.

On the other hand, in other low-temperature B_4C synthesis methods, the multi-stage production method and non-standardized product quality reduce the usability of the product in qualified sectors. Ball-to-powder ratio (BPR), milling speed (RPM), and milling time are critical for mechanochemical alloying, which is the first step in this two-step production method. In the BPR optimization 10:1, 15:1, and 20:1 ratios were tested. It was seen that the ratio of 15:1 provided the optimum efficiency. 200, 350, 450 and 550 RPM values were tried for RPM optimization. When timing and product quality were examined, it was seen that 450 RPM gave the most successful results. For the milling time, the previously optimized parameters were fused, and the samples were tested at 1-hour intervals starting from 1 hour up to 17 hours. At this stage, 8 hours of milling was found to be optimum when the effective reduction of the particle size paused. In order to produce higher amount of B_4C, scale up operation was performed with a special reaction chamber design. Some milling types (mixer mills etc.) used for production with this method, the production amount is limited to 4-5 grams. However, after a special chamber design is realized with the scale up operation, the amount of B_4C produced in a single run can reach up to 15 grams.

After this, the optimization of acid leaching parameters, the second step for this production method, was carried out. Acid type and molarity, leaching temperature, stirrer RPM, and acid leaching time were evaluated. For the HCl acid leaching operation, experiments were carried out under stoichiometric ratio, at stoichiometric ratio, and above stoichiometric ratio. It was observed that the most efficient operation was realized at stoichiometric ratio. For the other important parameters, leaching temperature, 40 and 70 ℃ were compared and it was observed that more successful purification was achieved in the experiments performed at 70 ℃. Magnetic stirrer RPM is important for leaching in an efficient time and 250 RPM value among the different ranges tried provides the most efficient stirring. In the last parameter, leaching time, it was observed that the impurities could be completely removed from the system after 20 minutes.

In the process of performing all these optimizations, different characterization techniques were used to compare the results. MasterSizer was used for particle size analysis. With the data obtained after XRD analysis, Rietveld analysis was performed to determine the phases and this process was performed in GSAS-II software. The particles were also subjected to SEM electron microscopy for efficient comparison.

Before the acid leaching operation, by-product formation and contamination were observed in the system. After 8 hours of mechanochemical operation, the amount of MgO, the man by-product, was 74.7%. Apart from this, unreacted carbon was found to be 1.2%. The final product also contained 5.9% iron, 3% unreacted magnesium, and 1.2% B_2O_3.

Rietveld analysis performed after the acid leaching operation showed that the first detected impurities disappeared. With this successful leaching operation, no detectable foreign matter other than B_4C and 1.92% carbon was found in the system. As can be seen in the section where the details of acid leaching are explained, removing the iron from the system with acid is not difficult after reaching the appropriate temperature and time. The waste B_2O_3 remaining in the system can be dissolved even with the help of hot water since it has weak bonds. MgO and Mg, on the other hand, have a structure that dissolves to a certain extent, even with unheated acid. As a result of all these, it is possible to obtain almost pure B_4C after a successful and efficient acid-leaching operation. Carbon contamination is a common problem in commercial powders. The main purpose here is to obtain the product with the lowest possible carbon content. Considering that it is possible to encounter examples with an approximate B_4C /C ratio of 92/8% in products produced by the carbothermic method, these ratios are suitable for use in critical industries.

As a result, mechanochemical milling was carried out for 8 hours at 450 RPM at a BPR ratio of 15:1, followed by acid leaching with hydrochloric acid for 20 minutes at 70 ℃ and 250 RPM. Finally, particles with a purity more than 98% and a particle size of less than 2 microns were synthesized.

REFERENCES

[1] H. F. Mark, N. Bikales, C. G. Overberger, and G. Menges, “Encyclopedia of polymer science and engineering,” *Photographic applications to polyesters, elastomeric*, vol. 11, 1987.

[2] G. Göller, “Bor karbür oluşum koşullarının belirlenmesi ve toz karakterizasyonu.” Fen Bilimleri Enstitüsü, 1992.

[3] F. Thevenot, “Boron carbide—a comprehensive review,” *Journal of the European Ceramic*, vol. 6, no. 4, pp. 205–225, 1990, Accessed: Dec. 02, 2022. [Online]. Available: https://www.sciencedirect.com/science/article/pii/095522199090048K

[4] A. Chauhan, M. C. Schaefer, R. A. Haber, and K. J. Hemker, “Experimental observations of amorphization in stoichiometric and boron-rich boron carbide,” *Acta Mater*, vol. 181, pp. 207–215, 2019, doi: 10.1016/j.actamat.2019.09.052.

[5] A. K. Suri, C. Subramanian, J. K. Sonber, and T. S. R. Ch Murthy, “Synthesis and consolidation of boron carbide: A review,” *International Materials Reviews*, vol. 55, no. 1, pp. 4–38, Jan. 2010, doi: 10.1179/095066009X12506721665211.

[6] R. A. Andrievski, “Micro- and nanosized boron carbide: synthesis, structure and properties,” *Russian Chemical Reviews*, vol. 81, no. 6, pp. 549–559, Jun. 2012, doi: 10.1070/rc2012v081n06abeh004287.

[7] K. Shirai, “Electronic structures and mechanical properties of boron and boron-rich crystals (Part I),” *Journal of Superhard Materials*, vol. 32, no. 3, pp. 205–225, Jun. 2010, doi: 10.3103/S1063457610030068.

[8] N. S. Hosmane, J. A. Maguire, and Z. Yinghuai, “Polyhedral boron cage compounds: An account,” in *Main Group Chemistry*, Dec. 2006, vol. 5, no. 4, pp. 251–265. doi: 10.1080/10241220701607501.

[9] W. Zhang, S. Yamashita, and H. Kita, “Progress in pressureless sintering of boron carbide ceramics–a review,” *Advances in Applied Ceramics*, vol. 118, no. 4. Taylor and Francis Ltd., pp. 222–239, May 19, 2019. doi: 10.1080/17436753.2019.1574285.

[10] G. S. Samy and S. T. Kumaran, “Measurement and analysis of temperature, thrust force and surface roughness in drilling of AA (6351)- B_4C composite,” *Measurement (Lond)*, vol. 103, pp. 1–9, 2017, doi: 10.1016/j.measurement.2017.02.016.

[11] A. B. Dresch, J. Venturini, S. Arcaro, O. R. K. Montedo, and C. P. Bergmann, “Ballistic ceramics and analysis of their mechanical properties for armour applications: A review,” *Ceramics International*, vol. 47, no. 7. Elsevier Ltd, pp. 8743–8761, Apr. 01, 2021. doi: 10.1016/j.ceramint.2020.12.095.

[12] A. Lipp, “Boron Carbide: Production, Properties, and Applications. | National Technical Reports Library - NTIS,” *Tech. Rundsch.*, vol. 58, no. 7, pp. 1–47, 1966.

[13] J. L. Hoard and R. E. Hughes, “Elemental Boron and Compounds of High Boron Content: Structure, Properties, and Polymorphism,” *The Chemistry of Boron and Its Compounds*, pp. 26–153, 1967, Accessed: Dec. 02, 2022. [Online]. Available: https://studylib.net/doc/8218794/boron-carbide--structure--properties--and-stability-under...

[14] H. Werheit *et al.*, “Raman effect in icosahedral boron-rich solids,” *Science and Technology of Advanced Materials*, vol. 11, no. 2. Taylor & Francis, 2010. doi: 10.1088/1468-6996/11/2/023001.

[15] E. D. Jemmis and M. M. Balakrishnarajan, “Ubiquitous icosahedral B12 in boron chemistry,” *Bulletin of Materials Science*, vol. 22, no. 5, pp. 863–867, 1999, doi: 10.1007/BF02745545.

[16] V. Domnich, S. Reynaud, R. A. Haber, and M. Chhowalla, “Boron carbide: Structure, properties, and stability under stress,” *Journal of the American Ceramic Society*, vol. 94, no. 11, pp. 3605–3628, 2011, doi: 10.1111/j.1551-2916.2011.04865.x.

[17] D. Emin, “Unusual properties of icosahedral boron-rich solids,” *J Solid State Chem*, vol. 179, no. 9, pp. 2791–2798, 2006.

[18] D. R. Tallant, T. L. Aselage, A. N. Campbell, and D. Emin, “Boron carbide structure by Raman spectroscopy,” *Phys Rev B*, vol. 40, no. 8, p. 5649, 1989.

[19] F. Mauri, N. Vast, and C. J. Pickard, “Atomic structure of icosahedral B 4 C boron carbide from a first principles analysis of NMR spectra,” *Phys Rev Lett*, vol. 87, no. 8, p. 85506, 2001.

[20] Y. Feng, G. T. Seidler, J. O. Cross, A. T. Macrander, and J. J. Rehr, “Role of inversion symmetry and multipole effects in nonresonant x-ray Raman scattering from icosahedral B 4 C,” *Phys Rev B*, vol. 69, no. 12, p. 125402, 2004.

[21] G. H. Kwei and B. Morosin, “Structures of the boron-rich boron carbides from neutron powder diffraction: Implications for the nature of the inter-icosahedral chains,” *J Phys Chem*, vol. 100, no. 19, pp. 8031–8039, 1996.

[22] G. Fanchini, J. W. McCauley, and M. Chhowalla, “Behavior of disordered boron carbide under stress,” *Phys Rev Lett*, vol. 97, no. 3, p. 35502, 2006.

[23] D. Jianxin, “Erosion wear of boron carbide ceramic nozzles by abrasive air-jets,” *Materials Science and Engineering: A*, vol. 408, no. 1–2, pp. 227–233, 2005.

[24] A. N. Caruso *et al.*, “The all boron carbide diode neutron detector: Comparison with theory,” *Materials Science and Engineering: B*, vol. 135, no. 2, pp. 129–133, 2006.

[25] Q. An and W. A. Goddard III, “Boron suboxide and boron subphosphide crystals: hard ceramics that shear without brittle failure,” *Chemistry of Materials*, vol. 27, no. 8, pp. 2855–2860, 2015.

[26] J. K. Sonber, T. S. R. C. Murthy, C. Subramanian, R. K. Fotedar, R. C. Hubli, and A. K. Suri, “Synthesis, densification and characterization of boron carbide,” *Transactions of the Indian Ceramic Society*, vol. 72, no. 2, pp. 100–107, 2013.

[27] Z. J. Li, F. Z. Fang, H. Gong, and X. D. Zhang, “Review of diamond-cutting ferrous metals,” *The International Journal of Advanced Manufacturing Technology*, vol. 68, no. 5, pp. 1717–1731, 2013.

[28] J.-L. Innocent, D. Portehault, G. Gouget, S. Maruyama, I. Ohkubo, and T. Mori, “Thermoelectric properties of boron carbide/HfB2 composites,” *Mater Renew Sustain Energy*, vol. 6, no. 2, pp. 1–7, 2017.

[29] A. P. Caricato *et al.*, “Wavelength, fluence and substrate-dependent room temperature pulsed laser deposited B-enriched thick films,” *Appl Surf Sci*, vol. 483, pp. 1044–1051, 2019.

[30] S. Li *et al.*, “One step co-sintering of silicon carbide ceramic membrane with the aid of boron carbide,” *J Eur Ceram Soc*, vol. 41, no. 2, pp. 1181–1188, 2021.

[31] N. Hynes, S. Raja, R. Tharmaraj, C. I. Pruncu, and D. Dispinar, “Mechanical and tribological characteristics of boron carbide reinforcement of AA6061 matrix composite,” *Journal of the Brazilian Society of Mechanical Sciences and Engineering*, vol. 42, no. 4, pp. 1–11, 2020.

[32] I. Huseyin, “Tribological properties of boron carbide reinforced copper based composites,” *European Journal of Engineering and Natural Sciences*, vol. 2, no. 1, pp. 102–107, 2017.

[33] U. Soy, A. Demir, and F. Findik, “Friction and wear behaviors of Al-SiC- B_4C composites produced by pressure infiltration method,” *Industrial lubrication and tribology*, 2011.

[34] A. Alizadeh and E. Taheri-Nassaj, “Wear behavior of nanostructured Al and Al– B_4C nanocomposites produced by mechanical milling and hot extrusion,” *Tribol Lett*, vol. 44, no. 1, pp. 59–66, 2011.

[35] F. Findik, “Latest progress on tribological properties of industrial materials,” *Mater Des*, vol. 57, pp. 218–244, 2014.

[36] Y. T. Yao and L. Q. Chen, “B_4C /Al composites processed by metal-assisted pressureless infiltration technique and its characterization,” *Materials and Manufacturing Processes*, vol. 31, no. 10, pp. 1286–1291, 2016.

[37] M. H. Shojaeefard, M. Akbari, A. Khalkhali, and P. Asadi, “Effect of tool pin profile on distribution of reinforcement particles during friction stir processing of B_4C /aluminum composites,” *Proceedings of the Institution of Mechanical Engineers, Part L: Journal of Materials: Design and Applications*, vol. 232, no. 8, pp. 637–651, 2018.

[38] F. Toptan, A. Rego, A. C. Alves, and A. Guedes, “Corrosion and tribocorrosion behavior of Ti– B_4C composite intended for orthopaedic implants,” *J Mech Behav Biomed Mater*, vol. 61, pp. 152–163, 2016.

[39] S. S. Bujari and R. v Kurahatti, “A review on processing and tribological properties of metal matrix composites,” *International Journal of Advancement in Engineering & Technology, Management & Applied Science*, vol. 3, no. 1, 2016.

[40] S. S. Rehman, W. Ji, S. A. Khan, Z. Fu, and F. Zhang, “Microstructure and mechanical properties of B_4C densified by spark plasma sintering with Si as a sintering aid,” *Ceram Int*, vol. 41, no. 1, pp. 1903–1906, 2015.

[41] M. S. Boldin, N. N. Berendeev, N. v Melekhin, A. A. Popov, A. v Nokhrin, and V. N. Chuvildeev, “Review of ballistic performance of alumina: Comparison of alumina with silicon carbide and boron carbide,” *Ceram Int*, vol. 47, no. 18, pp. 25201–25213, 2021.

[42] R. R. Ronald, “Boron carbide and method of making the same.” Google Patents, Feb. 14, 1933.

[43] M. T. Spohn, “Boron carbide,” *American Ceramic Society Bulletin*, vol. 72, no. 6, pp. 88–89, 1993.

[44] G. Goller, C. Toy, A. Tekin, and C. K. Gupta, “The production of boron carbide by carbothermic reduction,” *High Temperature Materials and Processes*, vol. 15, no. 1–2, pp. 117–122, 1996.

[45] Y. N. Tumanov, “The synthesis of boron carbide in a high frequency electromagnetic field,” *Journal of the Less Common Metals*, vol. 67, no. 2, pp. 521–529, 1979.

[46] W. Rafaniello and W. G. Moore, “Producing boron carbide.” Google Patents, Feb. 14, 1989.

[47] B. Z. Dacic, V. Jokanović, B. Jokanović, and M. D. Dramićanin, “Thermodynamics of gas phase carbothermic reduction of boron-anhydride,” *J Alloys Compd*, vol. 413, no. 1–2, pp. 198–205, 2006.

[48] I. A. Bairamashvili, “Experience in production of articles from boron carbide for fast rector control rods,” 1996.

[49] X. Guangshan, Z. Ruxian, L. Shikun, and W. Yonglan, “Control assembly to be used in CEFR,” 1996.

[50] A. W. Weimer, “Thermochemistry and kinetics,” in *Carbide, nitride and boride materials synthesis and processing*, Springer, 1997, pp. 79–113.

[51] K. U. Nair, D. K. Bose, and C. K. Gupta, “The production of elemental boron by fused salt electrolysis,” *Mineral Procesing and Extractive Metallurgy Review*, vol. 9, no. 1–4, pp. 283–291, 1992.

[52] A. Jain *et al.*, “Characterization of electrodeposited elemental boron,” *Mater Charact*, vol. 59, no. 7, pp. 890–900, 2008.

[53] G. E. Garry, “Process for the production of boron carbide.” Google Patents, May 13, 1958.

[54] M. Akinori, G. Tetsuo, and S. Masao, “Method for producing boron carbide.” Google Patents, Aug. 29, 1967.

[55] T. Zhang, “Preparation of Boron Carbide by Magnesium Reducing-SHS.,” *Journal of Northeastern University, Natural Science(China)*, vol. 24, no. 10, pp. 935–938, 2003.

[56] A. K. Khanra and M. M. Godkhindi, “Synthesis of boron carbide by self-propagating high temperature synthesis,” *Journal of the Australasian Ceramic Society*, vol. 41, no. 1, pp. 30–35, 2005.

[57] A. Aghaie, C. Falamaki, B. E. Yekta, and M. S. Afarani, “Effect of seeding on the synthesis of B sub 4 by the magnesiothermic reduction route,” *Industrial Ceramics(Italy)(Italy)*, vol. 22, no. 2, pp. 121–125, 2002.

[58] F. Deng, H.-Y. Xie, and L. Wang, “Synthesis of submicron B_4C by mechanochemical method,” *Mater Lett*, vol. 60, no. 13–14, pp. 1771–1773, 2006.

[59] L. L. Wang, Z. A. Munir, and J. B. Holt, “The feasibility of synthesis of B [sub 4] C fiber-MgO composites by combustion,” *Scripta Metallurgica et Materialia;(United States)*, vol. 31, no. 1, 1994.

[60] C. Suryanarayana, “Mechanical alloying and milling / C. Suryanarayana,” *SERBIULA (sistema Librum 2.0),* Jan. 2007.

[61] R. G. Bourdeau, “Process of preparing boron carbide from boron halide and a hydrocarbon.” Google Patents, Aug. 08, 1967.

[62] R. A. Clifton, “Production of boron carbide whiskers,” vol. 525, p. 589, May 1968.

[63] R. F. Cree and A. Gatti, “Catalyst for growth of boron carbide crystal whiskers.” Google Patents, Jan. 21, 1969.

[64] I. M. MacKinnon and B. G. Reuben, “The synthesis of boron carbide in an RF plasma,” *J Electrochem Soc*, vol. 122, no. 6, p. 806, 1975.

[65] G. L. Harris and D. S. Parsons, “Method of producing boron carbide from water-alcohol solution of carbon source.” Google Patents, May 20, 1975.

[66] S. Mondal and A. K. Banthia, “Low-temperature synthetic route for boron carbide,” *J Eur Ceram Soc*, vol. 25, no. 2–3, pp. 287–291, 2005.

[67] S. Cihangir, C. Ergun, S. Yılmaz, and F. Ç. Şahin, “Synthesis of B_4C /SiC composite from sugar based precursor,” in *Defect and Diffusion Forum*, 2009, vol. 283, pp. 268–272.

[68] L. Shi, Y. Gu, L. Chen, Y. Qian, Z. Yang, and J. Ma, “A low temperature synthesis of crystalline B_4C ultrafine powders,” *Solid State Commun*, vol. 128, no. 1, pp. 5–7, 2003.

[69] Y. Gu, L. Chen, Y. Qian, W. Zhang, and J. Ma, “Synthesis of nanocrystalline boron carbide via a solvothermal reduction of CCl_4 in the presence of amorphous boron powder,” *Journal of the American Ceramic Society*, vol. 88, no. 1, pp. 225–227, 2005.

[70] A. Sinha, T. Mahata, and B. P. Sharma, “Carbothermal route for preparation of boron carbide powder from boric acid–citric acid gel precursor,” *Journal of Nuclear Materials*, vol. 301, no. 2–3, pp. 165–169, 2002.

[71] M. Carlsson, F. J. García-García, and M. Johnsson, “Synthesis and characterisation of boron carbide whiskers and thin elongated platelets,” *J Cryst Growth*, vol. 236, no. 1–3, pp. 466–476, 2002.

[72] R. v Krishnarao and J. Subrahmanyam, “Studies on the formation of whiskers and platelets of B_4C and BN,” *J Mater Sci*, vol. 39, no. 20, pp. 6263–6269, 2004.

[73] R. Ma and Y. Bando, “Investigation on the growth of boron carbide nanowires,” *Chemistry of materials*, vol. 14, no. 10, pp. 4403–4407, 2002.

[74] X. K. Qian, “Methods of MAX-phase synthesis and densification–I,” in *Advances in Science and Technology of Mn+ 1axn Phases*, Elsevier, 2012, pp. 1–19.

[75] O. D. Neikov and N. A. Yefimov, *Handbook of non-ferrous metal powders: technologies and applications*. Elsevier, 2009.

[76] M. Chen, J. W. McCauley, and K. J. Hemker, “Shock-induced localized amorphization in boron carbide,” *Science (1979)*, vol. 299, no. 5612, pp. 1563–1566, 2003.

[77] K. M. Reddy, P. Liu, A. Hirata, T. Fujita, and M. W. Chen, “Atomic structure of amorphous shear bands in boron carbide,” *Nat Commun*, vol. 4, no. 1, pp. 1–5, 2013.

[78] S. Zhao *et al.*, “Directional amorphization of boron carbide subjected to laser shock compression,” *Proceedings of the National Academy of Sciences*, vol. 113, no. 43, pp. 12088–12093, 2016.

[79] D. Gosset, S. Miro, S. Doriot, G. Victor, and V. Motte, “Evidence of amorphisation of B_4C boron carbide under slow, heavy ion irradiation,” *Nucl Instrum Methods Phys Res B*, vol. 365, pp. 300–304, 2015.

[80] M. Chen and J. W. McCauley, “Mechanical scratching induced phase transitions and reactions of boron carbide,” *J Appl Phys*, vol. 100, no. 12, p. 123517, 2006.

[81] E. M. Heian, S. K. Khalsa, J. W. Lee, Z. A. Munir, T. Yamamoto, and M. Ohyanagi, “Synthesis of Dense, High-Defect-Concentration B_4C through Mechanical Activation and Field-Assisted Combustion,” *Journal of the American Ceramic Society*, vol. 87, no. 5, pp. 779–783, 2004.

[82] L. J. Berchmans, V. Mani, and K. Amalajyothi, “Synthesis of boron carbide by calciothermic reduction process,” *International Journal of Self-Propagating High-Temperature Synthesis*, vol. 18, no. 1, pp. 60–63, 2009.

[83] E. M. Sharifi, F. Karimzadeh, and M. H. Enayati, “Mechanochemical assisted synthesis of B_4C nanoparticles,” *Advanced Powder Technology*, vol. 22, no. 3, pp. 354–358, 2011.

[84] M. J. N. Isfahani, F. Payami, M. A. Asadabad, and A. A. Shokri, “Investigation of the effect of boron carbide nanoparticles on the structural, electrical and mechanical properties of Al- B_4C nanocomposites,” *J Alloys Compd*, vol. 797, pp. 1348–1358, 2019.

[85] B. Chang, B. L. Gersten, S. T. Szewczyk, and J. W. Adams, “Towards the preparation of boron carbide nanorods by carbothermal reaction method,” in *NSTI Nanotech*, 2006, pp. 369–372.

[86] G. B. Schaffer and P. G. McCormick, “Reduction of metal oxides by mechanical alloying,” *Appl Phys Lett*, vol. 55, no. 1, pp. 45–46, 1989.

[87] P. G. McCormick, V. N. Wharton, and G. B. Schaffer, “Physical chemistry of powder metals production and processing,” *Warrandale, PA: TMS*, pp. 19–34, 1989.

[88] M. C. Lea, “XLVI. Transformations of mechanical into chemical energy.(Third paper.) Action of shearing-stress (continued),” *The London, Edinburgh, and Dublin Philosophical Magazine and Journal of Science*, vol. 37, no. 228, pp. 470–475, 1894.

[89] P. G. McCormick, “Application of mechanical alloying to chemical refining (overview),” *materials Transactions, JIM*, vol. 36, no. 2, pp. 161–169, 1995.

[90] L. Takacs and C. Suryanarayana, “Processing and properties of nanocrystalline materials,” *Warrendale, PA, TMS*, pp. 453–464, 1996.

[91] C. Suryanarayana, “Mechanical alloying of nanocrystalline materials and nanocomposites,” *Madridge J. Nanotechnol. Nanosci*, vol. 4, no. 1, pp. 127–134, 2019.

[92] T. D. Shen, K. Y. Wang, J. T. Wang, and M. X. Quan, “Solid state displacement reaction of Fe and CuO induced by mechanical alloying,” *Materials Science and Engineering: A*, vol. 151, no. 2, pp. 189–195, 1992.

[93] D. Basset, P. Matteazzi, and F. Miani, “Measuring the impact velocities of balls in high energy mills,” *Materials Science and Engineering: A*, vol. 174, no. 1, pp. 71–74, 1994.

[94] G. B. Schaffer and P. G. McCormick, “Displacement reactions during mechanical alloying,” *Metallurgical Transactions A*, vol. 21, no. 10, pp. 2789–2794, 1990.

[95] G. B. Schaffer and P. G. McCormick, “Combustion and resultant powder temperatures during mechanical alloying,” *J Mater Sci Lett*, vol. 9, no. 9, pp. 1014–1016, 1990.

[96] G. B. Schaffer and P. G. McCormick, “On the kinetics of mechanical alloying,” *Metallurgical transactions A*, vol. 23, no. 4, pp. 1285–1290, 1992.

[97] A. O. Aning, C. Hong, and S. B. Desu, “Novel synthesis of lead titanate by mechanical alloying,” in *Materials Science Forum*, 1995, vol. 179, pp. 207–214.

[98] C. Suryanarayana, “Mechanical alloying and milling / C. Suryanarayana,” *SERBIULA (sistema Librum 2.0)*, Jan. 2007.

[99] C. C. Koch, “Temperature effect during mechanical attrition,” *Int. J. Mechanochem. Mech. Alloying*, vol. 1, no. 56, p. 7, 1994.

[100] D. R. Maurice and T. H. Courtney, “The physics of mechanical alloying: a first report,” *Metallurgical Transactions A*, vol. 21, no. 1, pp. 289–303, 1990.

[101] R. M. Davis, B. McDermott, and C. C. Koch, “Mechanical alloying of brittle materials,” *Metallurgical Transactions A*, vol. 19, no. 12, pp. 2867–2874, 1988.

[102] A. K. Bhattacharya and E. Arzt, “Temperature rise during mechanical alloying,” *Scripta metallurgica et materialia*, vol. 27, no. 6, pp. 749–754, 1992.

[103] M. Magini, C. Colella, W. Guo, S. Martelli, and F. Padella, “Some hints about energy transfer in the mechanosynthesis of materials,” *Int. J. Mechanochem. Mech. Alloying*, vol. 1, no. 1, p. 14, 1994.

[104] R. B. Schwarz and C. C. Koch, “Formation of amorphous alloys by the mechanical alloying of crystalline powders of pure metals and powders of intermetallics,” *Appl Phys Lett*, vol. 49, no. 3, pp. 146–148, 1986.

[105] A. Tonejc, D. Dužević, and A. M. Tonejc, “Effects of ball milling on pure antimony, on Ga□Sb alloy and on Ga+Sb powder mixture; oxidation, glass formation and crystallization,” *Materials Science and Engineering: A*, vol.

134, pp. 1372–1375, 1991, doi: https://doi.org/10.1016/0921-5093(91)90993-W.

[106] A. Tonejc, A. M. Tonejc, and D. Dužević, “Estimation of peak temperature reached by particles trapped among colliding balls in the ball-milling process using excessive oxidation of antimony,” *Scripta metallurgica et materialia*, vol. 25, no. 5, pp. 1111–1113, 1991.

[107] J. Ding, T. Tsuzuki, and P. G. McCormick, “Ultrafine alumina particles prepared by mechanochemical/thermal processing,” *Journal of the American Ceramic Society*, vol. 79, no. 11, pp. 2956–2958, 1996.

[108] C. Suryanarayana, “Mechanical alloying and milling,” *Prog Mater Sci*, vol. 46, no. 1–2, pp. 1–184, 2001.

[109] J. S. Benjamin, “Mechanical alloying,” *Sci Am*, vol. 234, no. 5, pp. 40–49, 1976.

[110] P.-Y. Lee, J.-L. Yang, and H.-M. Lin, “Amorphization behaviour in mechanically alloyed Ni—Ta powders,” *J Mater Sci*, vol. 33, no. 1, pp. 235–239, 1998.

[111] C. C. Koch, “The synthesis and structure of nanocrystalline materials produced by mechanical attrition: A review,” *Nanostructured materials*, vol. 2, no. 2, pp. 109–129, 1993.

[112] C. Suryanarayana, “Nanocrystalline materials,” *International materials reviews*, vol. 40, no. 2, pp. 41–64, 1995.

[113] A. Z. Juhász and B. Kolláth, “Mechanochemical reactions of OH-containing crystals,” *Acta chimica Hungarica*, vol. 130, no. 6, pp. 725–735, 1993.

[114] Z. Juhasz, “MECHANOCHEMISCHE AKTIVIERUNG VON SILIKATMINERALEN DURCH TROCHEN-FEINMAHLEN,” 1974.

[115] I. Kerr, “Laboratory mills for mechanical alloying,” *Metal Powder Rep*, vol. 48, pp. 36–38, 1993.

[116] L. M. Di and H. Bakker, “Phase transformation of the compound V3Ga induced by mechanical grinding,” *Journal of Physics: Condensed Matter*, vol. 3, no. 20, p. 3427, 1991.

[117] K. Tokumitsu, “Synthesis of metastable Fe3C, Co3C and Ni3C by mechanical alloying method,” in *Materials Science Forum*, 1997, vol. 235, pp. 127–132.

[118] B.-L. Chu, C.-C. Chen, and T.-P. Perng, “Amorphization of Ti1− x Mn x,” *Metallurgical Transactions A*, vol. 23, no. 8, pp. 2105–2110, 1992.

[119] M. S. El-Eskandarany, “Solid state nitrization reaction of amorphous tantalum aluminium nitride alloy powders: the role of amorphization by reactive ball milling,” *J Alloys Compd*, vol. 203, pp. 117–126, 1994.

[120] E.-E. M. Sherif, K. Sumiyama, K. Aoki, T. Masumoto, and K. Suzuki, “Mechanism of solid-gas reaction for formation of metastable niobium-nitride alloy powders by reactive ball milling,” *J Mater Res*, vol. 9, no. 11, pp. 2891–2898, 1994.

[121] C. H. Lee, T. Fukunaga, and U. Mizutani, “Mater Sci and Engng 1991,” *A134*, pp. 1334–1337.

[122] T. Fukunaga, M. Mori, K. Inou, and U. Mizutani, “Amorphization in an immiscible Cu□ V system by mechanical alloying and structure observed by neutron diffraction,” *Materials Science and Engineering: A*, vol. 134, pp. 863–866, 1991.

[123] T. Fukunaga, K. Nakamura, K. Suzuki, and U. Mizutani, “Amorphization of immiscible Cu□ Ta system by mechanical alloying and its structure observation,” *J Non Cryst Solids*, vol. 117, pp. 700–703, 1990.

[124] K. Sakurai, C. H. Lee, N. Kuroda, T. Fukunaga, and U. Mizutani, “Nitrogen effect in mechanical alloying of immiscible Cu-V: Extended x-ray absorption fine structure study,” *J Appl Phys*, vol. 75, no. 12, pp. 7752–7755, 1994.

[125] C. H. Lee, M. Mori, T. Fukunaga, K. Sakurai, and U. Mizutani, “Structural evidence for the amorphization of mechanically alloyed Cu-Ta powders studied by neutron diffraction and EXAFS,” in *Materials Science Forum*, 1992, vol. 88, pp. 399–406.

[126] C. Suryanarayana, E. Ivanov, R. Noufi, M. A. Contreras, and J. J. Moore, “Phase selection in a mechanically alloyed Cu2013; In–Ga–Se powder mixture,” *J Mater Res*, vol. 14, no. 2, pp. 377–383, 1999.

[127] B. K. Yen, T. Aizawa, and J. Kihara, “Mechanical alloying behavior in molybdenum-silicon system,” in *Materials Science Forum*, 1997, vol. 235, pp. 157–162.

[128] B. K. Yen, T. Aizawa, and J. Kihara, “Synthesis and formation mechanisms of molybdenum silicides by mechanical alloying,” *Materials Science and Engineering: A*, vol. 220, no. 1–2, pp. 8–14, 1996.

[129] T. Ohtani, K. Maruyama, and K. Ohshima, “Synthesis of copper, silver, and samarium chalcogenides by mechanical alloying,” *Mater Res Bull*, vol. 32, no. 3, pp. 343–350, 1997.

[130] M. S. El-Eskandarany, “Metall Mater Trans 1996,” *A27*, pp. 2374–2382.

[131] J. L. Harringa, B. A. Cook, and B. J. Beaudry, “Effects of vial shape on the rate of mechanical alloying in Si80Ge20,” *J Mater Sci*, vol. 27, no. 3, pp. 801–804, 1992.

[132] S. D. Kaloshkin, I. A. Tomilin, G. A. Andrianov, U. v Baldokhin, and E. v Shelekhov, “Phase transformations and hyperfine interactions in mechanically alloyed Fe-Cu solid solutions,” in *Materials Science Forum*, 1997, vol. 235, pp. 565–570.

[133] C. Kuhrt, H. Schropf, L. Schultz, and E. Arzt, “Mechanical alloying for structural applications,” *Materials Park, OH: ASM International*, pp. 269–273, 1993.

[134] A. Calka, J. I. Nikolov, and B. W. Ninham, “High Temperature Nitrides and Carbides for Structural Applications Synthesized by Mechanical Alloying,” *Mechanical Alloying for Structural Applications*, pp. 189–195, 1993.

[135] A. Calka and A. P. Radlinski, “Mater Sci and Engng 1991,” *A134*, pp. 1350–1353.

[136] C. Suryanarayana, “Does a disordered γ-TiAl phase exist in mechanically alloyed TiAl powders?,” *Intermetallics (Barking)*, vol. 3, no. 2, pp. 153–160, 1995.

[137] L. Lü and M. O. Lai, “Introduction to mechanical alloying,” in *Mechanical Alloying*, Springer, 1998, pp. 1–9.

[138] Y. H. Park, H. Hashimoto, and R. Watanabe, “Morphological evolution and amorphization of Ti/Cu and Ti/Al powder mixtures during vibratory ball milling,” in *Materials Science Forum*, 1992, vol. 88, pp. 59–66.

[139] W. Guo, A. Iasonna, M. Magini, S. Martelli, and F. Padella, “Synthesis of amorphous and metastable Ti40Al60 alloys by mechanical alloying of elemental powders,” *J Mater Sci*, vol. 29, no. 9, pp. 2436–2444, 1994.

[140] F. Padella *et al.*, “Mechanical alloying of the Pd-Si system in controlled conditions of energy transfer,” *Journal of the Less Common Metals*, vol. 175, no. 1, pp. 79–90, 1991.

[141] K. B. Gerasimov, A. A. Gusev, E. Y. Ivanov, and V. v Boldyrev, “Tribochemical equilibrium in mechanical alloying of metals,” *J Mater Sci*, vol. 26, no. 9, pp. 2495–2500, 1991.

[142] L. H. Liu, S. Casadio, M. Magini, C. A. Nannetti, Y. Qin, and K. Zhen, “Solid state reactions of V75Si25 driven by mechanical alloying,” in *Materials Science Forum*, 1997, vol. 235, pp. 163–168.

[143] M. Atzmon, “In situ thermal observation of explosive compound-formation reaction during mechanical alloying,” *Phys Rev Lett*, vol. 64, no. 4, p. 487, 1990.

[144] P. S. Gilman and J. S. Benjamin, “Mechanical alloying,” *Annual review of materials science*, vol. 13, no. 1, pp. 279–300, 1983.

[145] L. Takacs and M. Pardavi-Horvath, “Nanocomposite formation in the fe3o4-zn system by reaction milling,” *J Appl Phys*, vol. 75, no. 10, pp. 5864–5866, 1994.

[146] Z.-H. Chin and T. P. Perng, “Amorphization of Ni-Si-C ternary alloy powder by mechanical alloying,” in *Materials Science Forum*, 1997, vol. 235, pp. 121–126.

[147] M. Kis-Varga and D. L. Beke, “Phase transitions in Cu-Sb systems induced by ball milling,” in *Materials science forum*, 1996, vol. 225, pp. 465–470.

[148] S. Xi, J. Zhou, D. Zhang, and X. Wang, “Solid-state synthesis reaction between Al and Cu powders during ball milling,” *Mater Lett*, vol. 26, no. 4–5, pp. 245–248, 1996.

[149] J. Ding, W. F. Miao, P. G. McCormick, and R. Street, “Mechanochemical synthesis of ultrafine Fe powder,” *Appl Phys Lett*, vol. 67, no. 25, pp. 3804–3806, 1995.

[150] M. Miki, T. Yamasaki, and Y. Ogino, “Preparation of Nanocrystalline NbN and (Nb, Al)N Powders by Mechanical Alloying under Nitrogen Atmosphere,” *Materials Transactions, JIM*, vol. 33, no. 9, pp. 839–844, 1992, doi: 10.2320/matertrans1989.33.839.

[151] A. Calka and J. S. Williams, “Synthesis of nitrides by mechanical alloying,” in *Materials Science Forum*, 1992, vol. 88, pp. 787–794.

[152] Y. Chen and J. R. Williams, “Hydriding reactions induced by ball milling,” in *Materials Science Forum*, 1996, vol. 225, pp. 881–888.

[153] Y. Ogino, T. Yamasaki, S. Murayama, and R. Sakai, “Non-equilibrium phases formed by mechanical alloying of Cr Cu alloys,” *J Non Cryst Solids*, vol. 117, pp. 737–740, 1990.

[154] P. Y. Lee and C. C. Koch, “The formation and thermal stability of amorphous Ni-Nb alloy powder synthesized by mechanical alloying,” *J Non Cryst Solids*, vol. 94, no. 1, pp. 88–100, 1987.

[155] P. Y. Butyagin, “Disordering of structures and mechanochemical reactions in solids,” *Uspechi chimiji*, vol. 53, pp. 1769–1789, 1984.

[156] J. Viñals *et al.*, “Leaching of gold and palladium with aqueous ozone in dilute chloride media,” *Hydrometallurgy*, vol. 81, no. 2, pp. 142–151, 2006.

[157] T. Klassen, U. Herr, and R. S. Averback, “Ball milling of systems with positive heat of mixing: Effect of temperature in Ag-Cu,” *Acta Mater*, vol. 45, no. 7, pp. 2921–2930, 1997.

[158] G.-H. Chen, C. Suryanarayana, and F. H. Froes, “Structure of mechanically alloyed Ti-Al-Nb powders,” *Metallurgical and Materials Transactions A*, vol. 26, no. 6, pp. 1379–1387, 1995.

[159] P. S. Goodwin and C. M. Ward-Close, “Contamination control in the mechanical alloying of nanocrystalline intermetallic compound based alloys,” in *Materials Science Forum*, 1995, vol. 179, pp. 411–418.

[160] C. Suryanarayana, “Mechanical alloying of nanocrystalline materials and nanocomposites,” *Madridge J. Nanotechnol. Nanosci*, vol. 4, no. 1, pp. 127–134, 2019.

[161] G. M. Wang, S. J. Campbell, A. Calka, and W. A. Kaczmarek, “Synthesis and structural evolution of tungsten carbide prepared by ball milling,” *J Mater Sci*, vol. 32, no. 6, pp. 1461–1467, 1997.

[162] T. H. Courtney and Z. Wang, “Grinding media wear during mechanical alloying of Ni-W alloys in a SPEX mill,” *Scripta Metallurgica et Materialia;(United States)*, vol. 27, no. 6, 1992.

[163] S. Saji, S. Abe, and K. Matsumoto, “Formation Process of Amorphous Phase during Mechanical Alloying for Al-6 and 12 AT% Ti Mixed Powders,” in *Materials Science Forum*, 1992, vol. 88, pp. 367–374.

[164] W. Guo *et al.*, “FCC metastable phase induced in the Ti-Al system by mechanical alloying of pure elemental powders,” in *Materials Science Forum*, 1992, vol. 88, pp. 139–146.

[165] P. K. Ivison, I. Soletta, N. Cowlam, G. Cocco, S. Enzo, and L. Battezzati, “Evidence of chemical short-range order in amorphous CuTi alloys produced by mechanical alloying,” *Journal of Physics: Condensed Matter*, vol. 4, no. 7, p. 1635, 1992.

[166] E. Gaffet, M. Harmelin, and F. Faudot, “Far-from-equilibrium phase transition induced by mechanical alloying in the Cu□ Fe system,” *J Alloys Compd*, vol. 194, no. 1, pp. 23–30, 1993.

[167] P. Amin, A. Nourbakhsh, P. Asgarian, and R. Ebrahimi Kahrizsangi, “THE EFFECT OF TEMPERATURE AND MAGNESIUM SIZE ON LOW TEMPERATURE MAGNESIOTHERMIC SYNTHESIS OF NANO STRUCTURES BORON CARBIDE BY MESOPOROUS CARBON (CMK-1),” *Iranian Journal of Materials Science and Engineering*, vol. 13, no. 3, pp. 12–18, 2016.

[168] M. Alkan, M. S. Sonmez, B. Derin, and O. Yücel, “Effect of initial composition on boron carbide production by SHS process followed by acid leaching,” *Solid State Sci*, vol. 14, no. 11–12, pp. 1688–1691, 2012.

[169] I. Avramov, “Kinetics of distribution of infections in networks,” *Physica A: Statistical Mechanics and its Applications*, vol. 379, no. 2, pp. 615–620, 2007.

[170] M. Avrami, “Kinetics of phase change. I General theory,” *J Chem Phys*, vol. 7, no. 12, pp. 1103–1112, 1939.

[171] M. Avrami, “Kinetics of phase change. II transformation-time relations for random distribution of nuclei,” *J Chem Phys*, vol. 8, no. 2, pp. 212–224, 1940.

[172] M. Avrami, “Kinetics of phase change. III: Granulation, phase change and microstructure,” *Journal of chemical physics*, vol. 9, pp. 177–184, 1941.

[173] A. K. Jena and M. C. Chaturvedi, *Phase transformation in materials*. Prentice Hall, 1992.

[174] J. W. Cahn, “Transformation kinetics during continuous cooling,” *Acta Metallurgica*, vol. 4, no. 6, pp. 572–575, 1956.

[175] P. Y. Lee, J. U. L. Yang, C. K. Lin, and H. M. Lin, “Amorphization reaction of Ni-Ta powders during mechanical alloying,” *Metallurgical and Materials Transactions A 1997 28:7*, vol. 28, no. 7, pp. 1429–1435, 1997, doi: 10.1007/S11661-997-0205-4.

[176] J. S. Benjamin, “Mechanical alloying,” *Sci Am*, vol. 234, no. 5, pp. 40–49, 1976.

[177] C. Suryanarayana, E. Ivanov, R. Noufi, M. A. Contreras, and J. J. Moore, “Phase selection in a mechanically alloyed Cu2013; In–Ga–Se powder mixture,” *J Mater Res*, vol. 14, no. 2, pp. 377–383, 1999.

[178] B.-L. Chu, C.-C. Chen, and T.-P. Perng, “Amorphization of Ti1− x Mn x,” *Metallurgical Transactions A*, vol. 23, no. 8, pp. 2105–2110, 1992.

[179] K. Tokumitsu, “Synthesis of metastable Fe3C, Co3C and Ni3C by mechanical alloying method,” in *Materials Science Forum*, 1997, vol. 235, pp. 127–132.

[180] O. Kobayashi, T. Aizawa, and J. Kihara, “High speed, bulk mechanical alloying of Cu/Ag/Co systems,” *Materials Transactions, JIM*, vol. 37, no. 9, pp. 1497–1504, 1996.

[181] A. Biswas, G. K. Dey, A. J. Haq, D. K. Bose, and S. Banerjee, “A study of solid-state amorphization in Zr–30 at.% Al by mechanical attrition,” *J Mater Res*, vol. 11, no. 3, pp. 599–607, 1996.

[182] J. Katamura, T. Yamamoto, X. Qin, and T. Sakuma, “Mechanical alloying in the system ZrO2-ZrN,” *J Mater Sci Lett*, vol. 15, no. 1, pp. 36–37, 1996.

[183] S. D. Kaloshkin, I. A. Tomilin, G. A. Andrianov, U. v Baldokhin, and E. v Shelekhov, “Phase transformations and hyperfine interactions in mechanically alloyed Fe-Cu solid solutions,” in *Materials Science Forum*, 1997, vol. 235, pp. 565–570.

[184] C. Kuhrt, H. Schropf, L. Schultz, and E. Arzt, “Mechanical alloying for structural applications,” *Materials Park, OH: ASM International*, pp. 269–273, 1993.

[185] P. Millet, A. Calka, and B. W. Ninham, “Reduction of ilmenite by surfactant-assisted mechanochemical treatment,” *J Mater Sci Lett*, vol. 13, no. 19, pp. 1428–1429, 1994.

[186] A. Calka and A. P. Radlinski, “Mater Sci and Engng 1991,” *A134*, pp. 1350–1353.

[187] C. Suryanarayana, “Mechanical alloying and milling / C. Suryanarayana,” *SERBIULA (sistema Librum 2.0)*, Jan. 2007.

[188] C. Subramanian and A. K. Suri, “Development of boron based neutron absorber materials,” *Met. Mater. Process*, vol. 16, no. 1, pp. 39–52, 2004.

[189] A. K. Suri, C. Subramanian, J. K. Sonber, and T. S. R. Ch Murthy, “Synthesis and consolidation of boron carbide: A review,” *International Materials*

Reviews, vol. 55, no. 1, pp. 4–38, Jan. 2010, doi: 10.1179/095066009X12506721665211.

[190] Y. H. Park, H. Hashimoto, and R. Watanabe, "Morphological evolution and amorphization of Ti/Cu and Ti/Al powder mixtures during vibratory ball milling," in *Materials Science Forum*, 1992, vol. 88, pp. 59–66.

[191] W. Guo, A. Iasonna, M. Magini, S. Martelli, and F. Padella, "Synthesis of amorphous and metastable Ti40Al60 alloys by mechanical alloying of elemental powders," *J Mater Sci*, vol. 29, no. 9, pp. 2436–2444, 1994.

[192] K. B. Gerasimov, A. A. Gusev, E. Y. Ivanov, and V. v Boldyrev, "Tribochemical equilibrium in mechanical alloying of metals," *J Mater Sci*, vol. 26, no. 9, pp. 2495–2500, 1991.

[193] M. Kis-Varga and D. L. Beke, "Phase transitions in Cu-Sb systems induced by ball milling," in *Materials science forum*, 1996, vol. 225, pp. 465–470.

[194] Z.-H. Chin and T. P. Perng, "Amorphization of Ni-Si-C ternary alloy powder by mechanical alloying," in *Materials Science Forum*, 1997, vol. 235, pp. 121–126.

[195] A. K. Suri, C. Subramanian, J. K. Sonber, and T. S. R. Ch Murthy, "Synthesis and consolidation of boron carbide: A review," *International Materials Reviews*, vol. 55, no. 1, pp. 4–38, Jan. 2010, doi: 10.1179/095066009X12506721665211.

[196] M. Avrami, "Kinetics of phase change. I General theory," *J Chem Phys*, vol. 7, no. 12, pp. 1103–1112, 1939.

[197] M. Avrami, "Kinetics of phase change. II transformation-time relations for random distribution of nuclei," *J Chem Phys*, vol. 8, no. 2, pp. 212–224, 1940.

[198] U. M. Rao Seelam, C. Suryanarayana, H. Heinrich, T. Ohkubo, K. Hono, and N. S. Cheruvu, "Structural characterization of sputter-deposited 304 stainless

Steel+10 wt pct Al coatings," *Metall Mater Trans A Phys Metall Mater Sci*, vol. 43, no. 8, pp. 2945–2954, Aug. 2012, doi: 10.1007/S11661-012-1128-2.

[199] A. Kocjan, P. J. McGuiness, and S. Kobe, "The impact of ambient gas on the magnetic properties of Ti 40Zr40Ni20 powders during mechanical alloying," *J Magn Magn Mater*, vol. 323, no. 3–4, pp. 301–305, Feb. 2011, doi: 10.1016/J.JMMM.2010.09.023.

[200] M. J. N. Isfahani, F. Payami, M. A. Asadabad, and A. A. Shokri, "Investigation of the effect of boron carbide nanoparticles on the structural, electrical and mechanical properties of Al- B_4C nanocomposites," *J Alloys Compd*, vol. 797, pp. 1348–1358, 2019.